(NASA-CR-173514) THE BOUNDARY LAYER ON COMPRESSOR CASCADE BLADES Semiannual Progress Report, 1 Dec. 1983 - 1 Jun. 1984 (Pennsylvania State Univ.) 76 p HC A05/MF A01 CSCL 20D G3/34

N84-25001

Unclas 19326

SEMI-ANNUAL PROGRESS REPORT

1 December 1983 to 1 June 1984

to

National Aeronautics and Space Administration

on

NASA Grant NSG-3264

Entitled

"THE BOUNDARY LAYER ON COMPRESSOR CASCADE BLADES"

Submitted by:

Steven Deutsch and William C. Zierke

Applied Research Laboratory
The Pennsylvania State University
Post Office Box 30
State College, PA 16804

A. INTRODUCTION

The purpose of NASA Research Grant NSG-3264 is to characterize the flowfield about an airfoil in a cascade at chord Reynolds number (R_c) near 5×10^5. The program is experimental and combines Laser Doppler Anemometry (LDA) with flow visualization techniques in order to obtain detailed flow data [e.g., boundary layer profiles, points of separation and the transition zone] on a cascade of highly-loaded compressor blades. The information provided by this study is to serve as benchmark data for the evaluation of current and future compressor cascade predictive models, in this way aiding in the compressor design process.

This report summarizes the research activity for the period 1 December 1983 through 1 June 1984. Progress made from 1 June 1979 through 1 December 1983 is presented in Refs. (1) through (9). The current report presents the completed suction surface mean velocity and turbulence intensity profiles, at a single incidence angle.

B. PROGRESS DURING THE PERIOD 1 DECEMBER 1983 TO 1 JUNE 1984

B.1 Description of the Experiment

The ARL/PSU cascade tunnel is shown in Figure 1. With the current fan system, maximum inlet speed to the cascade section is near 35 m/sec. Inlet turbulence intensity, as measured with a hot-wire anemometer, is below 0.2% as shown in Figure 2. All data to be presented in this report were taken on the suction surface of a double circular arc compressor blade at a cascade inlet angle of 53° (see Figure 7).

The cascade test section is detailed in Figure 3. It is worth noting that blade pack side suction, as normally employed in cascade testing to maintain two-dimensionality, is not possible because of the need for an LDA window. Instead, a strong upstream side suction, controllable in the blade-to-blade direction, is employed. Tailboards are used to control the periodicity of the flow.

As current computer codes assume a two-dimensional, periodic cascade flow, data must be taken in such a flow field to be useful. Here, two-dimensionality is taken to imply that the velocities and angles of the flow are substantially the same in spanwise planes, while periodicity means that velocities and flow angles in planes normal to the blades leading and trailing edges are functions only of the distance from a blade (independent of which blade). In a successful two-dimensional, periodic, cascade flow, the ratio of axial velocity from the leading to trailing edge is one. A typical outlet flow profile is shown in Figure 4, the corresponding turning angle in Figure 5, and the blade static pressure distribution in Figure 6. Interpretation of these figures can be facilitated by referring to the definitions of cascade flow angles given in Figure 7. The periodicity of the flow is clearly excellent. Also apparent from the pressure gradient plot is the strong adverse gradient on the suction surface and strong favorable gradient on the pressure surface near the leading edge of the blade. One might then anticipate at this incidence angle, a separation at the leading edge of the suction surface and some laminar flow near the leading edge of the pressure surface. The axial flow ratio, found to be one, is determined by averaging the local axial velocity over three blade passages, centered at the minimum velocity ratio point of the central blade wake. On a day-to-day basis, the variation in axial flow ratio was within 3%, while the variation in chord Reynolds number was within 1%. A more detailed exposition of the experimental techniques may be found in [10].

A specially designed traversing mechanism which matches the arc of motion of an optics cradle to that of the blade curvature is used for the LDA measurements. All measurements then were made in the plane of the local blade normal. Translation of the optics cradle normal to the blade can be accomplished in step intervals as small as 0.0254 mm. Prior to LDA measurements, a reference distance was established by focusing the LDA control volume on an insert which fit over the central measuring blade. Narrow lines are etched on the insert so as to be at known locations from the blade surface. Repeatability in establishing a measurement reference was estimated to be ± 0.05 mm, and this uncertainty is probably the major source of scatter in the velocity data.

A schematic of the LDA optics system is shown in Figure 8. A two Watt Spectra-Physics Argon-Ion laser was used for the measurements. Power on the blue line employed (488 nm) ranged between 0.6 to 0.8 Watts. Standard TSI optical components were used: the focusing lens (focal distance = 371.3 mm) allowed the measurements to be made at the blade mid-span. The focal volume was ellipsoidal and was predicted to be 0.56 mm × 0.037 mm in the direction normal to the blade. Optical shifting at 5 Mhz was employed as needed. To measure close to the surface the optical cradle was tilted 1°. Silicon carbide particles having a mean diameter of 1.5 μm were used for laser seeding. In an attempt to maintain a uniform distribution, seed was injected well upstream of the measurement station (see Figure 1) at the flexible coupling.

LDA data acquisition and reduction was accomplished by using a direct link to a VAX 11/782 computer. Software allowed selection of focusing lens half angle, laser wavelength, frequency shift, minimum cycles employed in the calculation and number of particle counts per run (up to 4000). Initial output was in the form of a velocity histogram. Minimum and maximum velocity limits were set by a cursor from the histogram to eliminate obvious noise. Final output was mean velocity, turbulence intensity and percent of particle counts employed in the calculation. The latter served as a signal-to-noise indicator. It is probably fair to state that at least 98% of the total particle counts were employed for measurement stations in the boundary layer; at least 95% were employed for points in the free stream. Mean velocity here was taken as a simple arithmetic average

$$u = \frac{1}{N} \sum_{n=1}^{N} u_n \quad , \tag{1}$$

and local turbulence intensity (L.T.I.) as

$$\frac{u'}{u} = \frac{1}{u} \left(\frac{1}{N} \sum_{n=1}^{N} (u_n - u)^2 \right)^{1/2} \tag{2}$$

Experience has shown that quite satisfactory repeatability of the mean and turbulence intensity can be guaranteed in boundary layer flows by using N = 1000 particle counts in regions in which the L.T.I. exceeds 5%, 500 points for L.T.I. less than 5% and 200 points for the free stream.

B.2 Results and Discussion

Eleven velocity profiles were measured between 2.6% and 94.9% chord. Consider these measurement stations in conjunction with the blade static pressure distribution, Figure 9; particularly the strong adverse gradient on the suction surface. Clearly the pressure gradient (hence Coles' wake parameter Π) is varying throughout the region in which the profiles have been measured, so that the boundary layers cannot be considered to be in equilibrium.

At each of the stations the velocity profile was defined by statistically treating the data taken for six individual profiles (seven at 2.6% chord). Some appreciation of the day-to-day variation in the data may be gained by considering the individual profiles shown in Figure 10 for the data taken at 53.6% chord. Mean velocity profiles taken at chord locations of 2.6% through 94.9% are shown in Figures 11 through 21, respectively. The profiles are plotted semi-logarithmically to highlight the inner part of the boundary layer. Also shown on these plots are error bars. These represent 95% confidence levels as determined by a small sample Student T-Test. For the attached boundary layers the level of scatter is about the same as was measured earlier for a flat plate geometry; that is, for a 2% local turbulence level the 95% confidence band represents a roughly 0.4% variation in velocity, a 1.5% variation 15% and a 3% variation 25%, independent of chord position. More than half of this scatter can probably be accounted for by considering the positional uncertainty. The separated profiles at 84.2 and 94.9% chord show somewhat more scatter. This is perhaps due to the flow's heightened sensitivity to background conditions at these points.

At the present time, only the data at the first seven chord locations has been thoroughly analyzed. We shall consider these first. This data has been previously reported in Reference [11].

Perhaps the most interesting feature of the seven profiles is the fall-off of velocity with distance from the wall in the inviscid region. This is, of course, a consequence of the blade-to-blade normal pressure gradient. On a linear plot (c.f., see Figures 29-35) it may be shown that the decay of velocity with distance is linear for 53.6%, 43.3%, 33.3% and 23.0% chord, but that some significant profile curvature occurs at the remaining three chord locations. Note also that the near wall profile at 2.6% chord has a distinctly different shape than the others.

Local turbulence intensities are shown at each of the chord locations in Figures 22 through 28. With the exception of the 2.6% chord location (and perhaps the 7.6% chord location) the profiles may be observed to have a classical shape. The increase in uncertainty near the strong mean profile curvature at the edge of the boundary layer, which is particularly noticeable in the 23.0%, 12.7% and 7.6% chord location data, is a consequence of the very large skewness of the velocity histograms there. The intensity profile at 2.6% chord is interesting. The decrease of the local turbulence with decreasing distance to the wall is perhaps indicating a profile just recovering from separation. It is also worth noting that the free stream intensity level near 2%, which is roughly a factor of ten too high, is characteristic of laser anemometry. This LDA bias may be accounted for by requiring that the free stream have the correct value (0.18%, say, as measured by a hot-wire). The correction factor found in this way can be used as a correction throughout. The change in L.T.I. value in the boundary layer, however, can be shown to be small.

As will be shown in the next section, the turbulence intensity profiles may be of more than academic interest. They provide at least a rough indication of the boundary layer thickness and in this way give an indication of the acceptability of the analysis to be presented next. In this light, it would seem that values of the skewness and kurtosis would also be of interest, as one way of assessing the effect of the normal pressure gradient on the turbulence.

C. AN ANALYSIS

The presence of a normal pressure gradient makes the interpretation of the boundary layer profiles difficult. In particular, we wish to determine the shear velocity, u_{τ}, Coles' wake function Π, and a host of integral parameters. To do this we must, following References [12, 13], account for the effect of the normal pressure gradient. Assume that the measured profiles represent a composite velocity profile. This implies that each of the profiles have, to zero order, a region where viscous effects predominate, a region in which viscous effects are negligible (and the normal gradient acts) and an intermediate region in which the viscid-inviscid results match. Mathematically, the measured profile is the sum of a boundary layer profile and an inviscid profile less what appears in both. The last quantity is commonly called the edge velocity, U_e. That is

$$u_{meas} = u + u_{inv} - U_e \quad .$$

Clearly both the boundary layer velocity u and the measured velocity u_{meas} must go to zero at the wall, so that

$$U_e = (u_{inv})_w$$

and the scheme reduces to finding that value.

Consider each of the profiles as shown in Figures 29 through 35. Here the circles represent the measured values of average velocity. One must determine a way to extrapolate the inviscid portion of the profile to the wall. A rigorous approach does not appear possible so one must settle for a self consistent attack which produces plausible results. Consider Figure 31 (12.7%) as a representative profile. We note that there are 26 data points (say, N_{inv}) from the position of maximum velocity to the measurement position furthest from the blade. One might argue then that the actual inviscid region contains anywhere from one to 26 data points. In addition, it is clear that the inviscid profile exhibits some curvature. If one least square fits each of these possible inviscid regions with a quadratic, one finds that there is a region in which U_e changes only slightly with the number of points. Specifically, this region is well represented by choosing $N_{inv}/2 \pm N_{inv}/4$ points for each of the profiles. In Figures 29 through 35, the triangles represent the boundary layer plots reconstructed by choosing the inviscid region to contain $N_{inv}/2$ points. Also shown in Figures 29 through 35, on the velocity axis, is the average value of U_e which was determined by assuming the inviscid region is represented by each of the $N_{inv}/2 \pm N_{inv}/4$ points in turn. In general, these values are quite close. The average values of U_e along with its standard deviation (the plus and minus values) are given in Table 1.

The boundary layer thickness, δ, was chosen as the position at which

$$u = 0.99\ U_e \quad .$$

One can test the plausibility of the U_e and δ values by noting that in a classical equilibrium boundary layer the turbulence intensity has a higher than free stream value at positions $y/\delta \overset{\sim}{<} 1.25$. We may use $y = 1.25\delta$ and the turbulence intensity measurement (Figures 22 through 28) to define δ. The results of this comparison are shown in Table 2. As a second check on the plausibility of the calculations, the U_e determined can be compared to the surface velocity. The last may be found from

$$U_{e_s} = V_1 \sqrt{1 - C_p}$$

where

$$C_p = \frac{p_s - p_i}{1/2\ \rho\ V_1^2}$$

The surface velocities are compared with the U_e determined from the composite solution in Table 2. Though not a proof, the good comparisons indicate that the technique produces plausible results. Comparison of the triangles and circles in Figure 29 through 35 indicate that the near wall region is hardly changed in the analysis. That is, for example, the inner variables (e.g., the shear velocity, u_τ) are reasonably independent of the choice of U_e. We note further that all the derived boundary layers show a constant free stream velocity with the exception of that at 2.6% chord. This profile, of course, contains the largest inviscid curvature, and the smallest measurable free stream region (due to geometric constraints); possibly these effects combine to produce this discrepancy.

With δ known, Coles' velocity profiles for the wall/wake region of the turbulent boundary layer

$$\frac{u}{u_\tau} = \frac{1}{\kappa} \ln \left(\frac{y u_\tau}{\nu}\right) + C + \frac{\Pi}{\kappa} W \left(\frac{y}{\delta}\right)$$

where

$$W \left(\frac{y}{\delta}\right) = 1 - \cos \left(\frac{y \pi}{\delta}\right)$$

can be used to determine Π and u_τ. Here Π and u_τ were determined by minimizing the error between the data and the expressions above: the constants were chosen from the 1970 Stanford Convention [14]. The resulting simultaneous non-linear equations were solved using a standard IMS (International Mathematical Subroutine Library) routine. As noted by White [15], Coles' profile does not fit the entire boundary layer precisely; for the results presented here the Coles' profile was assumed valid for positions between 5 and 80% of the boundary layer thickness. Note that measurements were made at points above and below these values. The velocity profile was taken to be

$$\frac{u}{u_\tau} = \frac{yu_\tau}{\nu}$$

for the lower portion of the boundary layer. The profiles were numerically joined near a y^+ of 10.7 -- thus defining the sublayer thickness. A spline curve was used to fit the data above 80% of the boundary layer thickness.

In Table 1, the common parameters for the reconstructed turbulent boundary are given as a function of chord location. A complete nomenclature is given in Table 3. Error estimates are based on the deviations in U_e over the range $N_{inv}/2 \pm N_{inv}/4$. We note that R_θ varies from 1174 to 4015, and the boundary layer thickness from 0.206 cm to 1.148 cm from 2.6 to 53.6% chord . The large values of G at both 2.6% and 53.6% chord indicate that those boundary layers are near separation. Also note the good agreement between the values of u_τ determined by measurement with those determined by the Ludwing-Tillman relation. For the profile at 12.7%, H (and β) indicates a near zero pressure gradient boundary layer -- although, of course, comparisons must be made with care as the measured profiles are non-equilibrium. For the same reason, it is not really worthwhile to compare the pressure gradient parameter β with the derived quantity Π. The trends, however, are the same for each.

The boundary layer profiles are shown in inner variables in Figures 36 through 42. Note the striking effect on the outer part of the boundary layer (or the extent of the logarithmic region) with increasing and decreasing values of the wake parameter Π. In Figure 36 through 42 the circles represent the measured data points, the triangles the derived boundary layer profile and the solid line the least squares fit law of the wall/wake to the derived profile. The data are replotted in terms of u/U_e vs y/δ in Figure 43 through 49, a form which best emphasizes the evolution of the boundary layer. One can clearly observe, in following the data from 2.6% to 53.6% chord, a boundary layer recovering from a separation at the leading edge only to approach separation again somewhere beyond the 53.6% chord location.

As noted earlier, profile data taken at 63.2, 74.0, 84.2 and 94.9% chord have not been thoroughly analyzed as yet. The mean velocity data is presented in linear format in Figures 50-53. At each of these locations the velocity is instantaneously negative (backflow) for some range of distance from the wall some of the time as shown in Figures 54-57. At 63.2 percent chord the backflow region is quite small, involving only the region within 0.1 cm from the wall; the maximum percent backflow is about 5. At 94.9% chord, the backflow region has spread to encompass about the first two centimeters from the blade, maximum time in backflow approaches 65%. For the 94.9% and the 84.2% chord locations the point of maximum backflow is not at the measurement station nearest the wall.

In Figure 58 the maximum percent backflow as a function of percent chord is given. Simpson [16] reported on a set of proposed quantitative definitions for the state of flow detachment in near wall region; incipient detachment (ID) occurs with 1% instantaneous backflow; intermittent transitory detachment (ITD) occurs with 20% instantaneous backflow; transitory detachment (TD) occurs with 50% instantaneous backflow; and detachment occurs where the wall shear is zero. The first three of these states are also indicated in Figure 58. A measure of wall shear stress would be useful here.

Analysis of the profile data taken for 63.2 to 94.9% chord is continuing.

C. GOALS FOR THE NEXT REPORTING PERIOD

During the next six month period, it is anticipated that:

- Analysis of the profile data at 63.2 to 94.9% chord will be completed.
- Boundary layer profile measurements on the pressure surface of the blade will be completed
- Flow visualization studies of the blades to determine transition and separated regions will be finished.
- Near wake profile measurements at the current incidence will be done.
- Flow studies at a second incidence will be underway.

D. REFERENCES

[1] Deutsch, S., Semi-Annual Progress Report for NASA Grant NSG-3264, January 1980.

[2] Deutsch, S., Semi-Annual Progress Report for NASA Grant NSG-3264, June 1980.

[3] Deutsch, S., Semi-Annual Progress Report for NASA Grant NSG-3264, January 1981.

[4] Deutsch, S., Semi-Annual Progress Report for NASA Grant NSG-3264, June 1981.

[5] Deutsch, S., Semi-Annual Progress Report for NASA Grant NSG-3264, January 1982.

[6] Deutsch, S., Semi-Annual Progress Report for NASA Grant NSG-3264, June 1982.

[7] Deutsch, S. and S. Gearhart, Semi-Annual Progress Report for NASA Grant NSG-3264, December 1982.

[8] Deutsch, S., Semi-Annual Progress Report for NASA Grant NSG-3264, May 1983.

[9] Deutsch, S. and W. C. Zierke, Semi-Annual Progress Report for NASA Grant NSG-3264, December 1983.

[10] Deutsch, S., S. A. Gearhart and R. E. Henderson, "A Two-Dimensional Cascade Tunnel Suitable for Blade Boundary Layer Measurements by Laser Doppler Anemometry," ARL/PSU TM 83-93, Applied Research Laboratory, The Pennsylvania State University (19 May 1983).

[11] Deutsch, S. and W. C. Zierke, "Some Measurements of Boundary Layers on the Suction Surface of Double Circular Arc Blades in Cascades," ARL/PSU TM 84-77, Applied Research Laboratory, The Pennsylvania State University (3 April 1984).

[12] Ball, C. L., L. Reid and J. F. Schmidt, "End-Wall Boundary Layer Measurements in a Two Stage Fan," NASA TM 83409 (June 1983).

[13] Mellor, G. L. and G. M. Wood, "An Axial Compressor End-Wall Boundary Layer Theory," Trans. of Basic Engr., Journal of Basic Engr. (June 1971).

[14] Coles, D. E. and E. A. Hirst, "Computation of Turbulent Boundary Layers," Proceedings of the 1968 AFOJR-IFP-Stanford Conference.

[15] White, F. M., Viscous Fluid Flow, McGraw-Hill, Inc. (1974).

[16] Simpson, R. L., Y.-T. Chow and B. G. Shivaprasad, "The Structure of a Separating Turbulent Boundary Layer. Part 1. Mean Flow and Reynolds Stresses," Journal of Fluid Mechanics, Vol. 113, pp. 23-51 (1981).

Table 1

% Chord	U_E (m/sec)	U_τ (m/sec)	$U_{\tau_{LT}}$ (m/sec)	δ (cm)	δ^* (cm)	θ (cm)	Π	G	β	R_θ
2.6	53.968 ± .207	1.429 ±.019	1.379 ±.014	0.2060 ±.0056	0.0722 ±.0003	0.0337 ±.0000	3.544 ±.169	20.1 ± .3	24.659 ± .751	1174 ± 5
7.7	46.286 ± .313	1.880 ±.051	1.886 ±.021	0.3817 ±.0636	0.0682 ±.0020	0.0448 ±.0013	1.405 ±.278	8.4 ± .1	2.195 ± .178	1339 ± 30
12.7	44.726 ± .082	1.938 ±.005	1.930 ±.005	0.4019 ±.0078	0.0729 ±.0002	0.0509 ±.0001	0.514 ±.028	7.0 ± .0	0.377 ± .003	1469 ± 2
23.0	41.750 ± .095	1.753 ±.006	1.750 ±.006	0.5242 ±.0088	0.0928 ±.0002	0.0643 ±.0001	0.611 ±.007	7.3 ± .0	1.177 ± .010	1733 ± 2
33.2	37.780 ± .083	1.409 ±.005	1.434 ±.005	0.8038 ±.0065	0.1658 ±.0004	0.1111 ±.0001	1.125 ±.002	8.8 ± .1	4.455 ± .041	2708 ± 3
43.3	35.310 ± .119	1.128 ±.008	1.160 ±.007	0.9259 ±.0106	0.2172 ±.0007	0.1308 ±.0002	2.415 ±.007	12.5 ± .1	3.841 ± .064	2979 ± 7
53.6	33.780 ± .130	0.822 ±.009	0.880 ±.007	1.1479 ±.0161	0.3512 ±.0013	0.1843 ±.0001	4.436 ±.007	15.5 ± .3	6.861 ± .176	4015 ± 15

$\rho = 1.0057 \frac{kg}{m^3}$

$\nu = 0.155 \frac{cm^2}{sec}$

Table 2

% Chord	U_e (m/sec) (Current Method)	U_e (C_p Dist.)	δ (cm) (Current Method)	δ (cm) (Turb. Int.)
2.6	53.968 ± 0.207	50.305	0.206 ± 0.0056	-----
7.7	46.286 ± 0.313	43.352	0.3817 ± 0.0636	0.457
12.7	44.726 ± 0.082	41.625	0.4019 ± 0.0078	0.406
23.0	41.750 ± 0.095	40.683	0.5242 ± 0.0088	0.508
33.2	37.780 ± 0.083	37.370	0.8038 ± 0.0065	0.813
43.3	35.310 ± 0.119	34.765	0.9259 ± 0.0106	0.914
53.2	33.780 ± 0.130	33.621	1.1479 ± 0.0161	1.11

Table 3

NOMENCLATURE

C	Law of the wall constant (= 5.0)
C_f	Skin friction coefficient $(= \frac{\tau_w}{1/2 \rho U_e^2})$
C_p	Local pressure coefficient $(= \frac{p_s - p_1}{1/2 \rho V_1^2})$
G	Clauser's shape factor $(= \frac{1}{\Delta} \int_0^\omega (\frac{U_e - u}{u_\tau})^2 dy)$
H_{12}	First shape factor $(= \frac{\delta^*}{\theta})$
H_{32}	Second shape factor $(= \frac{\delta_3}{\theta})$.
N	Number of particle counts per run
N_{inv}	Number of data points in the inviscid region
p_e	Static pressure at the bounday layer edge
p_1	Static pressure upstream of the cascade
p_s	Local static pressure on the blade surface
R_θ	Momentum thickness boundary layer $(= \frac{\theta U_e}{\nu})$
u	Boundary layer velocity
u_{inv}	Inviscid velocity
u_{meas}	Measured composite velocity
u_n	Particle velocity.
u^+	= Dimensionless velocity in the inner boundary layer $(= \frac{u}{u_\tau})$

u_τ	Friction velocity $(= \sqrt{\frac{\tau_w}{\rho}})$
U_e	Velocity at the boundary layer edge
U_{e_s}	Velocity at the boundary layer-edge as derived from the local pressure coefficient
V_1	Velocity upstream of the cascade
W	Coles' universal wake function
x	Streamwise coordinate
y	Coordinate normal to the blade surface
y^+	Dimensionless coordinate normal to the blade surface in the inner boundary layer
β	Clauser's equilibrium parameter $(= \frac{\delta^*}{\tau_w} \frac{\partial p_e}{\partial x})$
δ	Boundary layer thickness
δ^*	Displacement thickness $(= \int_0^\infty (1 - \frac{u}{U_e}) dy)$
δ_3	Energy thickness $(= \int_0^\infty \frac{u}{U_e} (1 - \frac{u^2}{U_e^2}) dy)$
Δ	Defect thickness $(= \int_0^\infty (\frac{U_e - u}{u_\tau}) dy)$
θ	Momentum thickness $(= \int_0^\infty \frac{u}{U_e} (1 - \frac{u}{u_e}) dy)$
κ	Karman's mixing length parameter (= 0.41)
ν	Kinematic viscosity
Π	Coles' wake parameter
ρ	Fluid density
τ_w	Wall shear stress

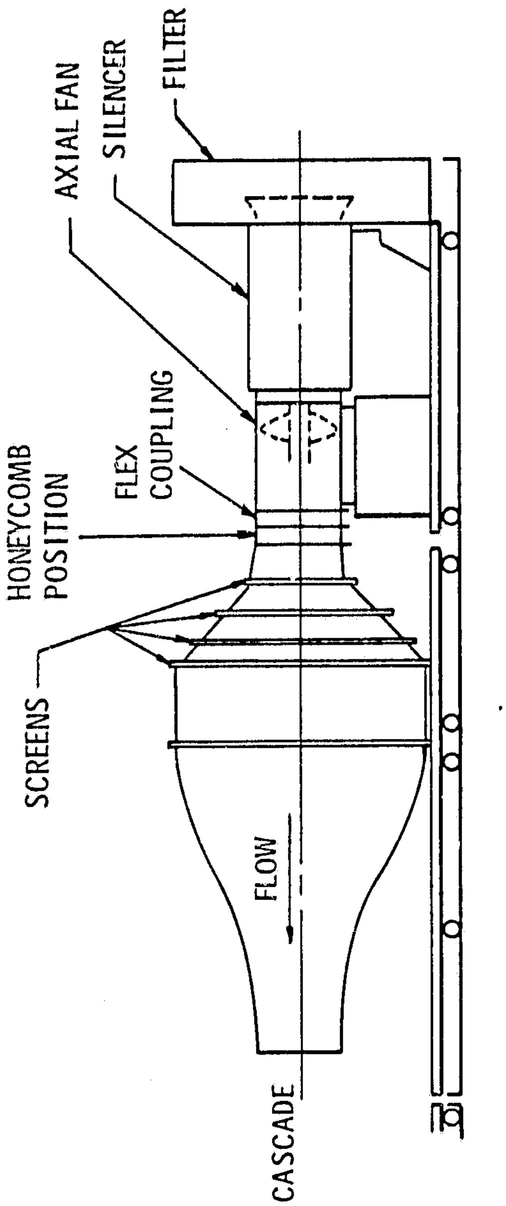
FILTER
SILENCER
AXIAL FAN
FLEX
COUPLING
HONEYCOMB
POSITION
SCREENS
FLOW
CASCADE

Figure 1.

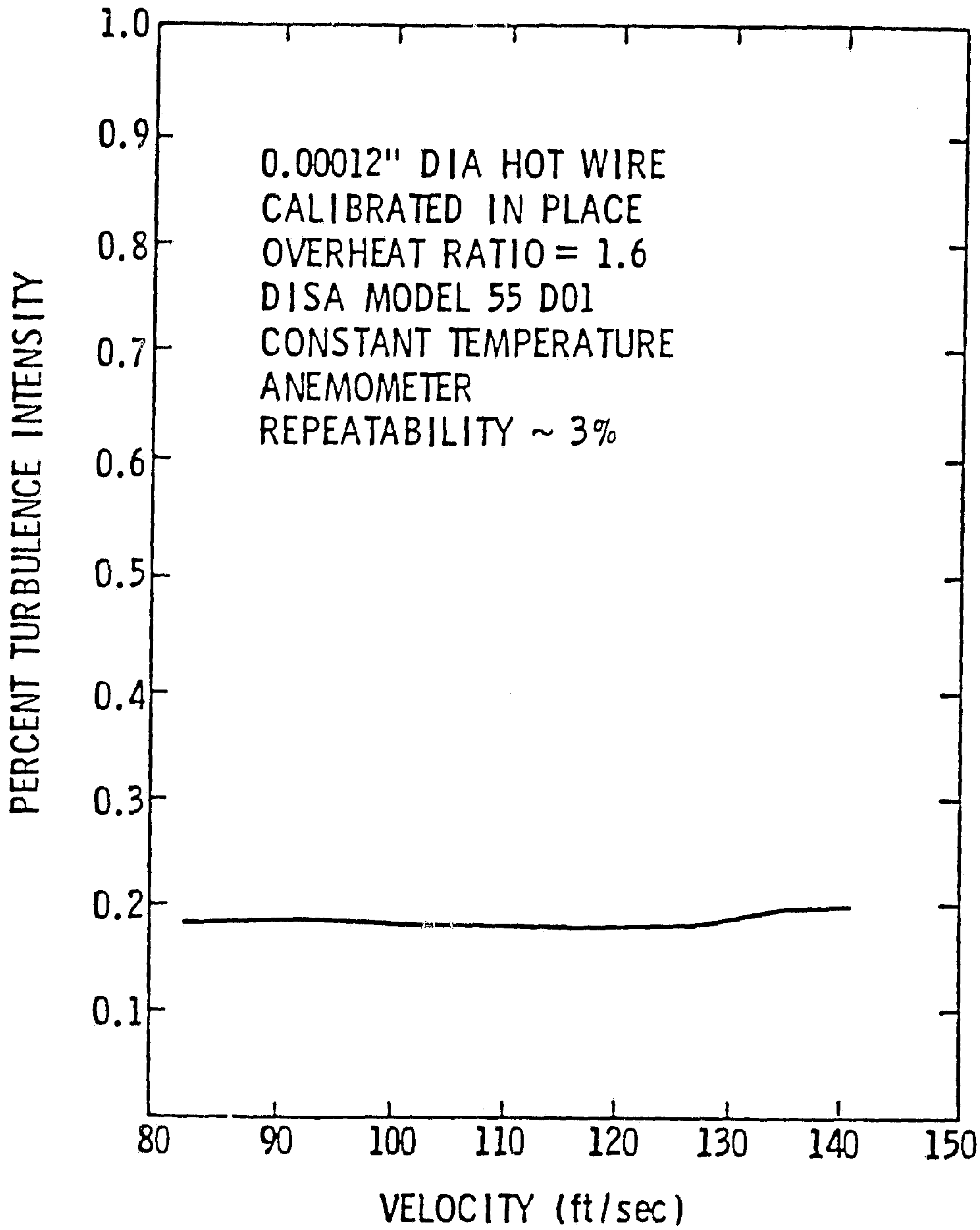
0.00012" DIA HOT WIRE
CALIBRATED IN PLACE
OVERHEAT RATIO = 1.6
DISA MODEL 55 D01
CONSTANT TEMPERATURE
ANEMOMETER
REPEATABILITY ~ 3%
PERCENT TURBULENCE INTENSITY
1.0
0.9
0.8
0.7
0.6
0.5
0.4
0.3
0.2
0.1
80
90
100
110
120
130
140
150
VELOCITY (ft/sec)

Figure 2.

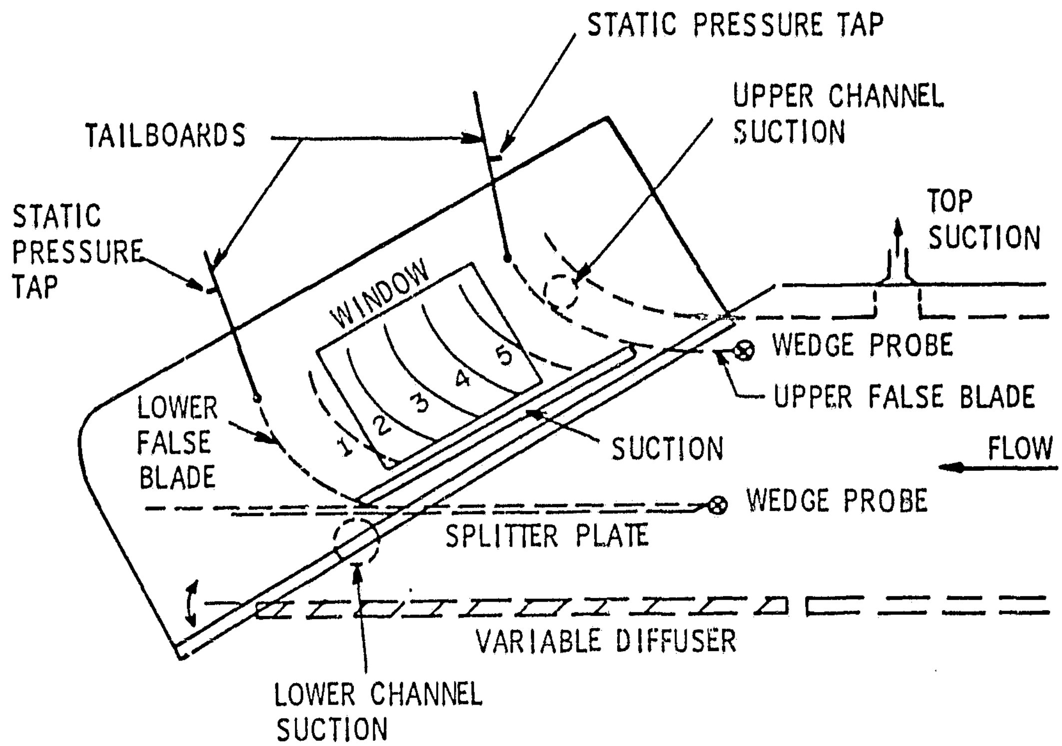
STATIC PRESSURE TAP
UPPER CHANNEL SUCTION
TAILBOARDS
STATIC PRESSURE TAP
TOP SUCTION
WINDOW
1
2
3
4
5
WEDGE PROBE
UPPER FALSE BLADE
LOWER FALSE BLADE
SUCTION
FLOW
WEDGE PROBE
SPLITTER PLATE
VARIABLE DIFFUSER
LOWER CHANNEL SUCTION

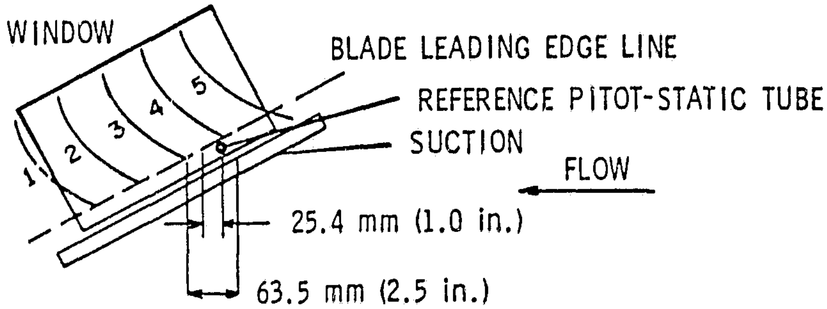
WINDOW
BLADE LEADING EDGE LINE
REFERENCE PITOT-STATIC TUBE
SUCTION
FLOW
1
2
3
4
5
25.4 mm (1.0 in.)
63.5 mm (2.5 in.)

Figure 3.

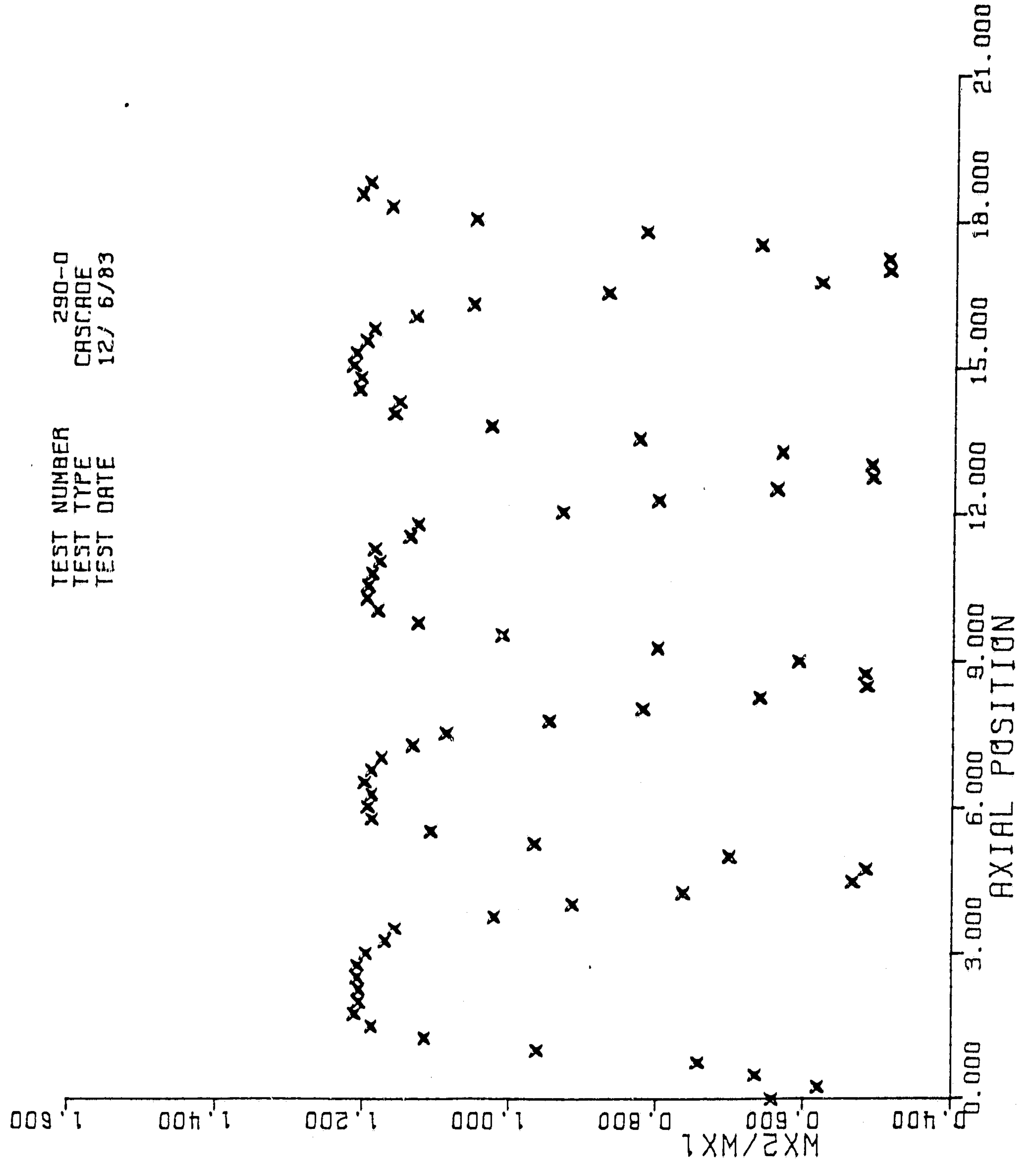
TEST NUMBER 290-0
TEST TYPE CASCADE
TEST DATE 12/ 6/83
MX2/MX1
0.400
0.600
0.800
1.000
1.200
1.400
1.600
AXIAL POSITION
0.000
3.000
6.000
9.000
12.000
15.000
18.000
21.000

Figure 4.

ORIGINAL PAGE IS
OF POOR QUALITY

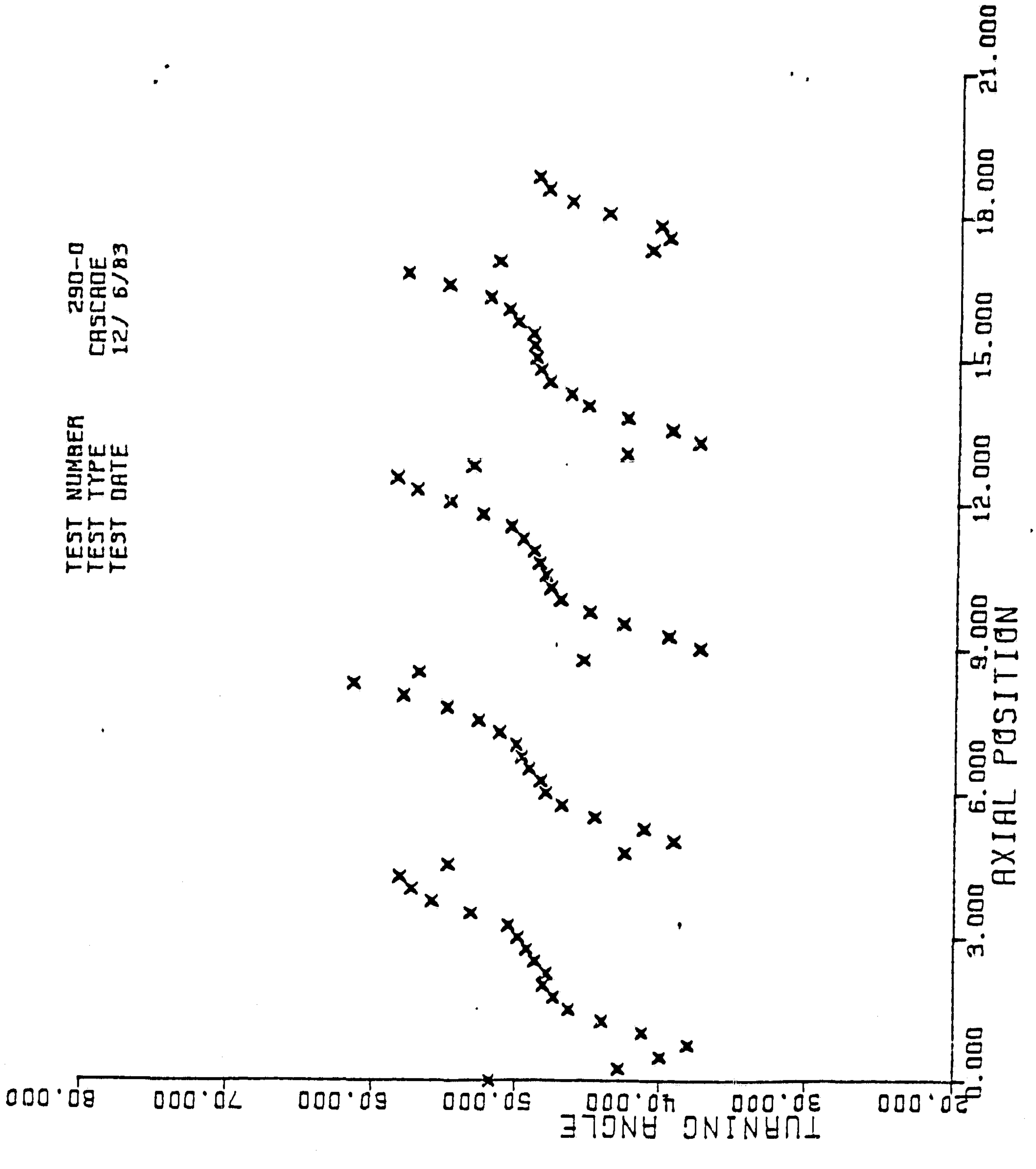

Figure 5.

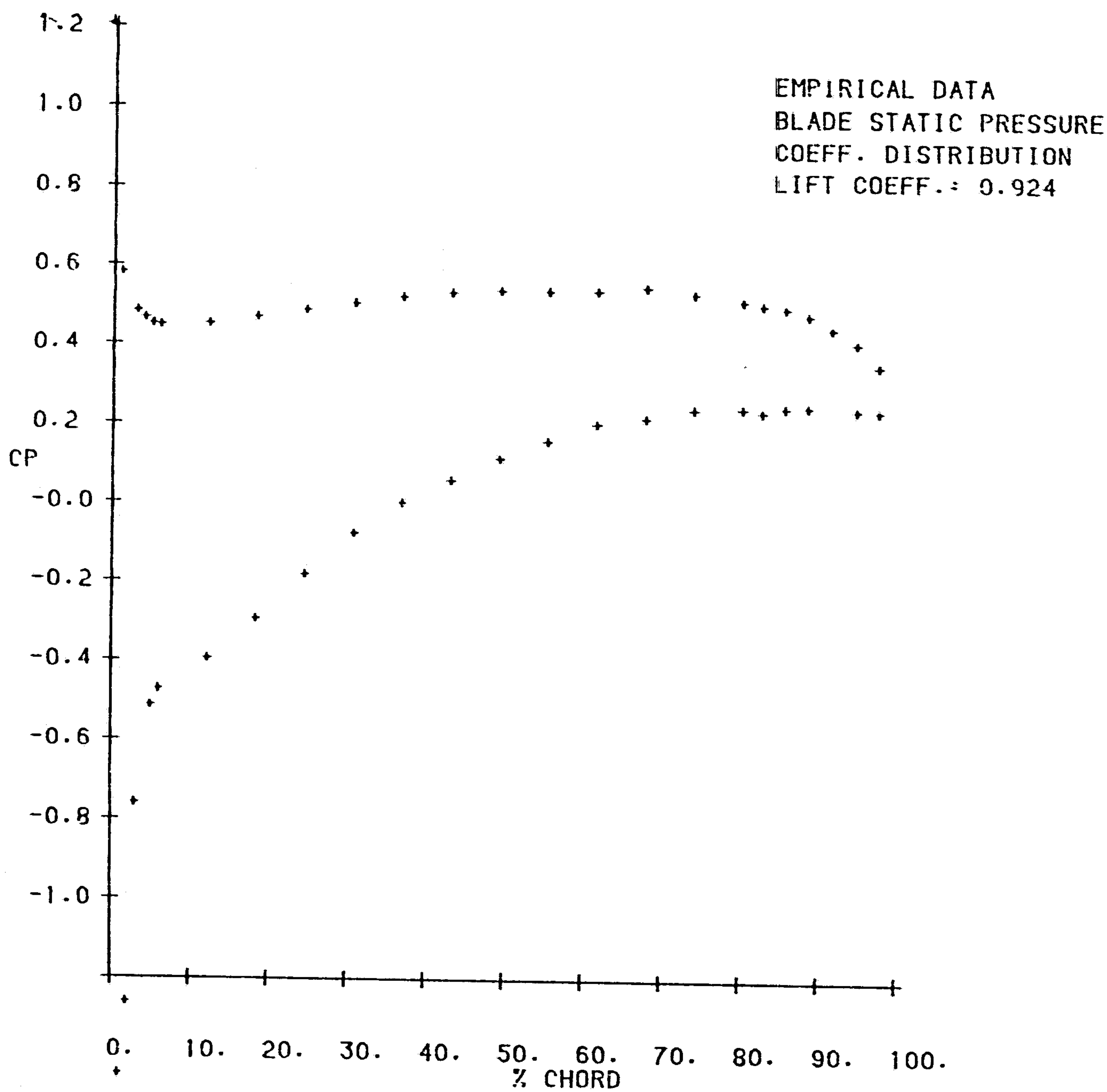
EMPIRICAL DATA
BLADE STATIC PRESSURE
COEFF. DISTRIBUTION
LIFT COEFF.: 0.924
CP
1.2
1.0
0.8
0.6
0.4
0.2
-0.0
-0.2
-0.4
-0.6
-0.8
-1.0
0.
10.
20.
30.
40.
50.
60.
70.
80.
90.
100.
% CHORD

Figure 6.

CASCADE ANGLES

W1 INLET VELOCITY
W2 OUTLET VELOCITY
β_1 INLET FLOW ANGLE
β_2 OUTLET FLOW ANGLE
WX1 INLET AXIAL VELOCITY
WX2 OUTLET AXIAL VELOCITY

TURNING ANGLE $\theta = \beta_1 + \beta_2$

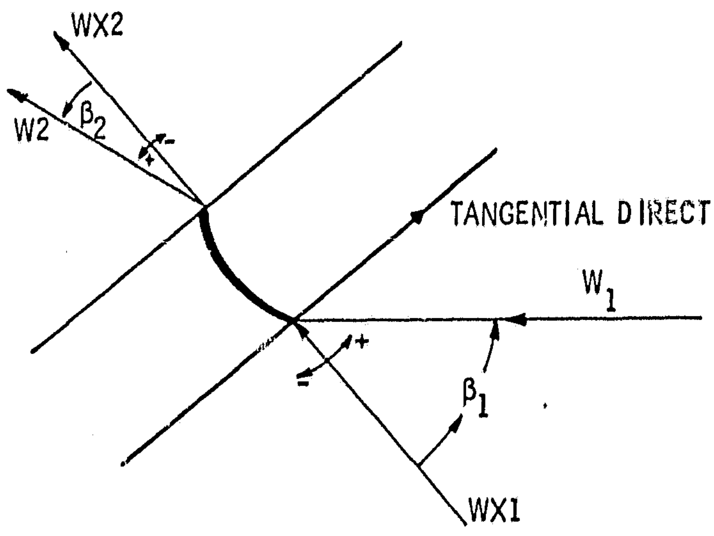

Figure 7.

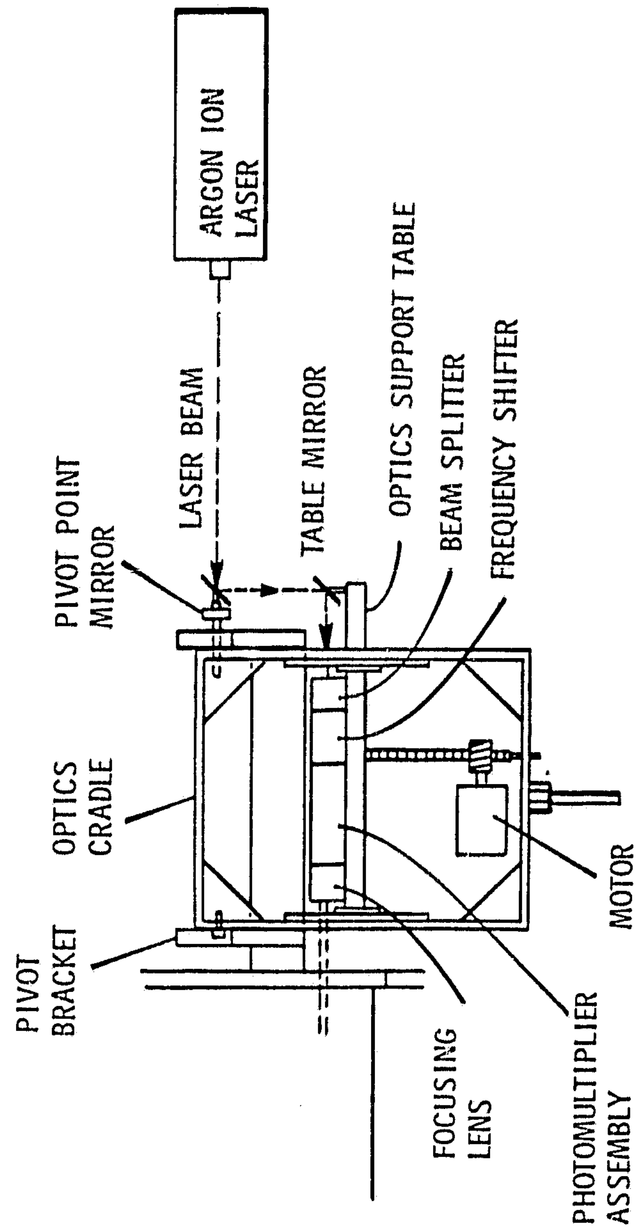
ARGON ION LASER
LASER BEAM
PIVOT POINT MIRROR
TABLE MIRROR
OPTICS SUPPORT TABLE
BEAM SPLITTER
FREQUENCY SHIFTER
OPTICS CRADLE
PIVOT BRACKET
MOTOR
FOCUSING LENS
PHOTOMULTIPLIER ASSEMBLY

Figure 8.

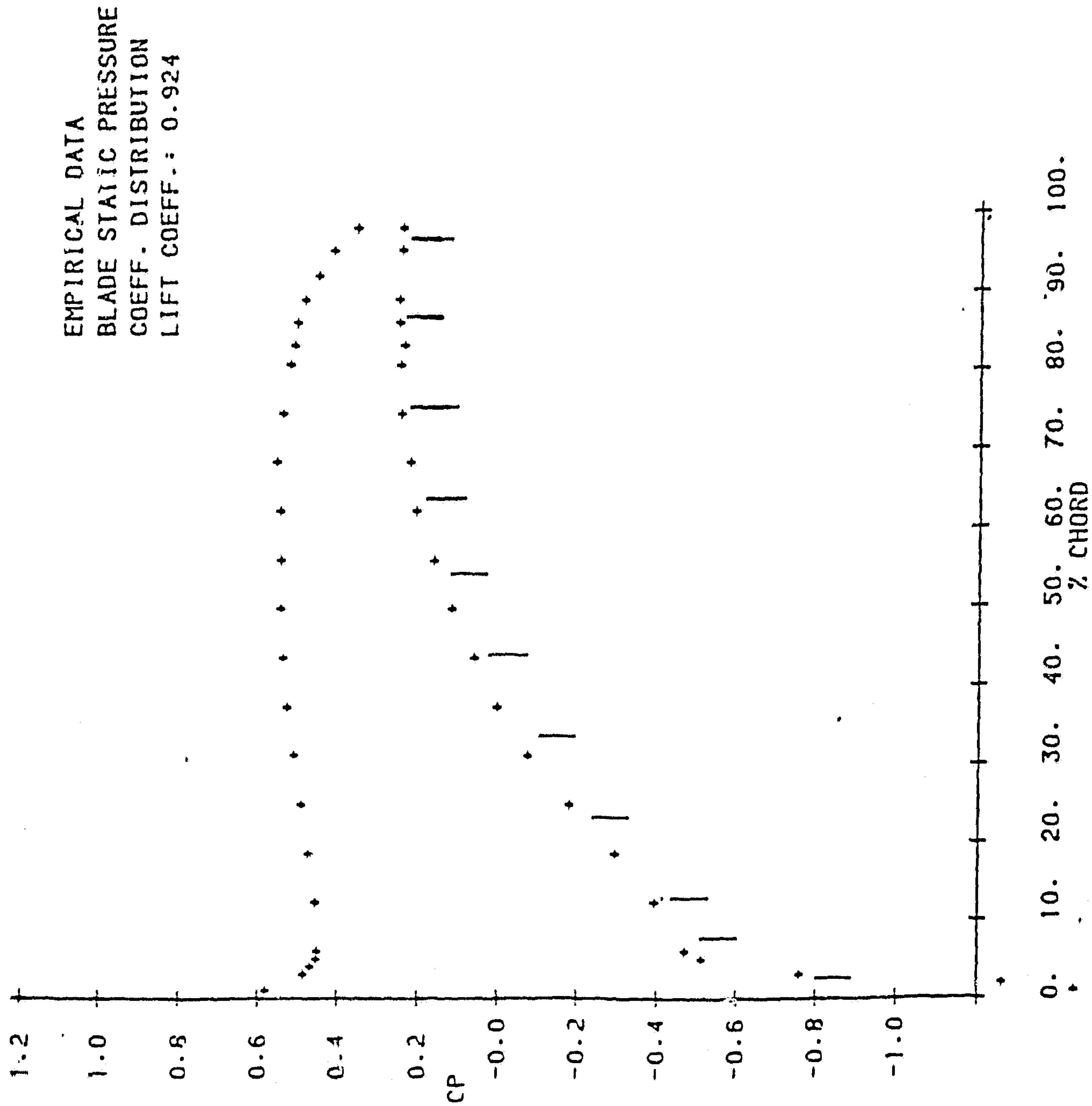
EMPIRICAL DATA
BLADE STATIC PRESSURE
COEFF. DISTRIBUTION
LIFT COEFF.: 0.924
CP
1.2
1.0
0.8
0.6
0.4
0.2
-0.0
-0.2
-0.4
-0.6
-0.8
-1.0
% CHORD
0.
10.
20.
30.
40.
50.
60.
70.
80.
90.
100.

ORIGINAL PAGE IS
OF POOR QUALITY

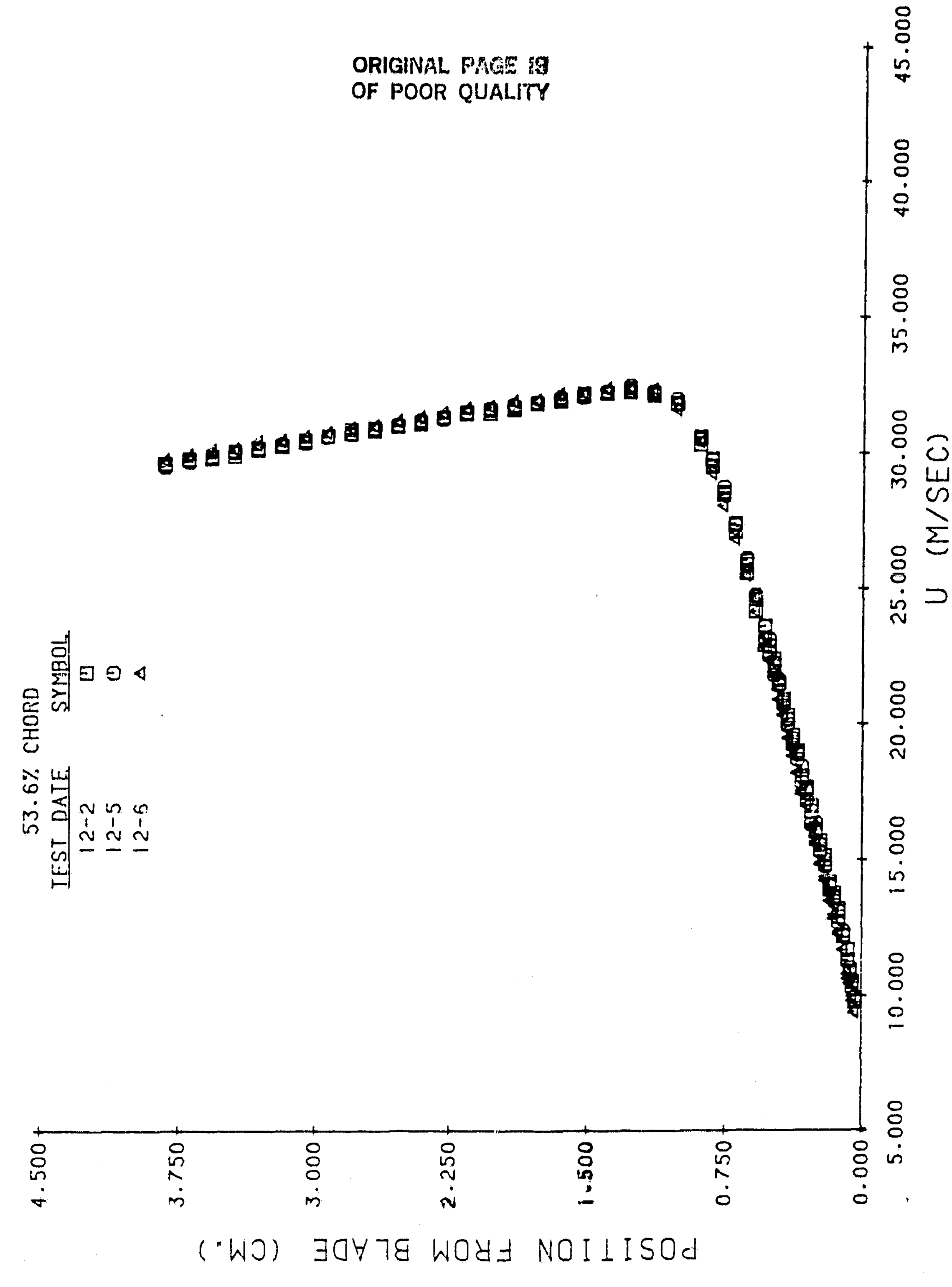

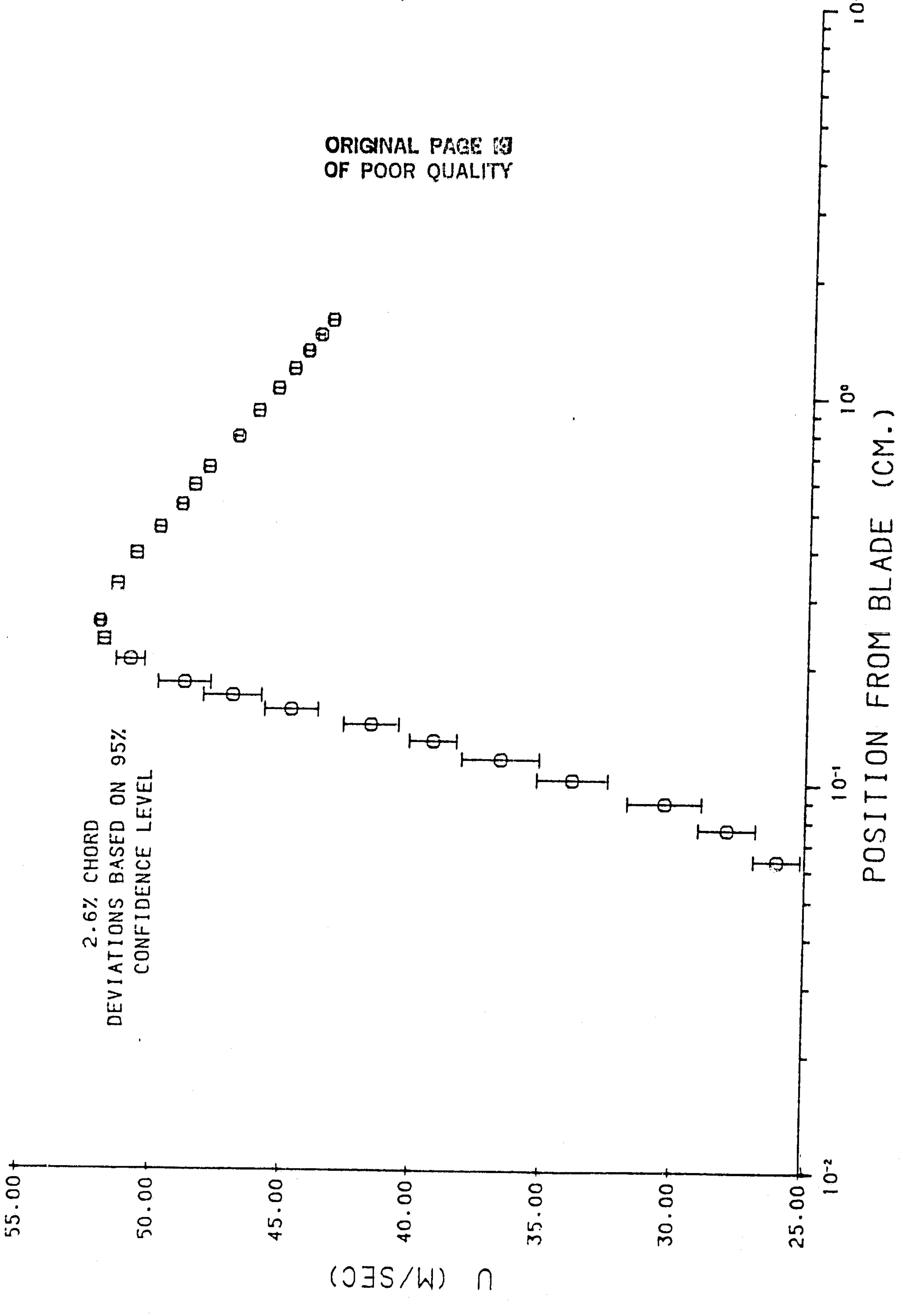
2.6% CHORD
DEVIATIONS BASED ON 95%
CONFIDENCE LEVEL
U (M/SEC)
55.00
50.00
45.00
40.00
35.00
30.00
25.00
POSITION FROM BLADE (CM.)
10^{-2}
10^{-1}
10^{0}
10^{1}

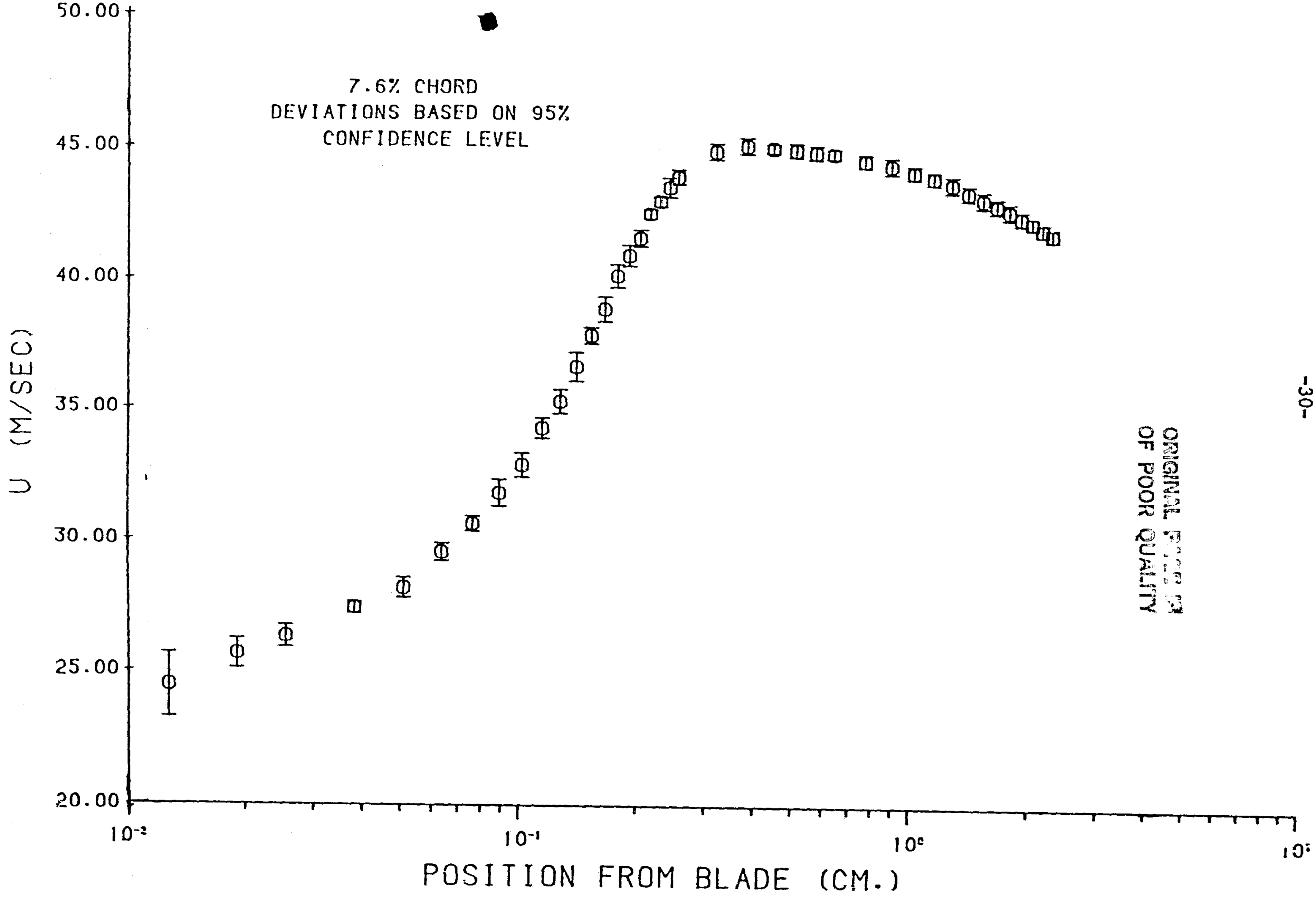
7.6% CHORD
DEVIATIONS BASED ON 95%
CONFIDENCE LEVEL
U (M/SEC)
50.00
45.00
40.00
35.00
30.00
25.00
20.00
10^{-2}
10^{-1}
10^{0}
10^{1}
POSITION FROM BLADE (CM.)

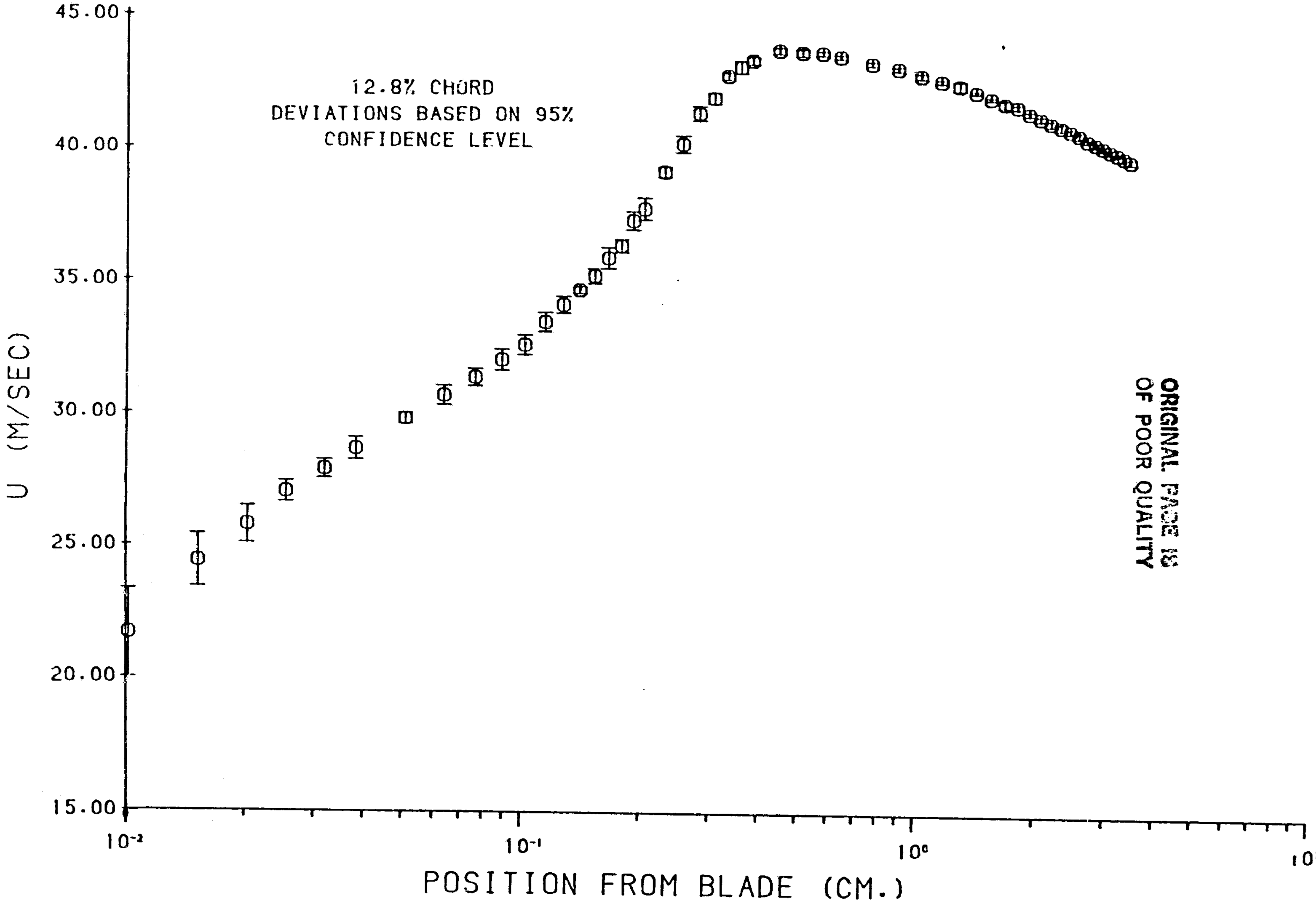
12.8% CHORD
DEVIATIONS BASED ON 95%
CONFIDENCE LEVEL
45.00
40.00
35.00
30.00
25.00
20.00
15.00
U (M/SEC)
10^{-2}
10^{-1}
10^{0}
10^{1}
POSITION FROM BLADE (CM.)

Figure 13.

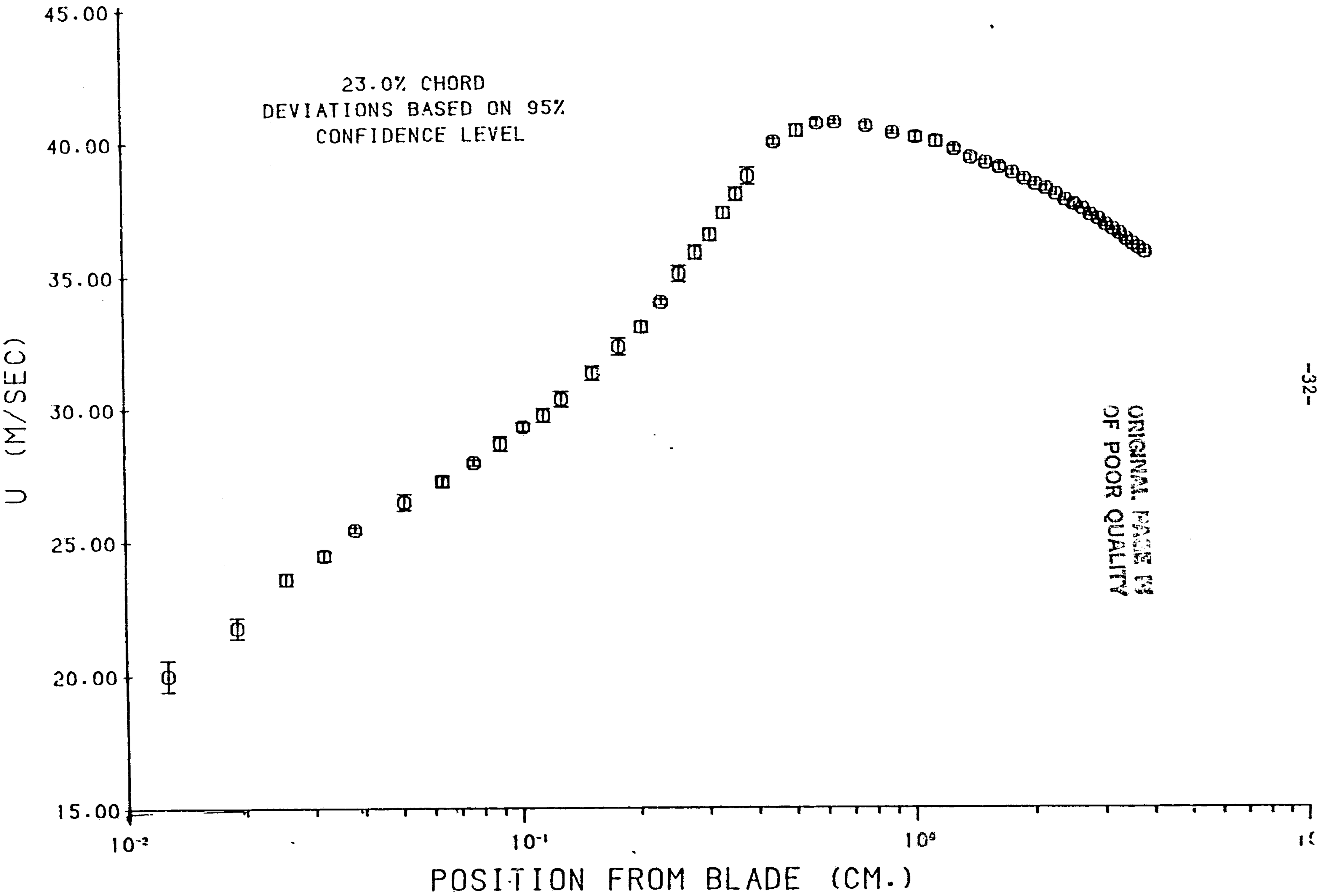
23.0% CHORD
DEVIATIONS BASED ON 95%
CONFIDENCE LEVEL
45.00
40.00
35.00
30.00
25.00
20.00
15.00
U (M/SEC)
10^{-2}
10^{-1}
10^{0}
POSITION FROM BLADE (CM.)

Figure 14.

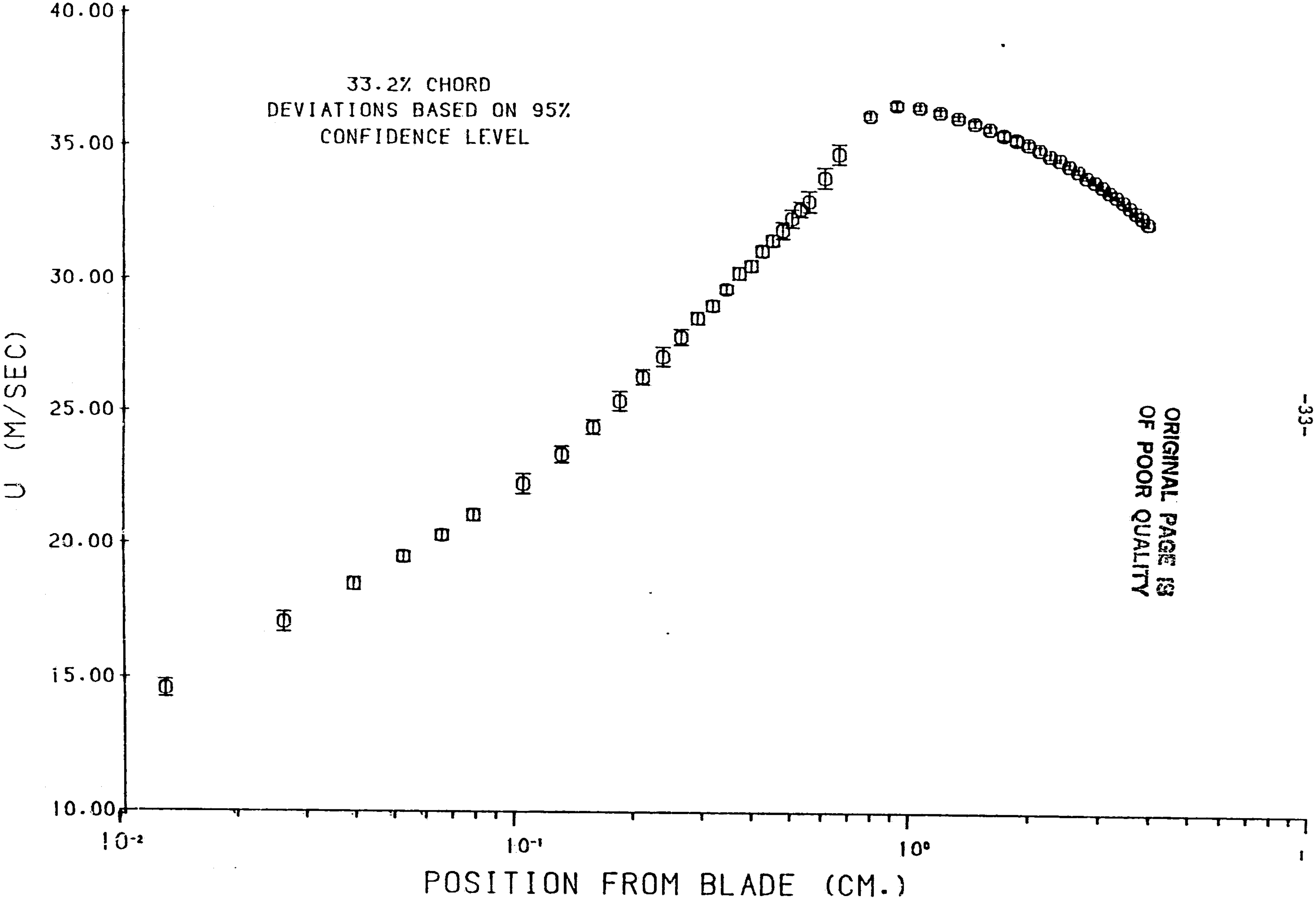
33.2% CHORD
DEVIATIONS BASED ON 95%
CONFIDENCE LEVEL
40.00
35.00
30.00
25.00
20.00
15.00
10.00
U (M/SEC)
10^{-2}
10^{-1}
10^{0}
POSITION FROM BLADE (CM.)

Figure 15

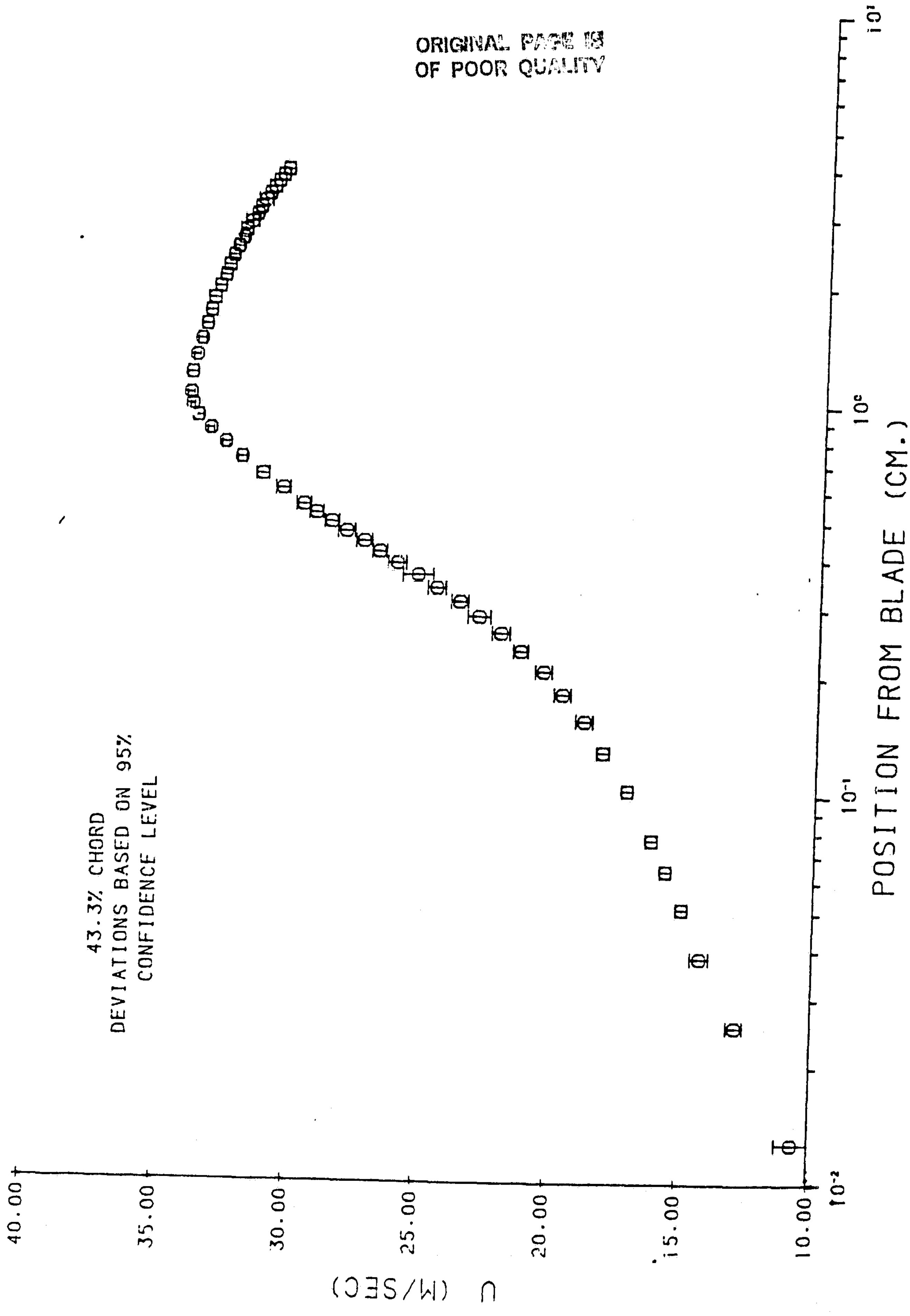
43.3% CHORD
DEVIATIONS BASED ON 95%
CONFIDENCE LEVEL
U (M/SEC)
10.00
15.00
20.00
25.00
30.00
35.00
40.00
10^{-2}
10^{-1}
10^{0}
10^{1}
POSITION FROM BLADE (CM.)

Figure 16.

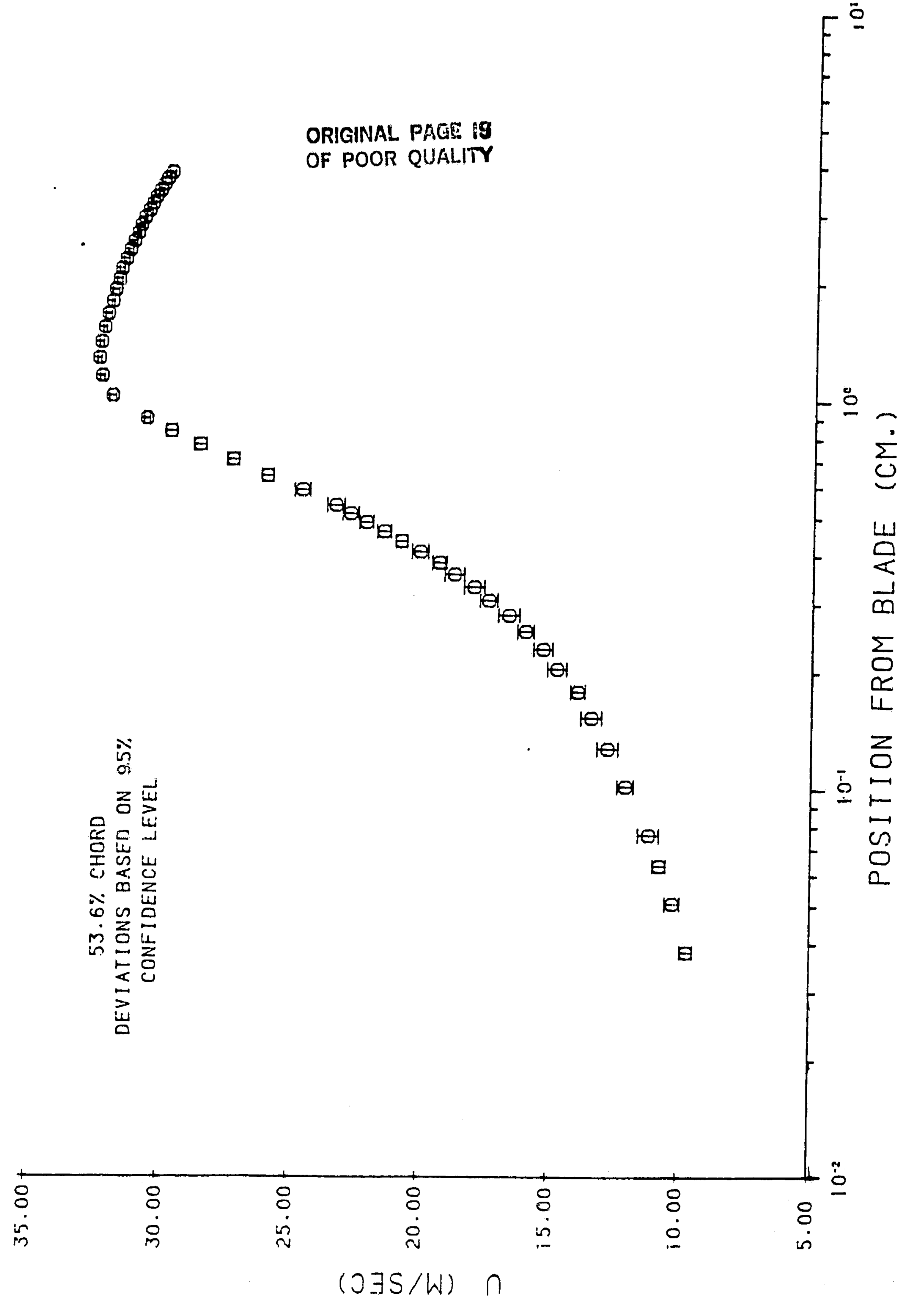
53.6% CHORD
DEVIATIONS BASED ON 95%
CONFIDENCE LEVEL
U (M/SEC)
35.00
30.00
25.00
20.00
15.00
10.00
5.00
POSITION FROM BLADE (CM.)
10^{-2}
10^{-1}
10^{0}
10^{1}

Figure 17.

ORIGINAL PAGE IS
OF POOR QUALITY

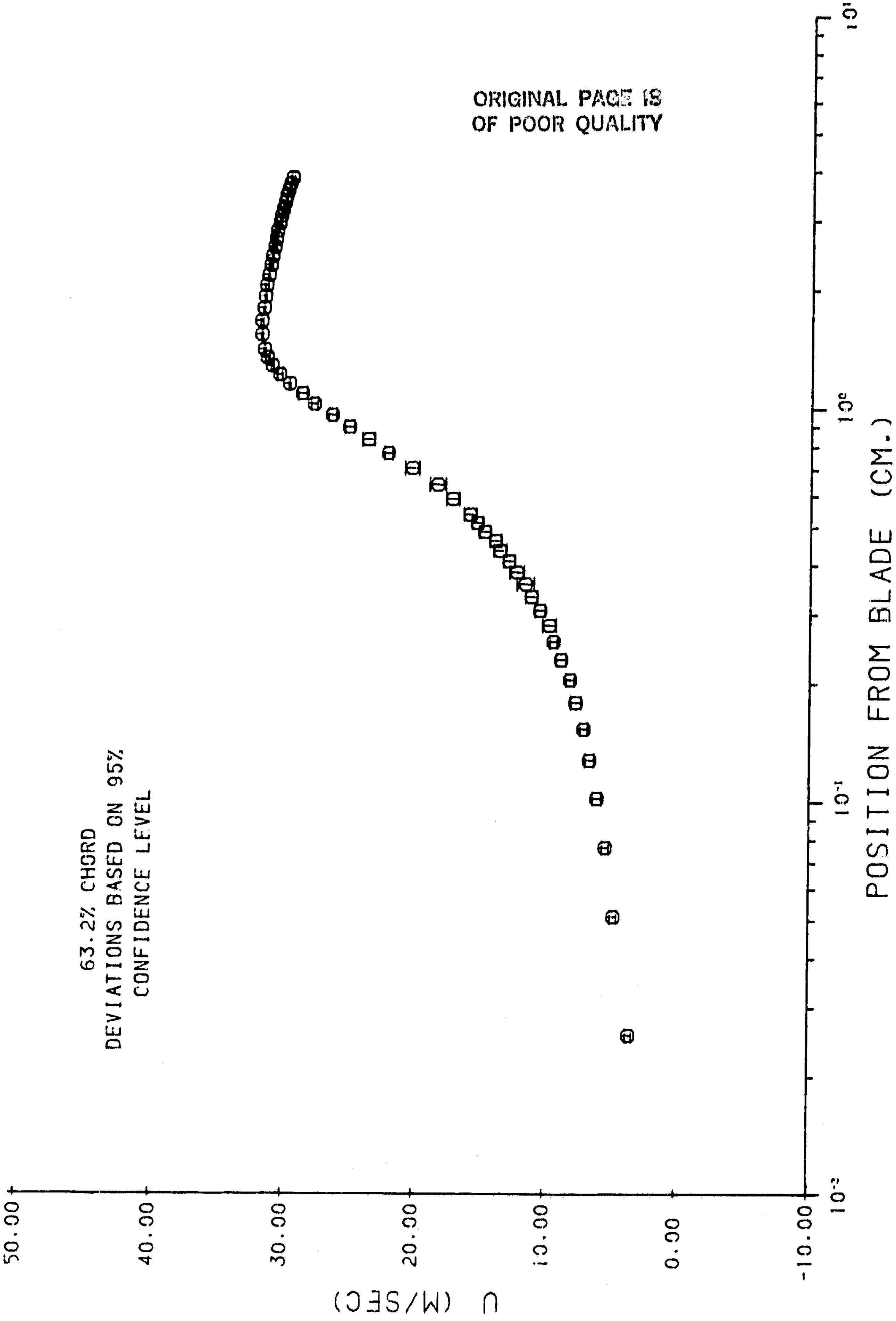

Figure 18.

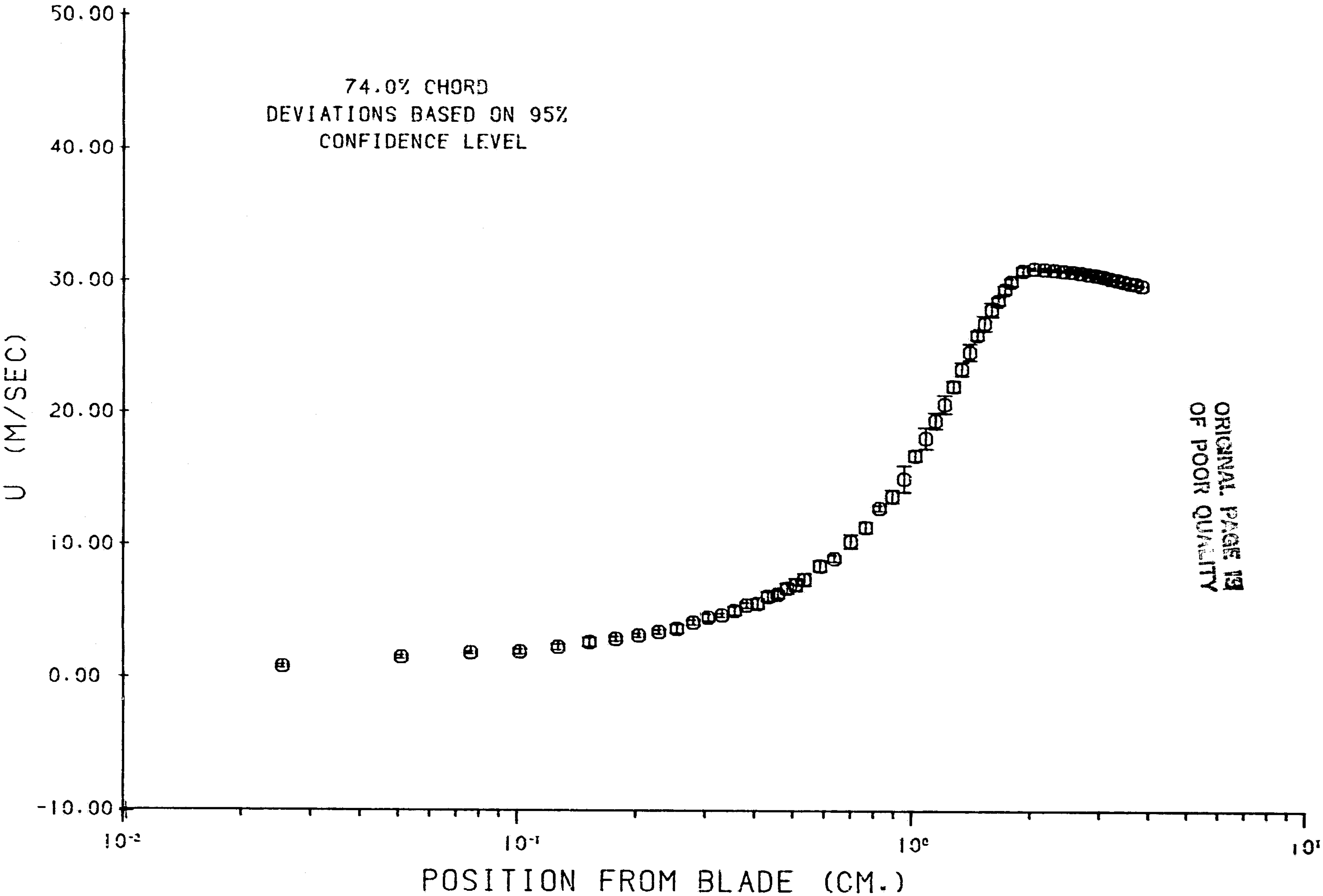

Figure 19.

ORIGINAL PAGE IS
OF POOR QUALITY

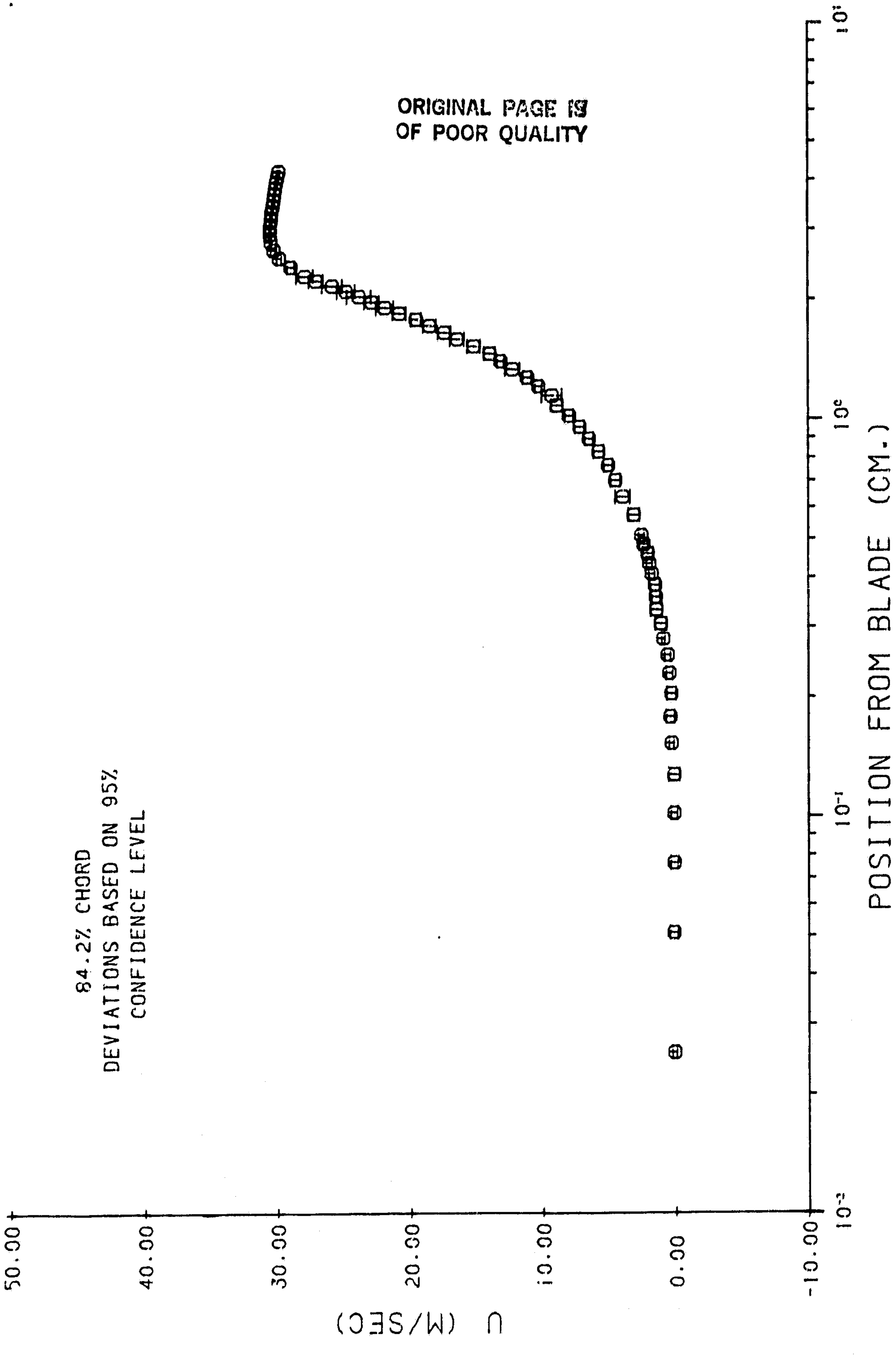
84.2% CHORD
DEVIATIONS BASED ON 95%
CONFIDENCE LEVEL
U (M/SEC)
50.00
40.00
30.00
20.00
10.00
0.00
-10.00
10⁻²
10⁻¹
10⁰
10¹
POSITION FROM BLADE (CM.)

Figure 20.

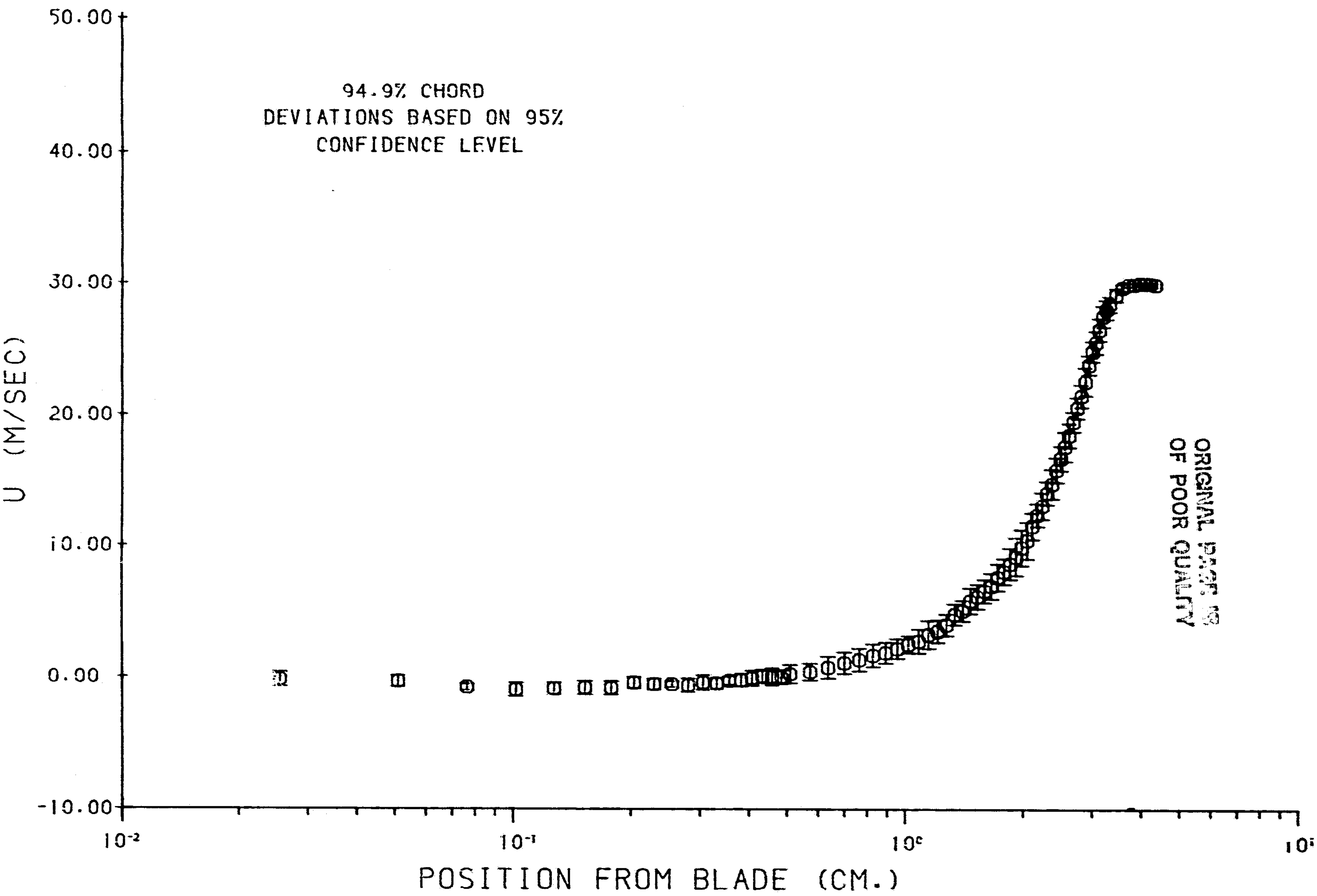
94.9% CHORD
DEVIATIONS BASED ON 95%
CONFIDENCE LEVEL
U (M/SEC)
50.00
40.00
30.00
20.00
10.00
0.00
-10.00
10^{-2}
10^{-1}
10^{0}
10^{1}
POSITION FROM BLADE (CM.)

Figure 21.

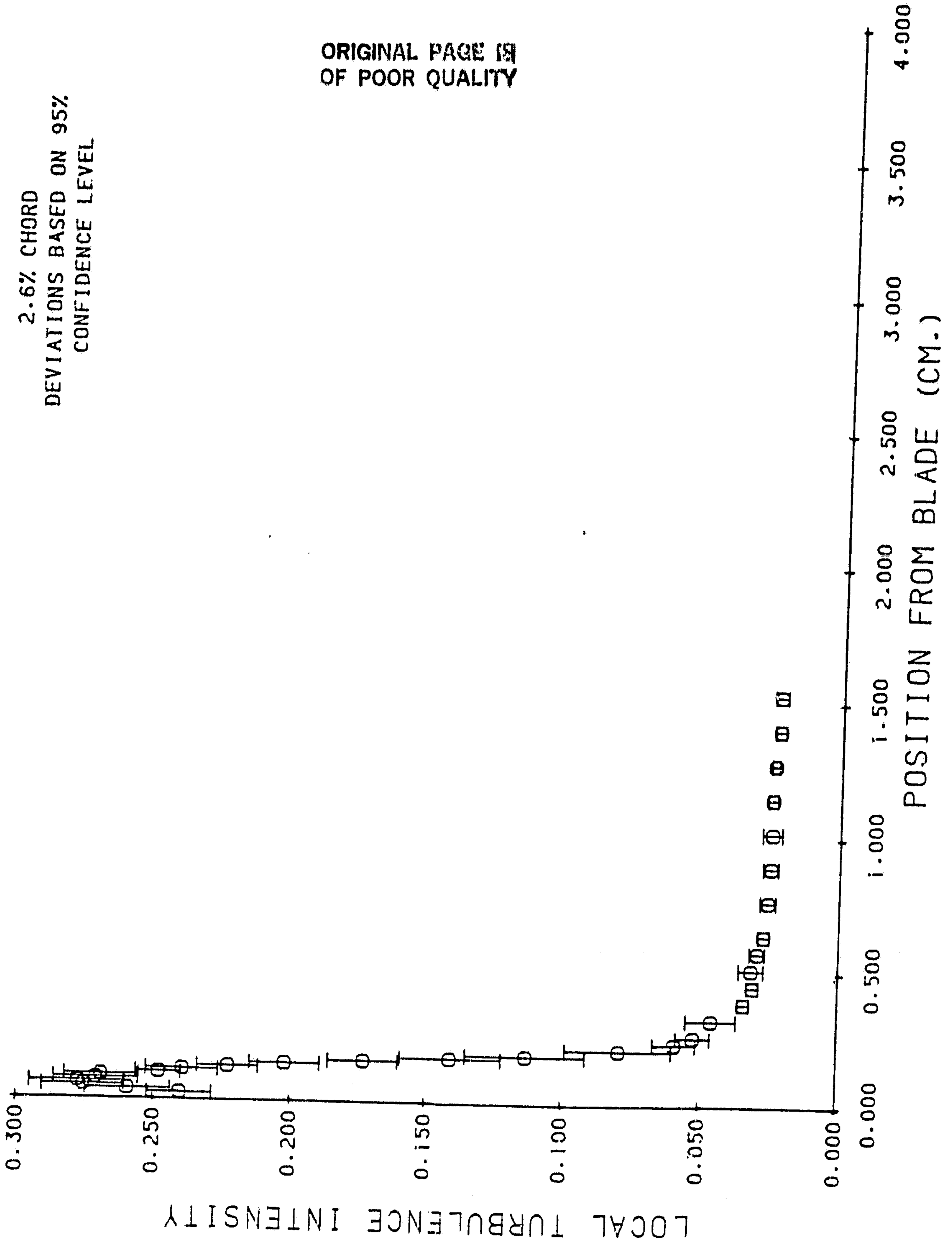
2.6% CHORD
DEVIATIONS BASED ON 95%
CONFIDENCE LEVEL
LOCAL TURBULENCE INTENSITY
0.000
0.050
0.100
0.150
0.200
0.250
0.300
POSITION FROM BLADE (CM.)
0.000
0.500
1.000
1.500
2.000
2.500
3.000
3.500
4.000

ORIGINAL PAGE IS
OF POOR QUALITY

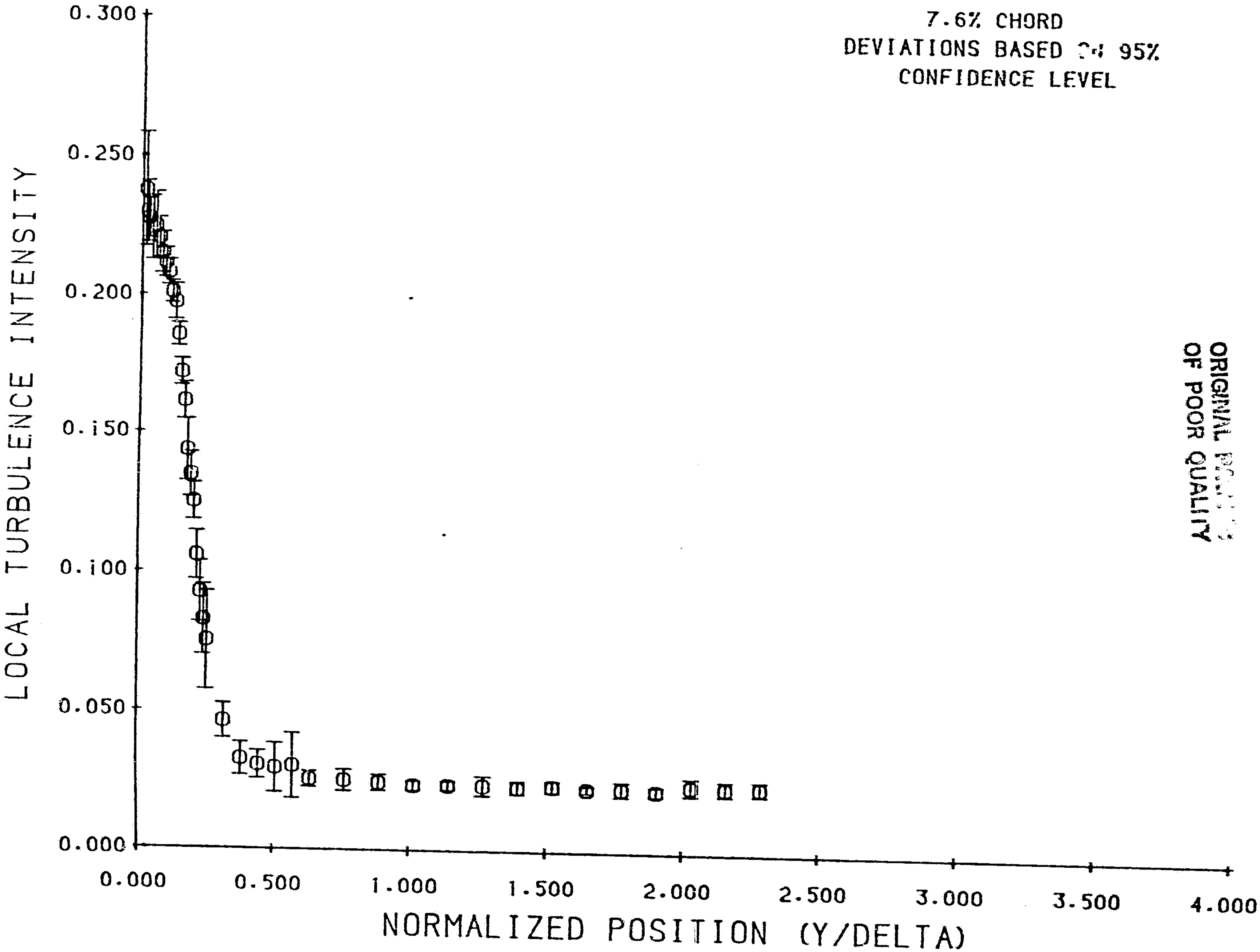

Figure 23

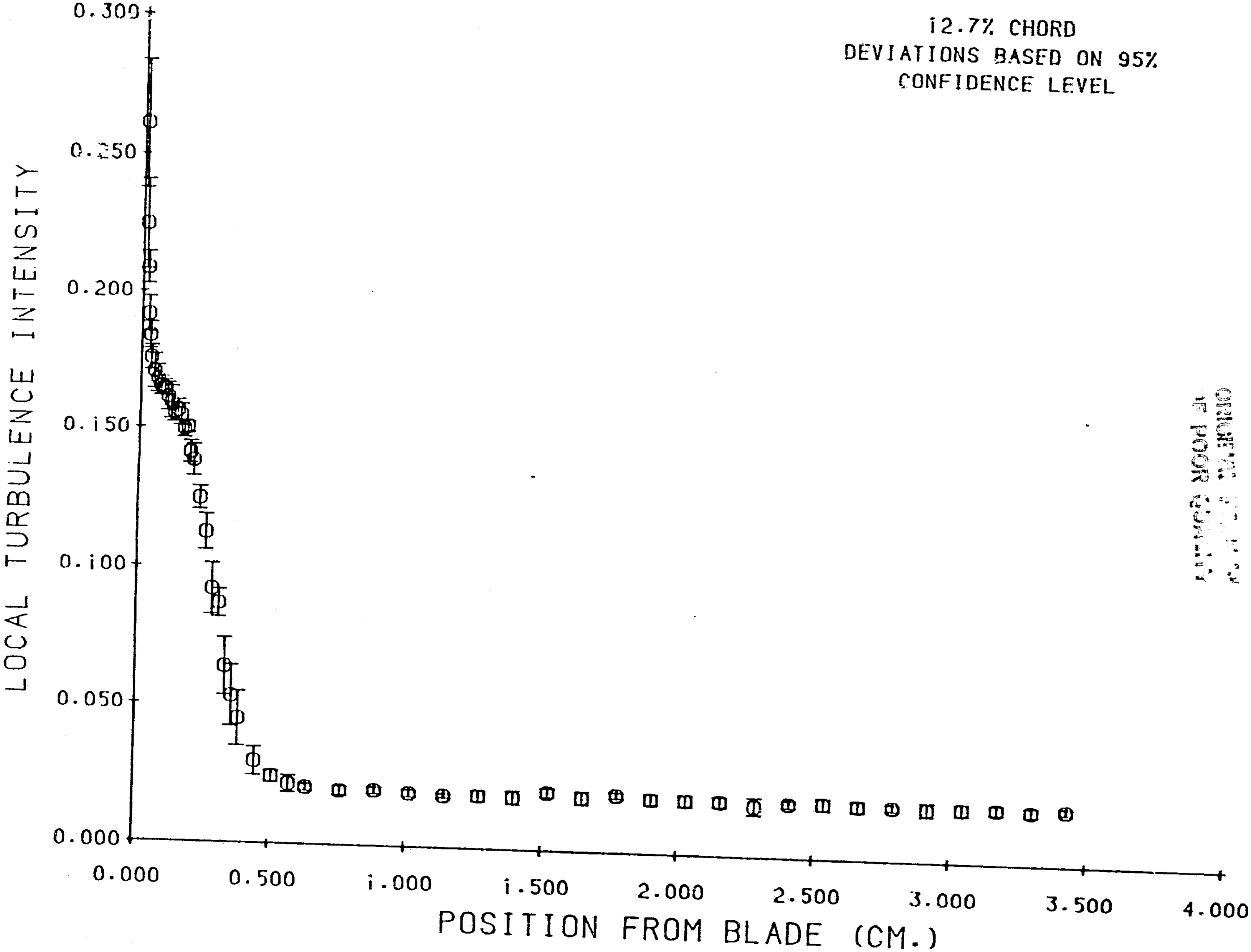
12.7% CHORD
DEVIATIONS BASED ON 95%
CONFIDENCE LEVEL
LOCAL TURBULENCE INTENSITY
0.000
0.050
0.100
0.150
0.200
0.250
0.300
0.000
0.500
1.000
1.500
2.000
2.500
3.000
3.500
4.000
POSITION FROM BLADE (CM.)

Figure 24.

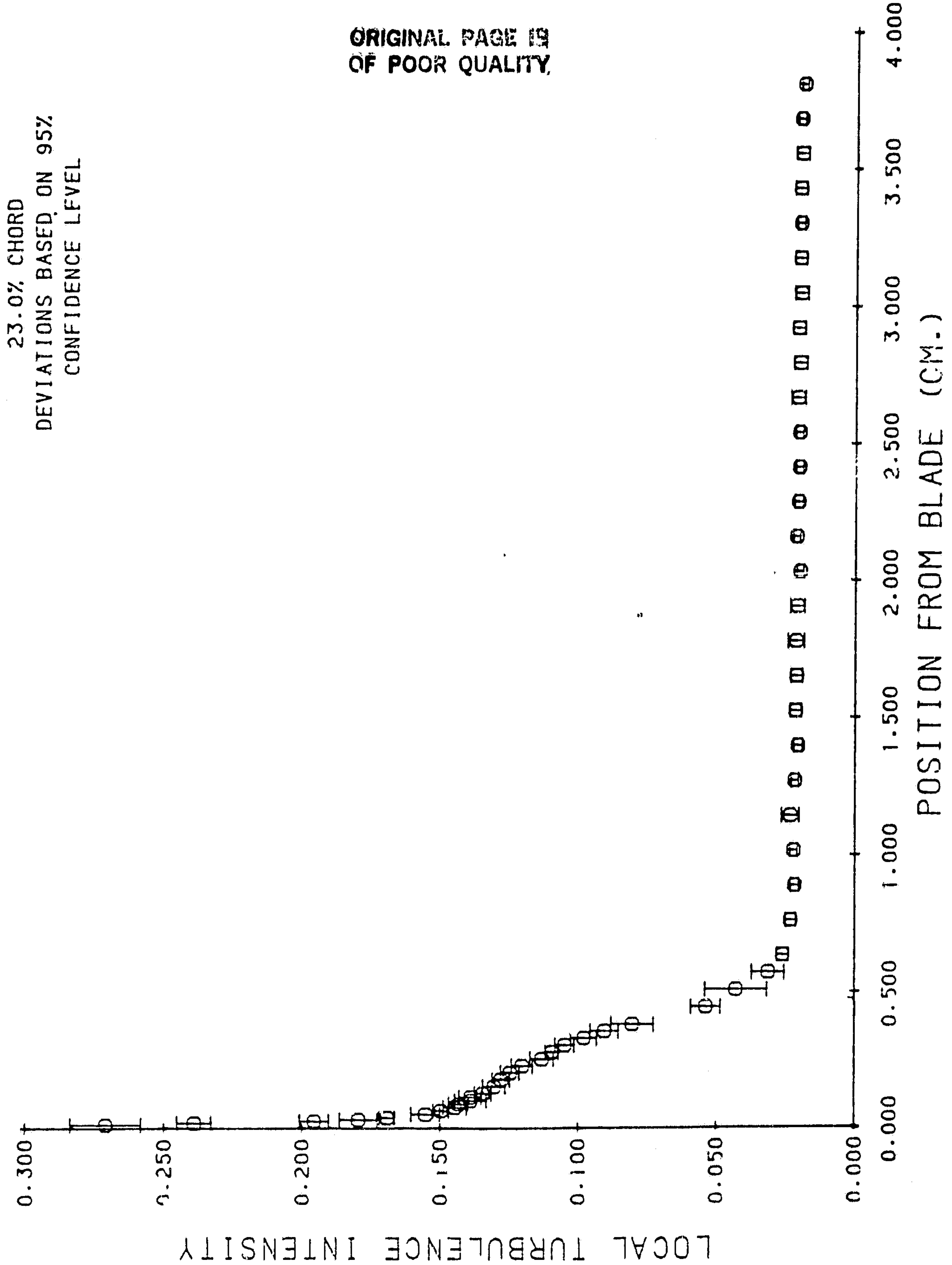
23.0% CHORD
DEVIATIONS BASED ON 95%
CONFIDENCE LEVEL
LOCAL TURBULENCE INTENSITY
0.000
0.050
0.100
0.150
0.200
0.250
0.300
POSITION FROM BLADE (CM.)
0.000
0.500
1.000
1.500
2.000
2.500
3.000
3.500
4.000

Figure 25.

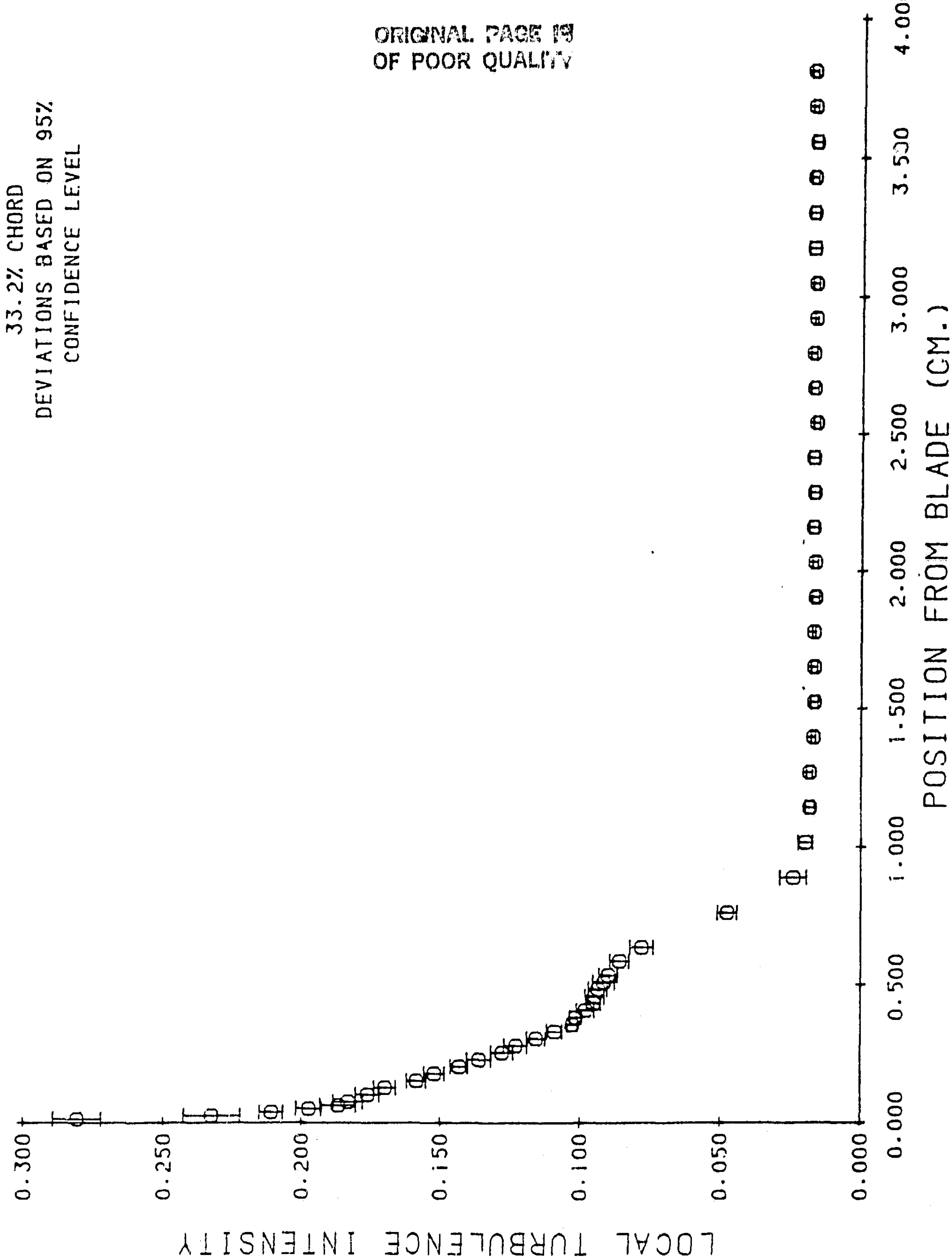
33.2% CHORD
DEVIATIONS BASED ON 95%
CONFIDENCE LEVEL
LOCAL TURBULENCE INTENSITY
0.000
0.050
0.100
0.150
0.200
0.250
0.300
POSITION FROM BLADE (CM.)
0.000
0.500
1.000
1.500
2.000
2.500
3.000
3.500
4.000

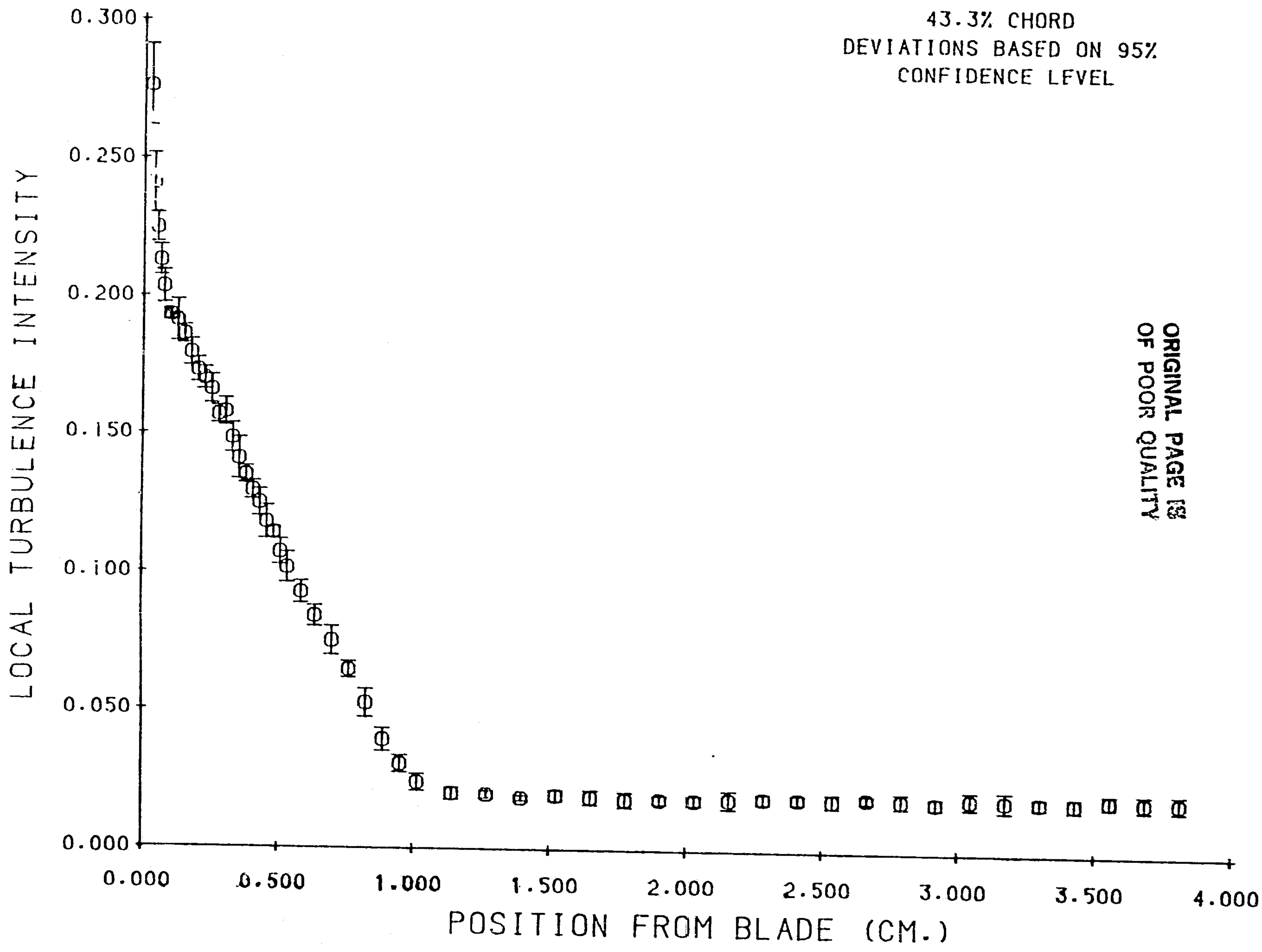
43.3% CHORD
DEVIATIONS BASED ON 95%
CONFIDENCE LEVEL
ORIGINAL PAGE IS
OF POOR QUALITY
LOCAL TURBULENCE INTENSITY
0.300
0.250
0.200
0.150
0.100
0.050
0.000
0.000
0.500
1.000
1.500
2.000
2.500
3.000
3.500
4.000
POSITION FROM BLADE (CM.)

Figure 27.

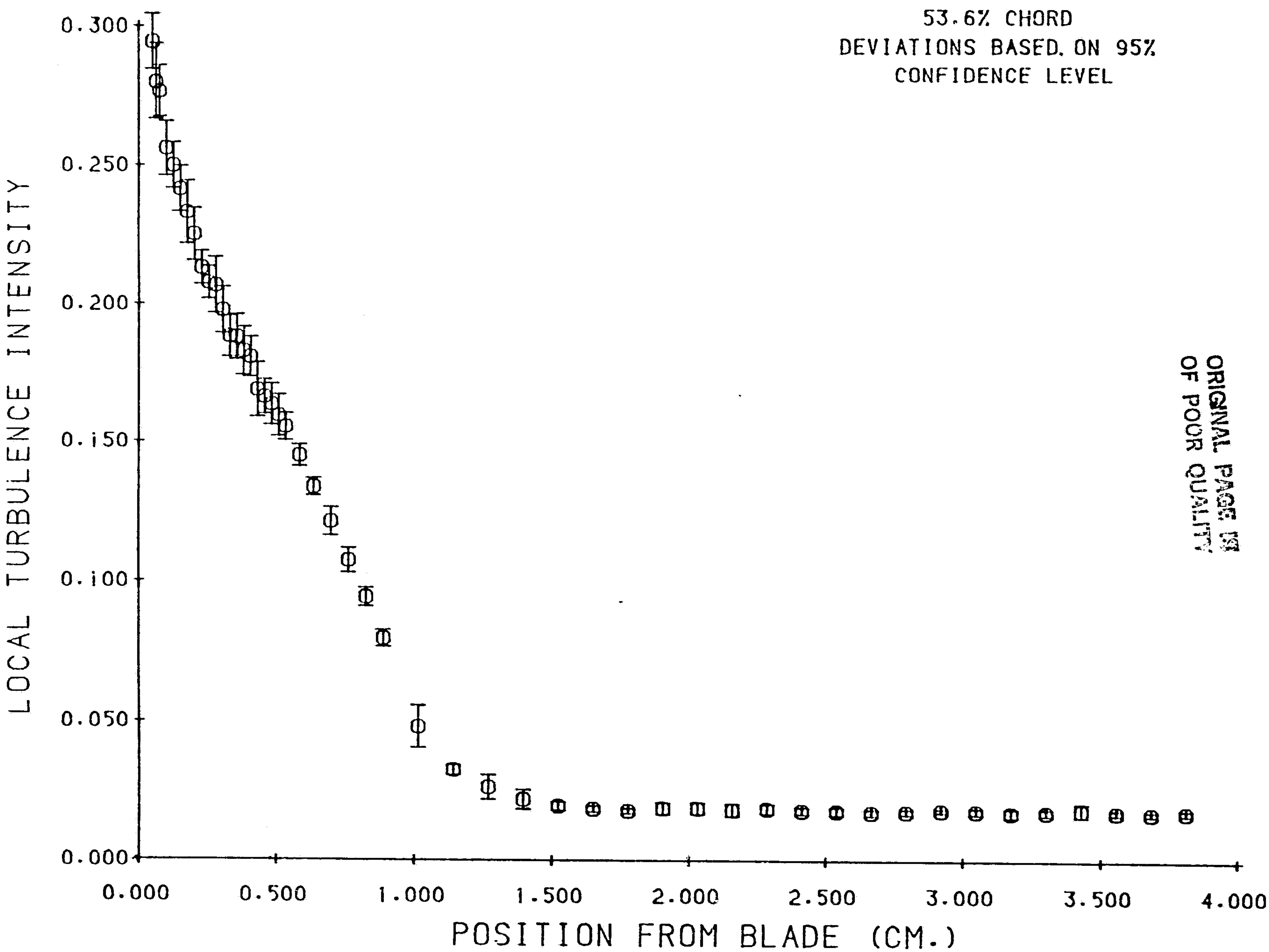

53.6% CHORD
DEVIATIONS BASED ON 95%
CONFIDENCE LEVEL
LOCAL TURBULENCE INTENSITY
0.300
0.250
0.200
0.150
0.100
0.050
0.000
0.000
0.500
1.000
1.500
2.000
2.500
3.000
3.500
4.000
POSITION FROM BLADE (CM.)

Figure 28.

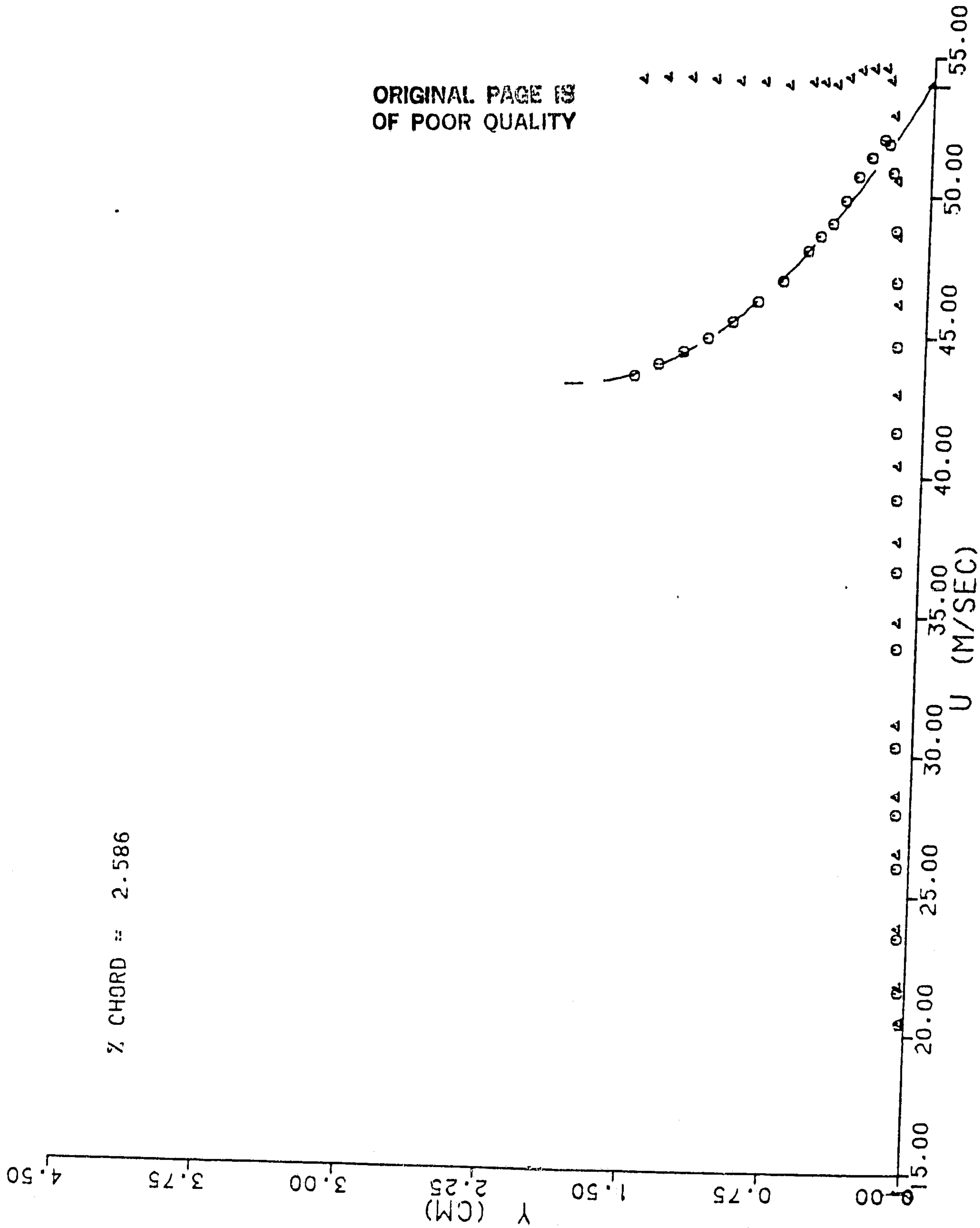
% CHORD = 2.586
U (M/SEC)
15.00
20.00
25.00
30.00
35.00
40.00
45.00
50.00
55.00
Y (CM)
0.00
0.75
1.50
2.25
3.00
3.75
4.50

Figure 29.

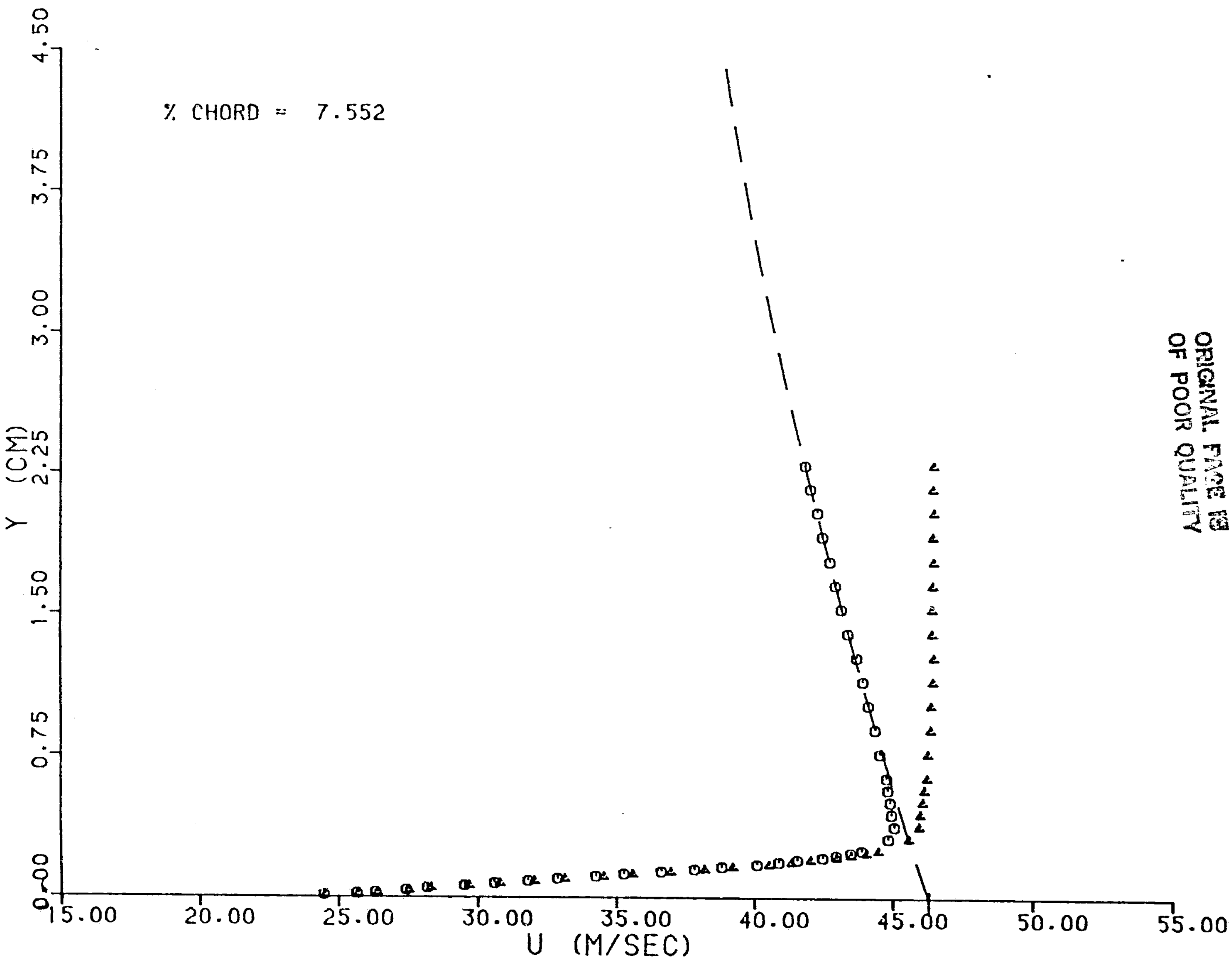
% CHORD = 7.552
Y (CM)
0.00
0.75
1.50
2.25
3.00
3.75
4.50
U (M/SEC)
15.00
20.00
25.00
30.00
35.00
40.00
45.00
50.00
55.00

Figure 30.

ORIGINAL PAGE IS
OF POOR QUALITY

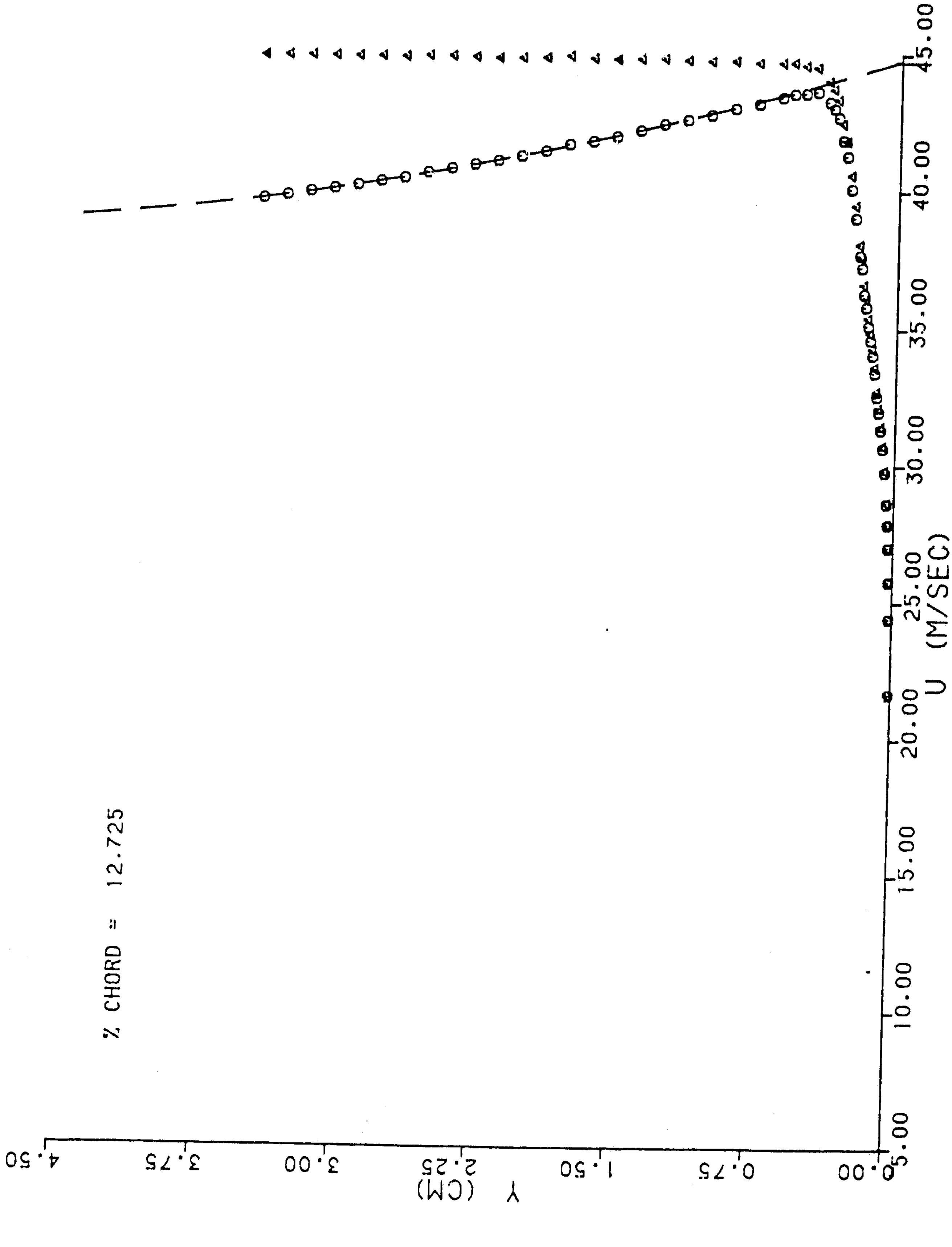

Figure 31.

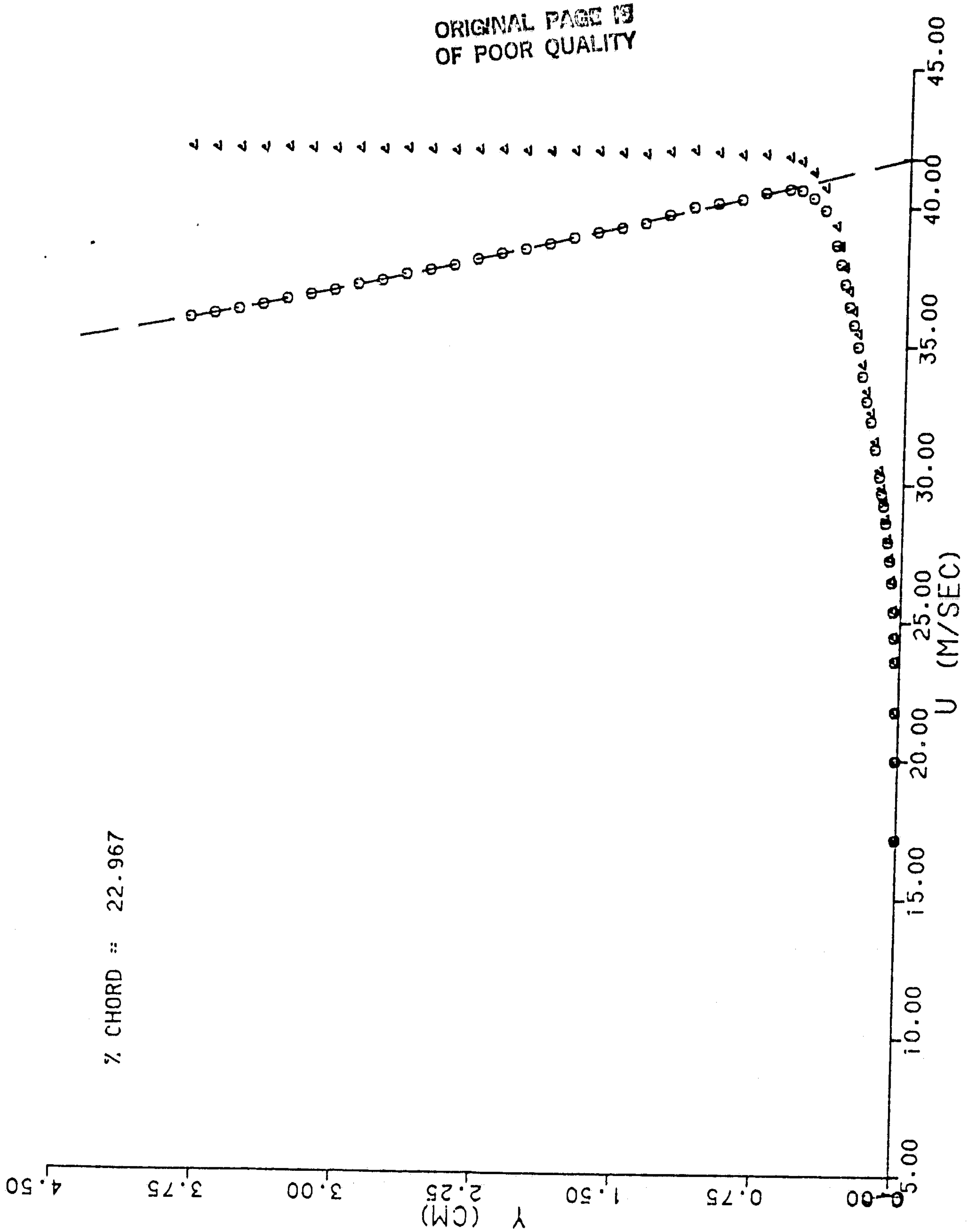
% CHORD = 22.967
U (M/SEC)
5.00
10.00
15.00
20.00
25.00
30.00
35.00
40.00
45.00
Y (CM)
0.00
0.75
1.50
2.25
3.00
3.75
4.50

Figure 32.

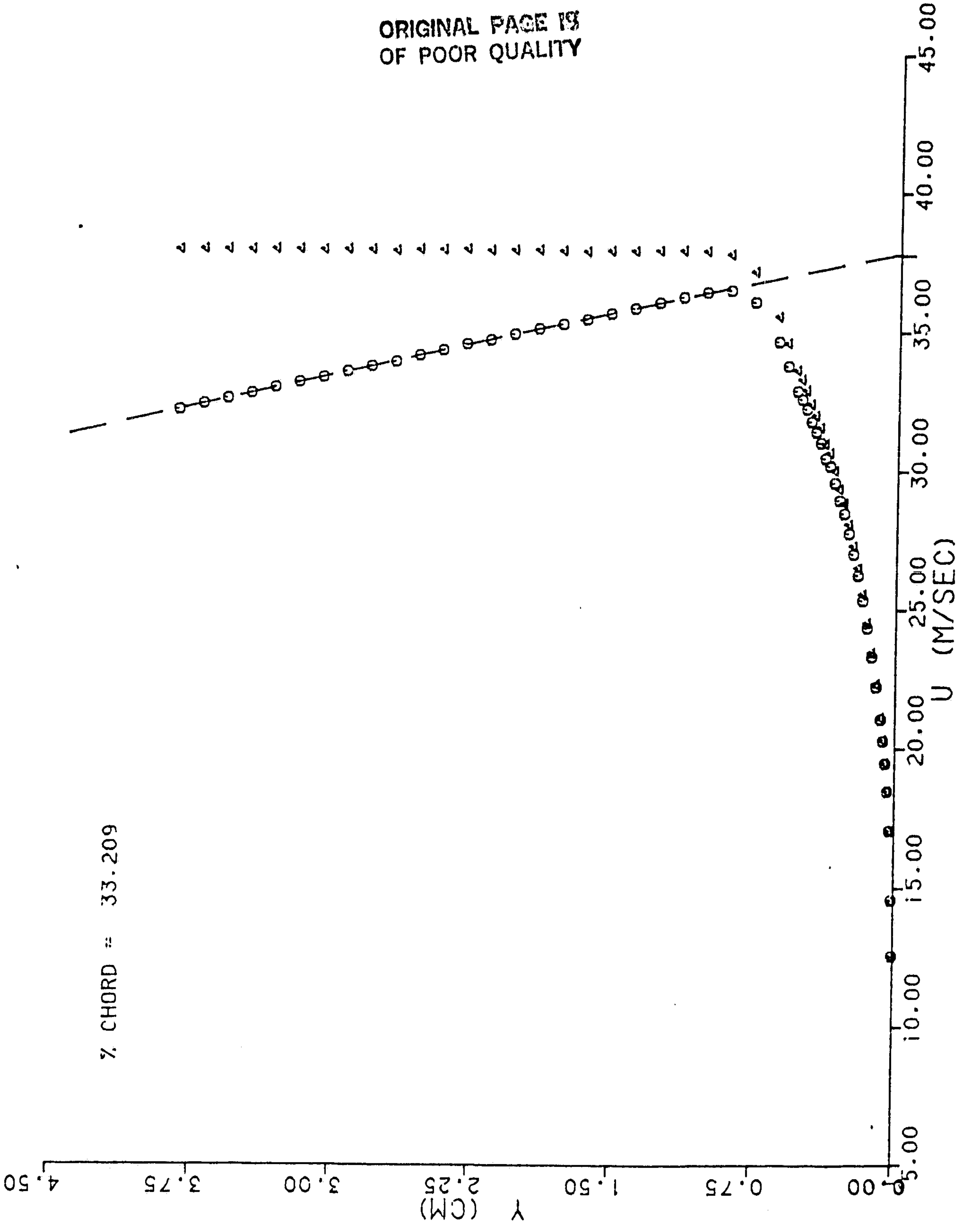
% CHORD = 33.209
U (M/SEC)
Y (CM)
5.00
10.00
15.00
20.00
25.00
30.00
35.00
40.00
45.00
0.00
0.75
1.50
2.25
3.00
3.75
4.50

Figure 33.

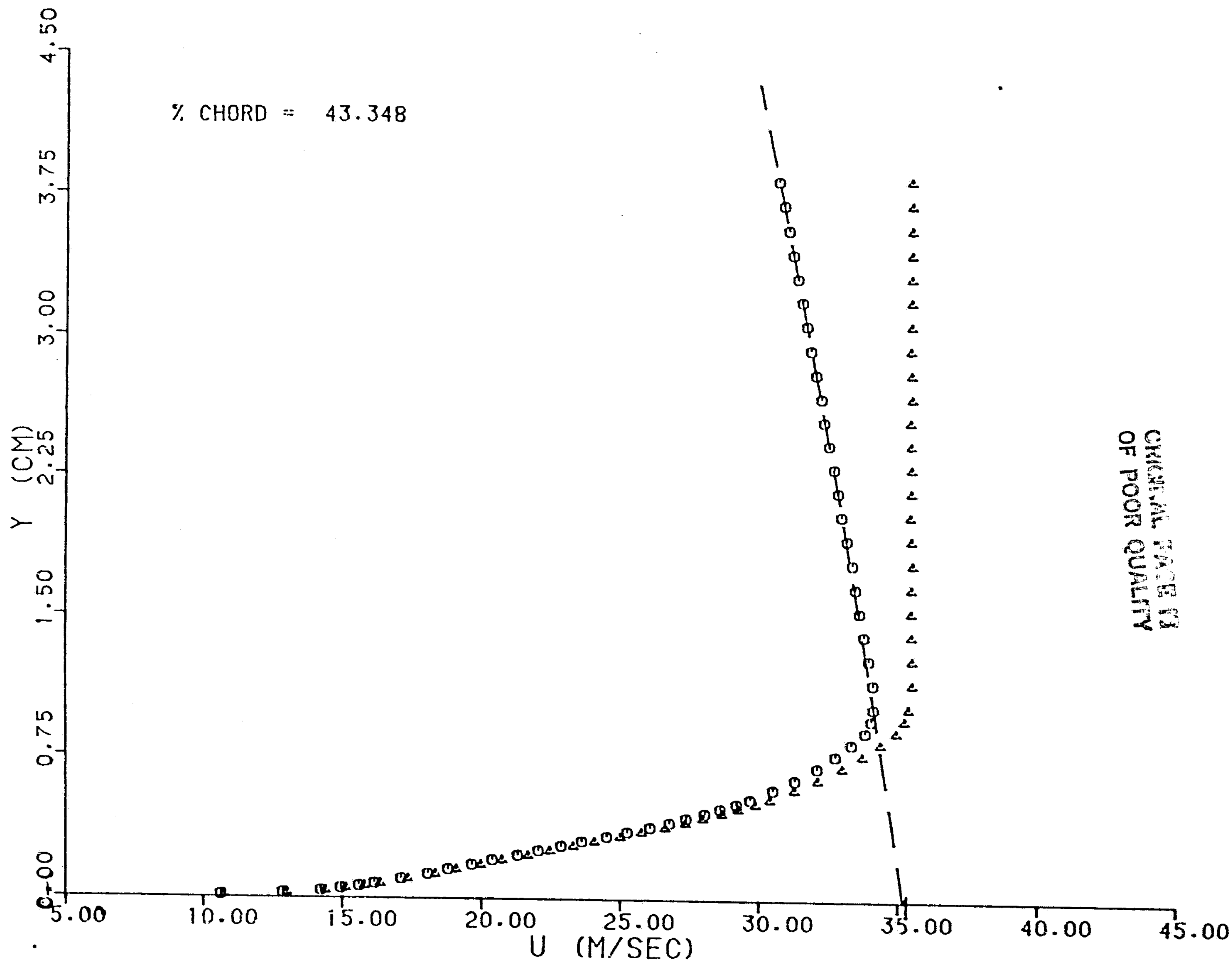
% CHORD = 43.348
Y (CM)
4.50
3.75
3.00
2.25
1.50
0.75
0.00
5.00
10.00
15.00
20.00
25.00
30.00
35.00
40.00
45.00
U (M/SEC)

Figure 34.

ORIGINAL PAGE IS
OF POOR QUALITY

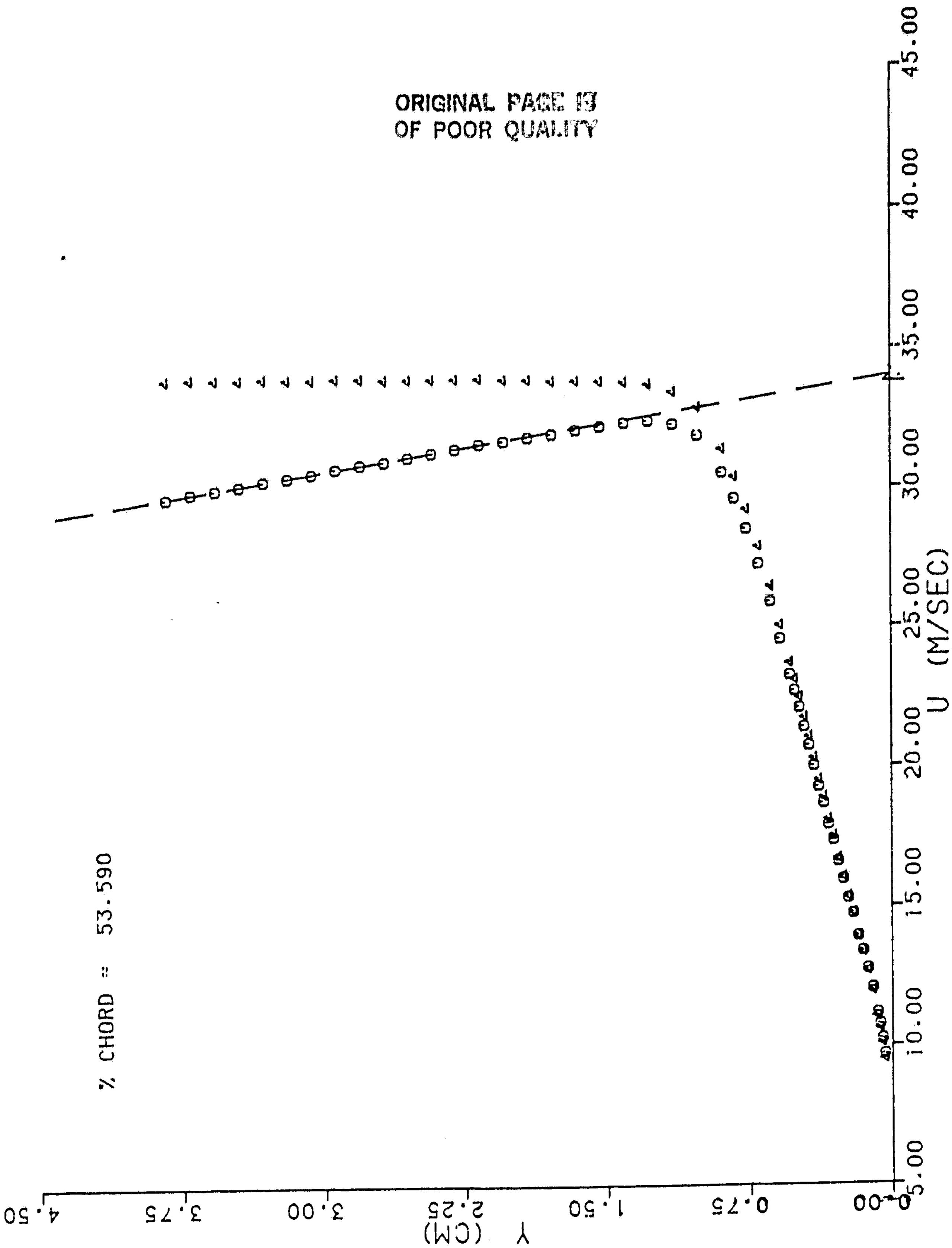

Figure 35.

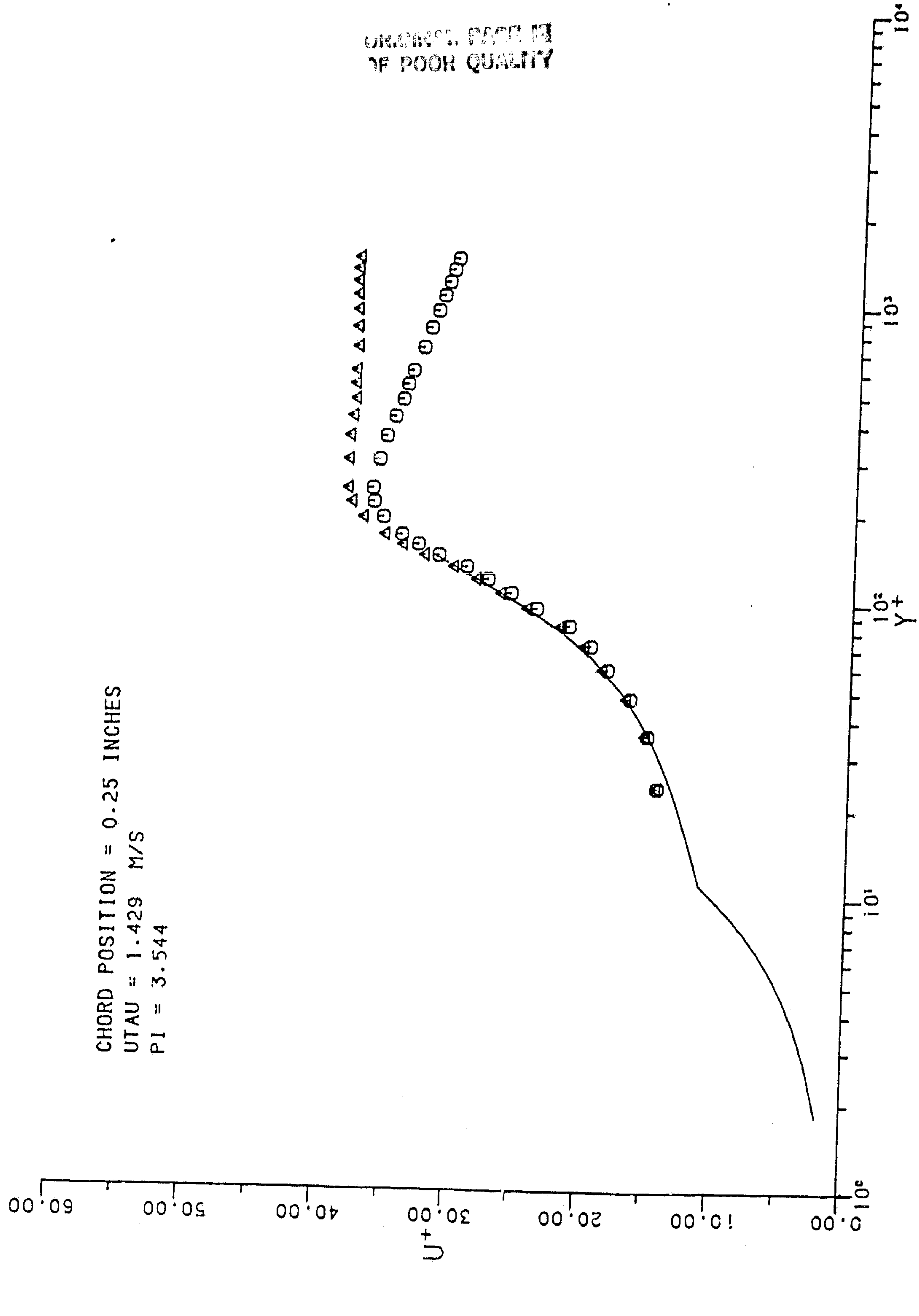
CHORD POSITION = 0.25 INCHES
UTAU = 1.429 M/S
PI = 3.544
U+
Y+
0.00
10.00
20.00
30.00
40.00
50.00
60.00
10⁰
10¹
10²
10³
10⁴

Figure 36.

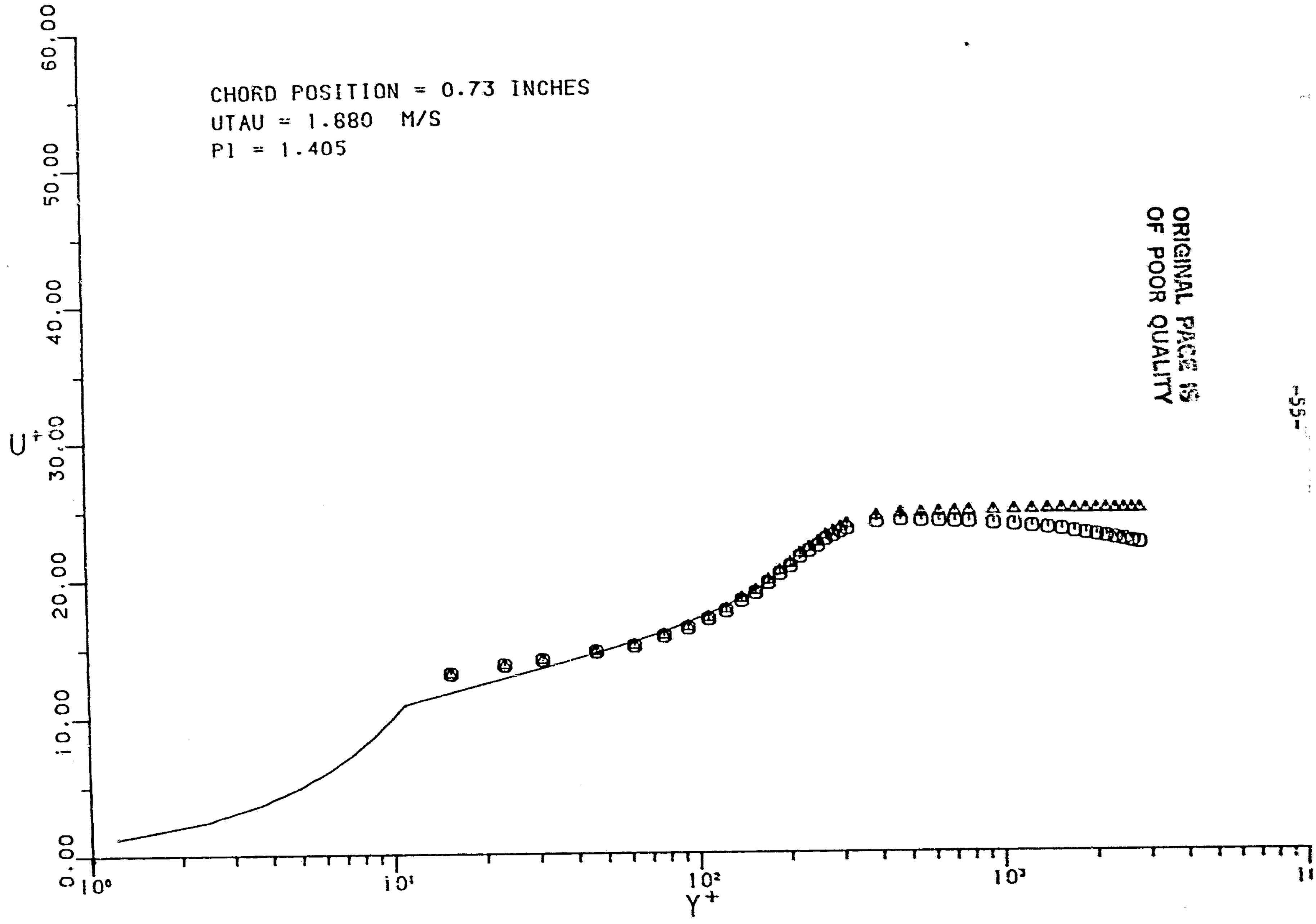
CHORD POSITION = 0.73 INCHES
UTAU = 1.880 M/S
PI = 1.405
U+
0.00
10.00
20.00
30.00
40.00
50.00
60.00
Y+
10⁰
10¹
10²
10³

Figure 37.

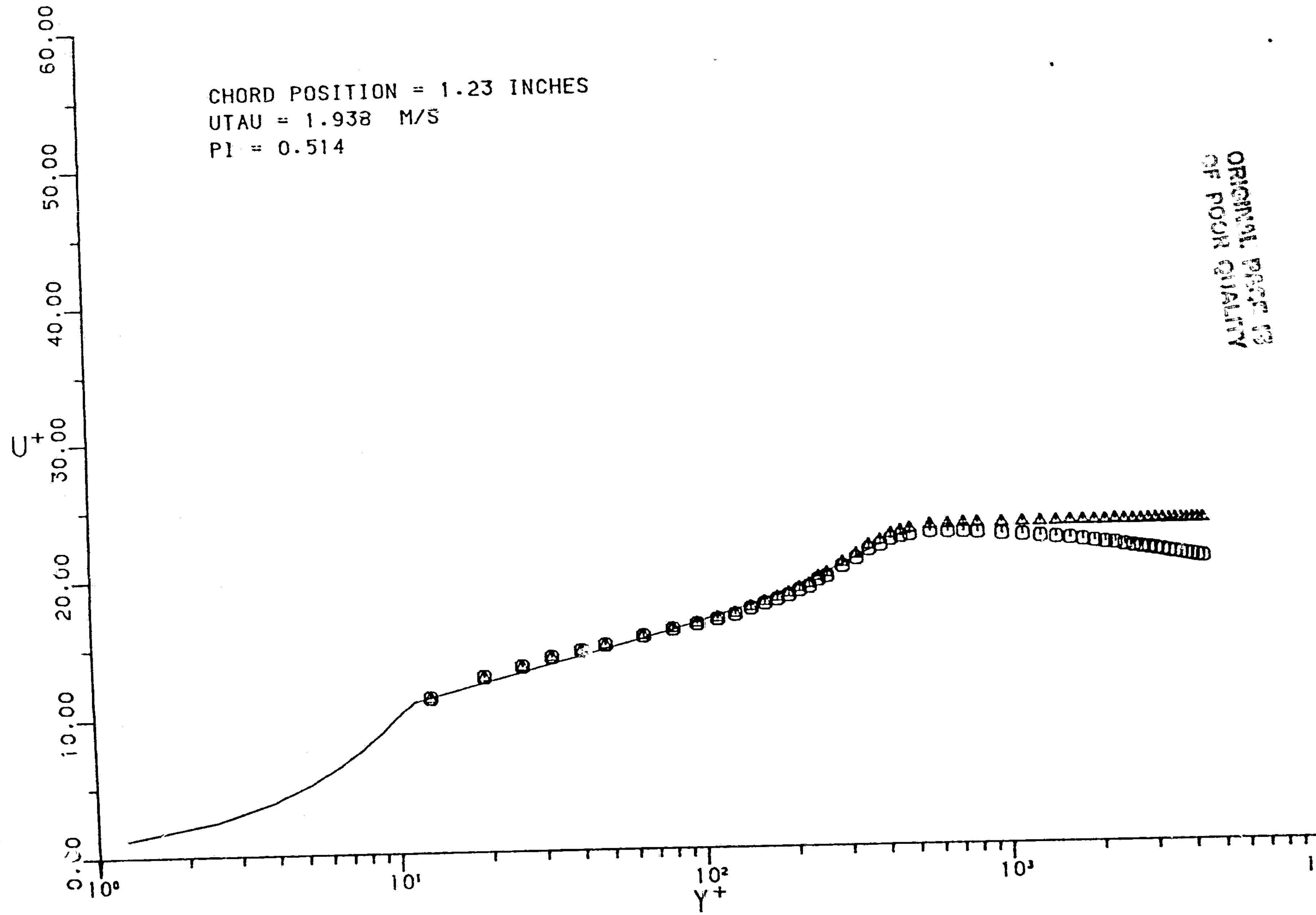
CHORD POSITION = 1.23 INCHES
UTAU = 1.938 M/S
PI = 0.514
U+
0.00
10.00
20.00
30.00
40.00
50.00
60.00
Y+
10⁰
10¹
10²
10³
10⁴

Figure 38.

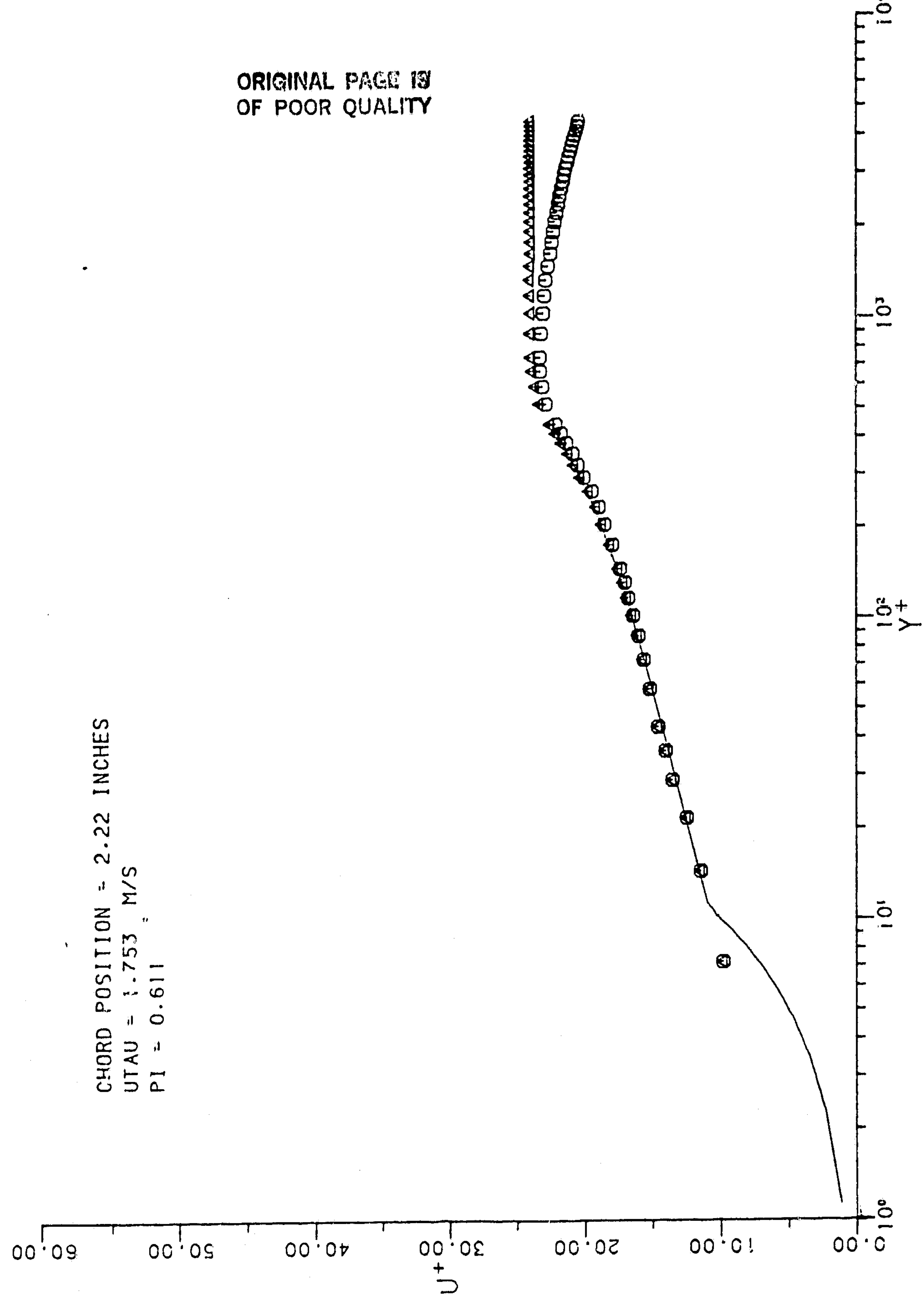
CHORD POSITION = 2.22 INCHES
UTAU = 1.753 M/S
PI = 0.611
U+
Y+
0.00
10.00
20.00
30.00
40.00
50.00
60.00

Figure 39.

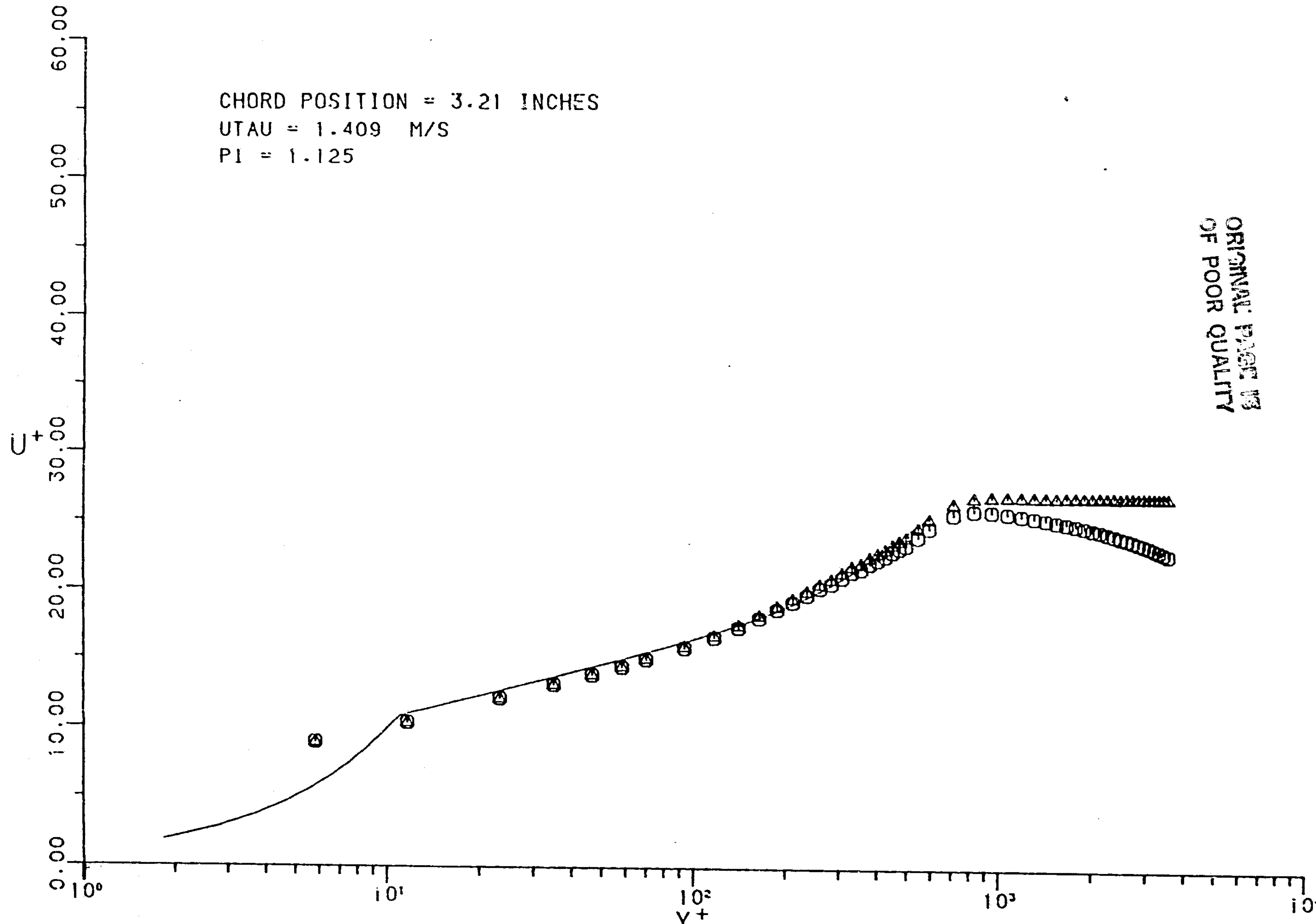
CHORD POSITION = 3.21 INCHES
UTAU = 1.409 M/S
PI = 1.125
U+
Y+
0.00
10.00
20.00
30.00
40.00
50.00
60.00
10⁰
10¹
10²
10³
10⁴

Figure 40.

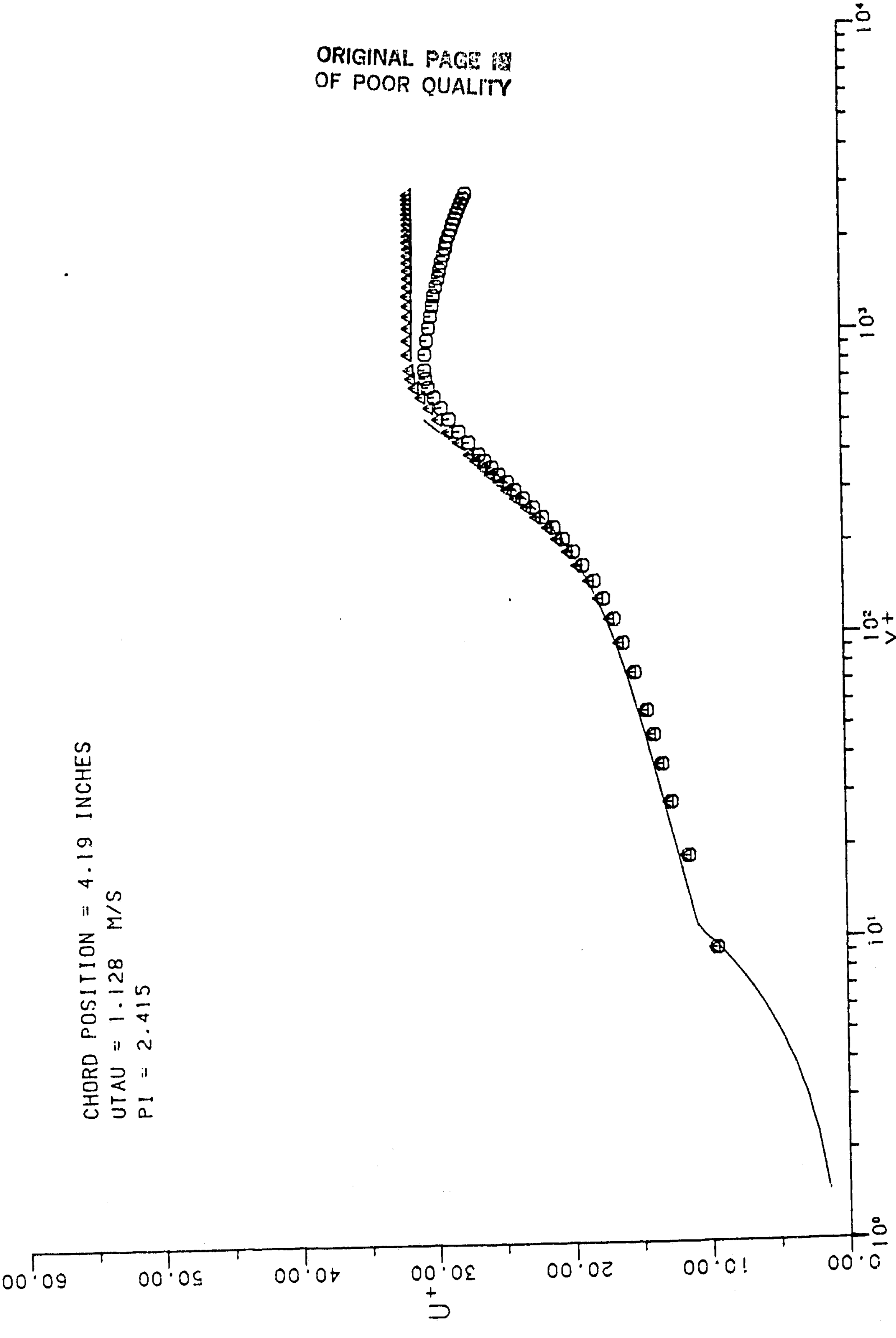
CHORD POSITION = 4.19 INCHES
UTAU = 1.128 M/S
PI = 2.415
U+
Y+
0.00
10.00
20.00
30.00
40.00
50.00
60.00
10⁰
10¹
10²
10³
10⁴

Figure 41.

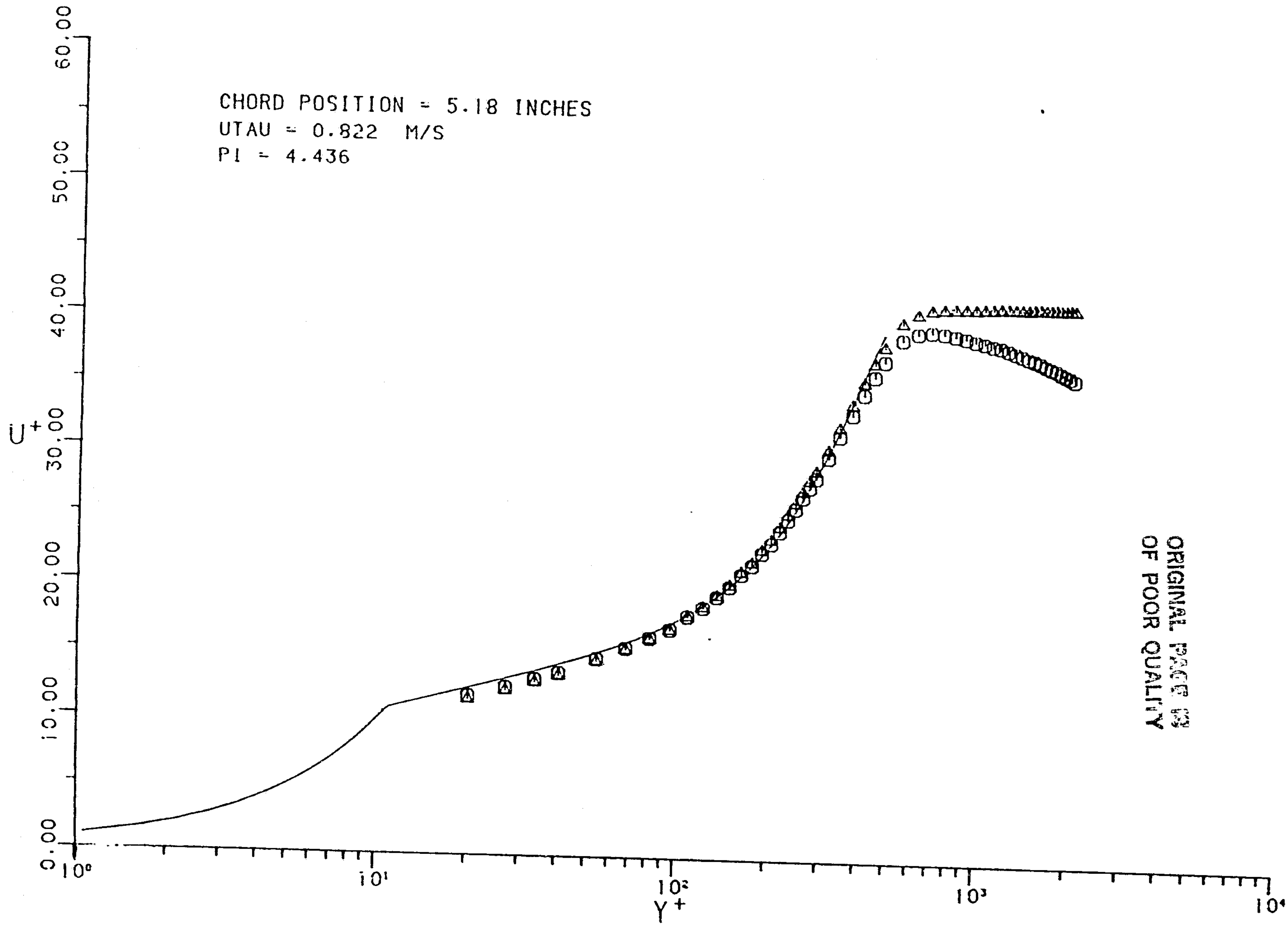
CHORD POSITION = 5.18 INCHES
UTAU = 0.822 M/S
PI = 4.436
U+
Y+
0.00
10.00
20.00
30.00
40.00
50.00
60.00
10⁰
10¹
10²
10³
10⁴

Figure 42.

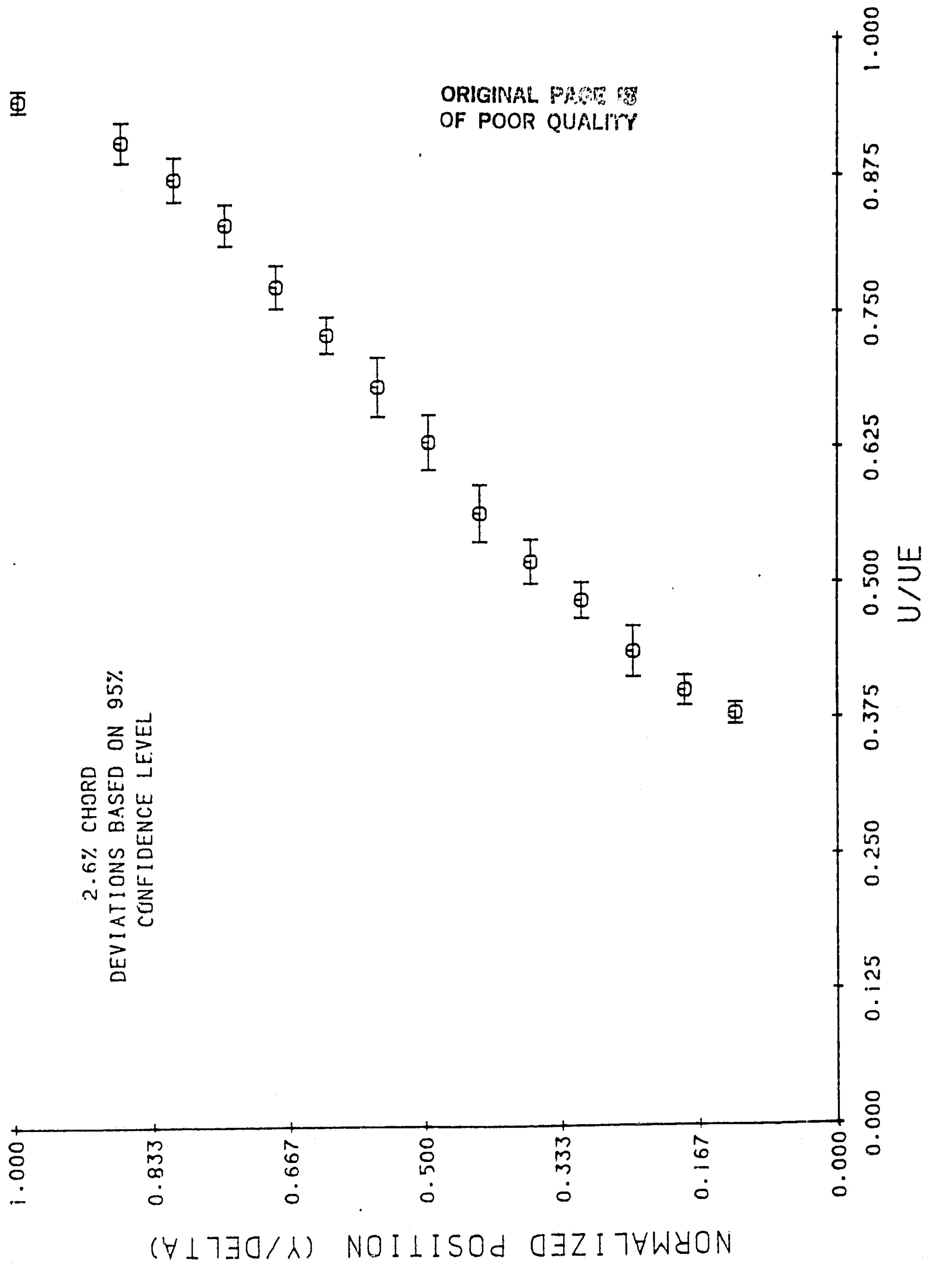
2.6% CHORD
DEVIATIONS BASED ON 95%
CONFIDENCE LEVEL
U/UE
0.000
0.125
0.250
0.375
0.500
0.625
0.750
0.875
1.000
NORMALIZED POSITION (Y/DELTA)
0.000
0.167
0.333
0.500
0.667
0.833
1.000

ORIGINAL PAGE IS
OF POOR QUALITY

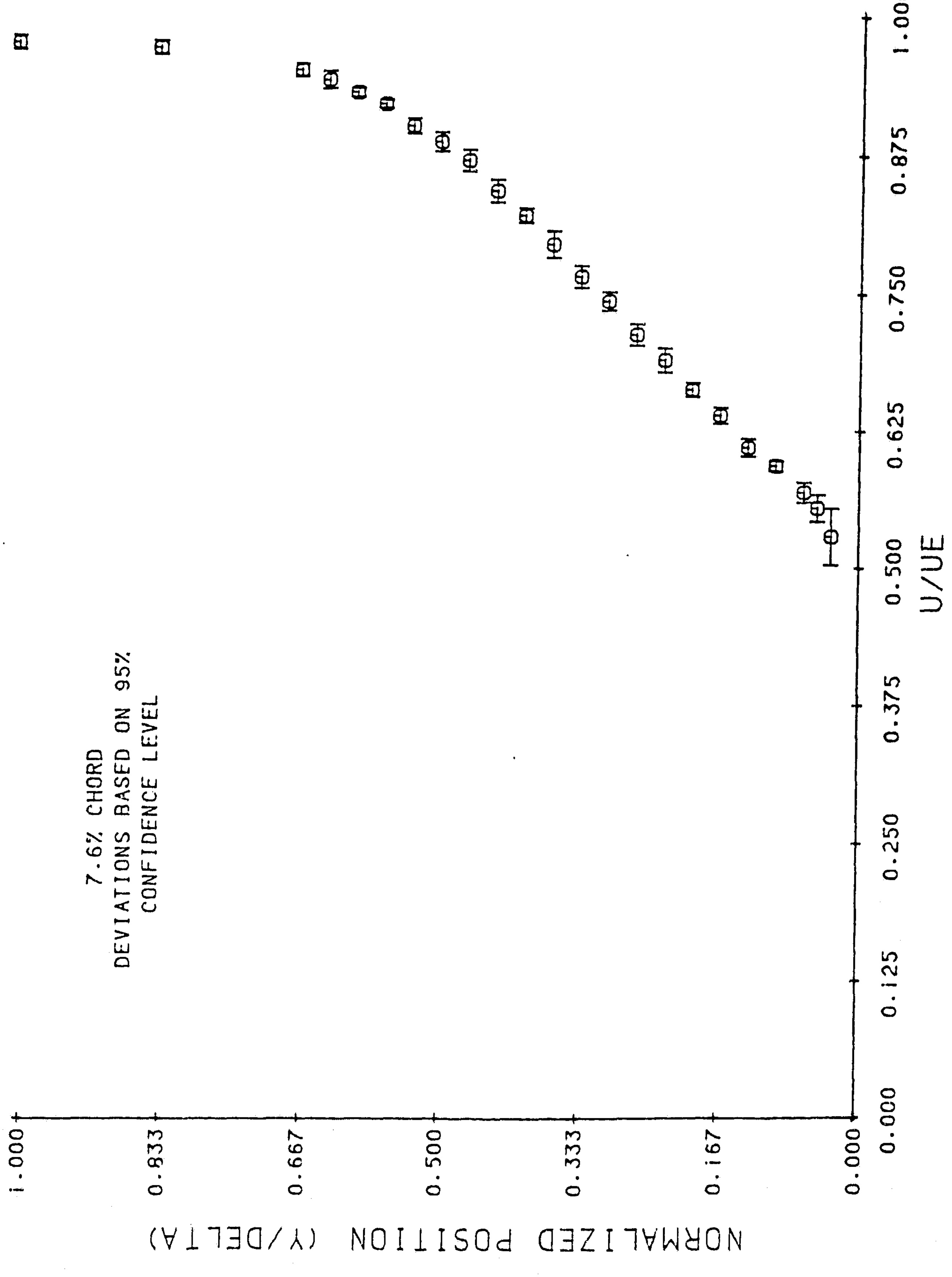

Figure 44.

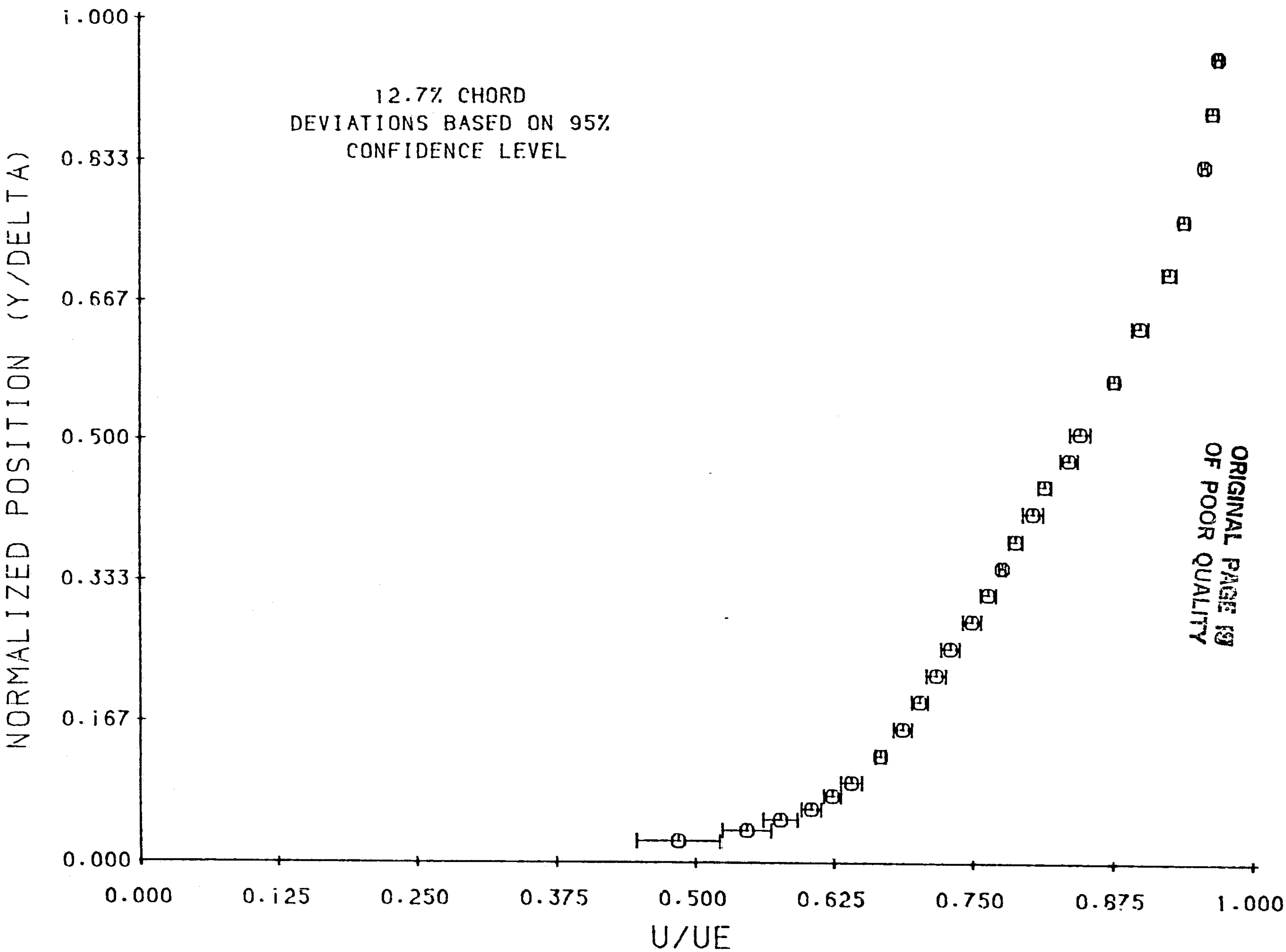

ORIGINAL PAGE IS
OF POOR QUALITY

Figure 45.

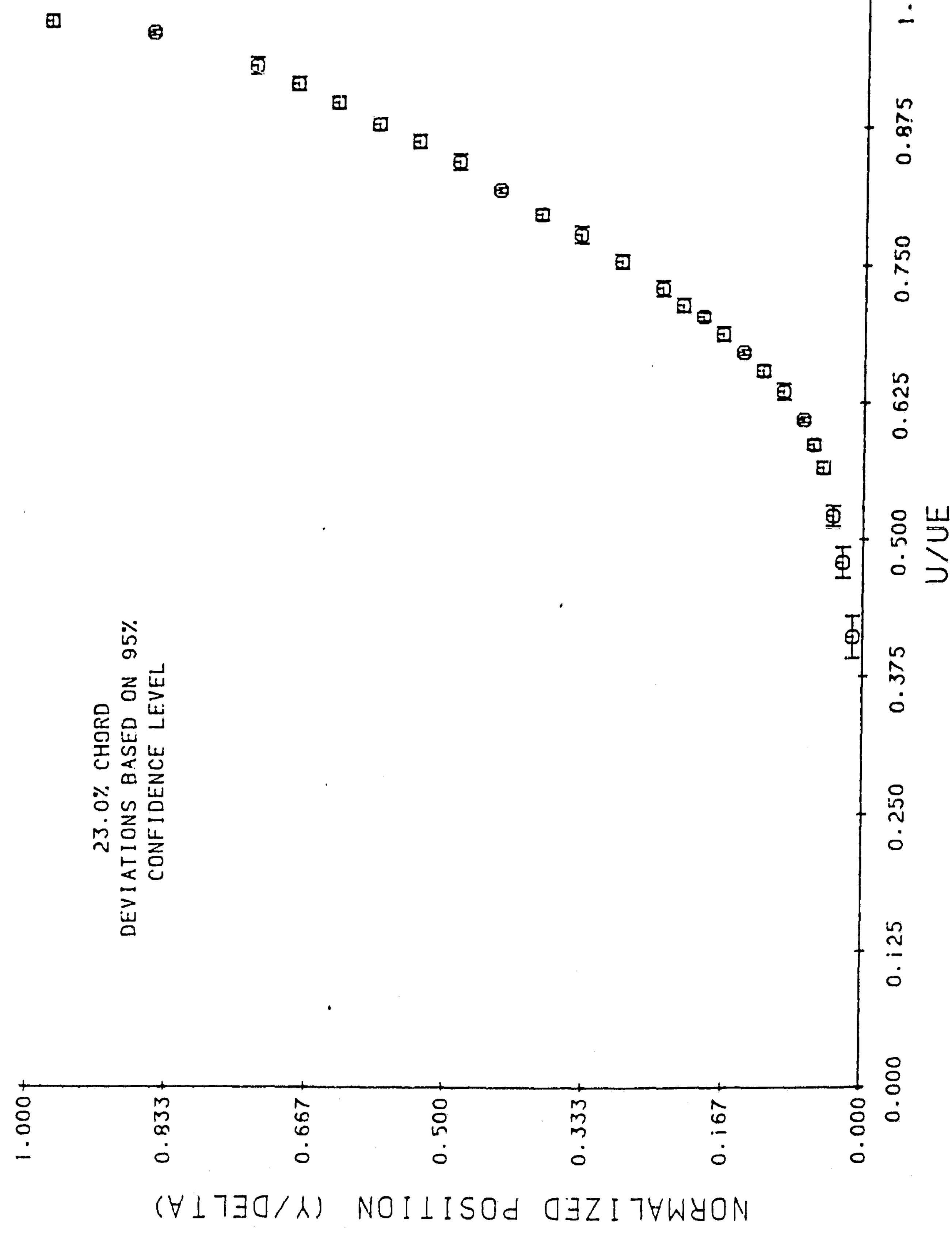
23.0% CHORD
DEVIATIONS BASED ON 95%
CONFIDENCE LEVEL
U/UE
NORMALIZED POSITION (Y/DELTA)
0.000
0.125
0.250
0.375
0.500
0.625
0.750
0.875
1.000
0.000
0.167
0.333
0.500
0.667
0.833
1.000

Figure 46.

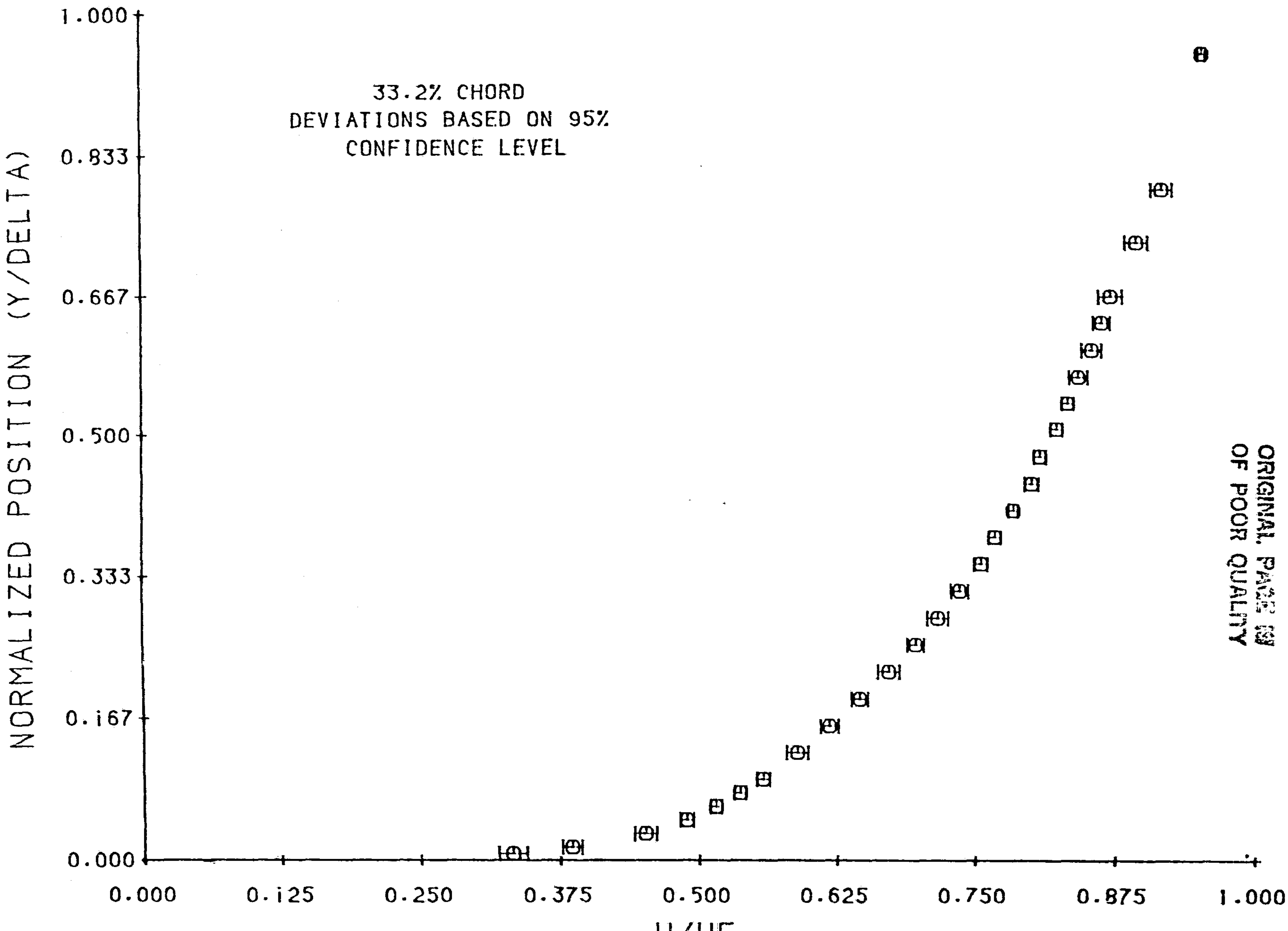
33.2% CHORD
DEVIATIONS BASED ON 95%
CONFIDENCE LEVEL
NORMALIZED POSITION (Y/DELTA)
U/UE
1.000
0.833
0.667
0.500
0.333
0.167
0.000
0.125
0.250
0.375
0.625
0.750
0.875

Figure 47.

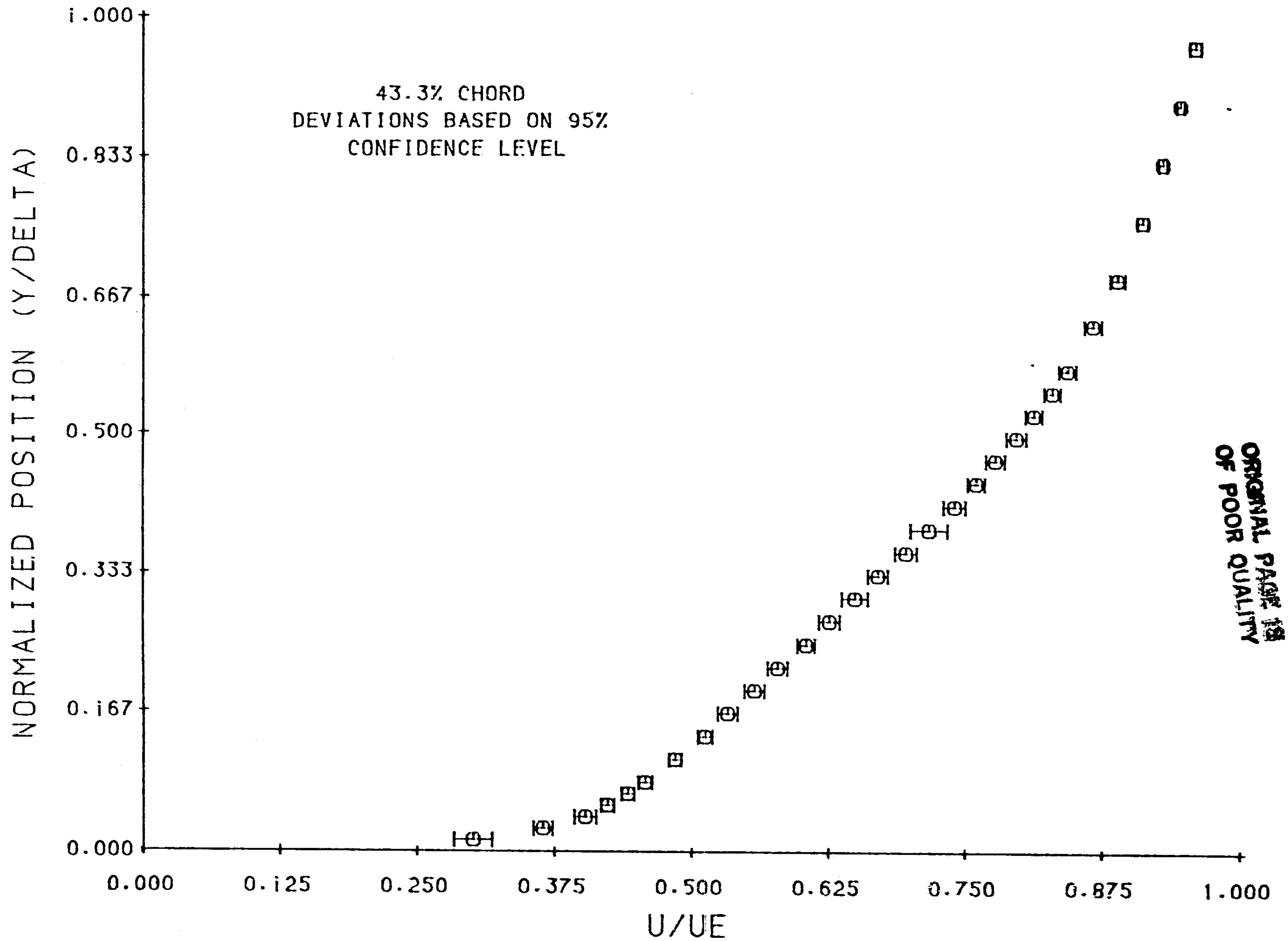
43.3% CHORD
DEVIATIONS BASED ON 95%
CONFIDENCE LEVEL
NORMALIZED POSITION (Y/DELTA)
1.000
0.833
0.667
0.500
0.333
0.167
0.000
0.000
0.125
0.250
0.375
0.500
0.625
0.750
0.875
1.000
U/UE

Figure 48.

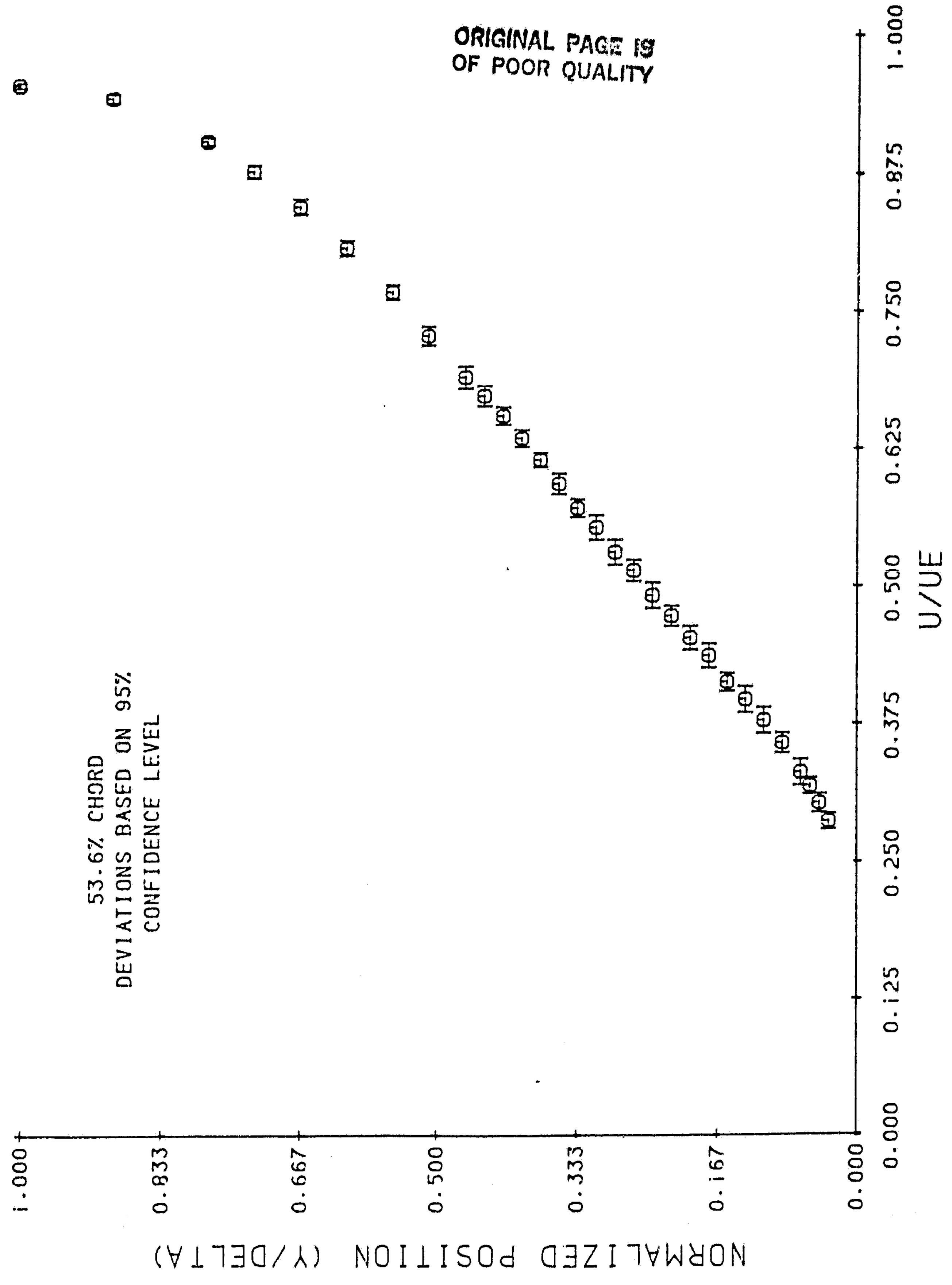
53.6% CHORD
DEVIATIONS BASED ON 95%
CONFIDENCE LEVEL
NORMALIZED POSITION (Y/DELTA)
1.000
0.833
0.667
0.500
0.333
0.167
0.000
U/UE
0.000
0.125
0.250
0.375
0.500
0.625
0.750
0.875
1.000

Figure 49

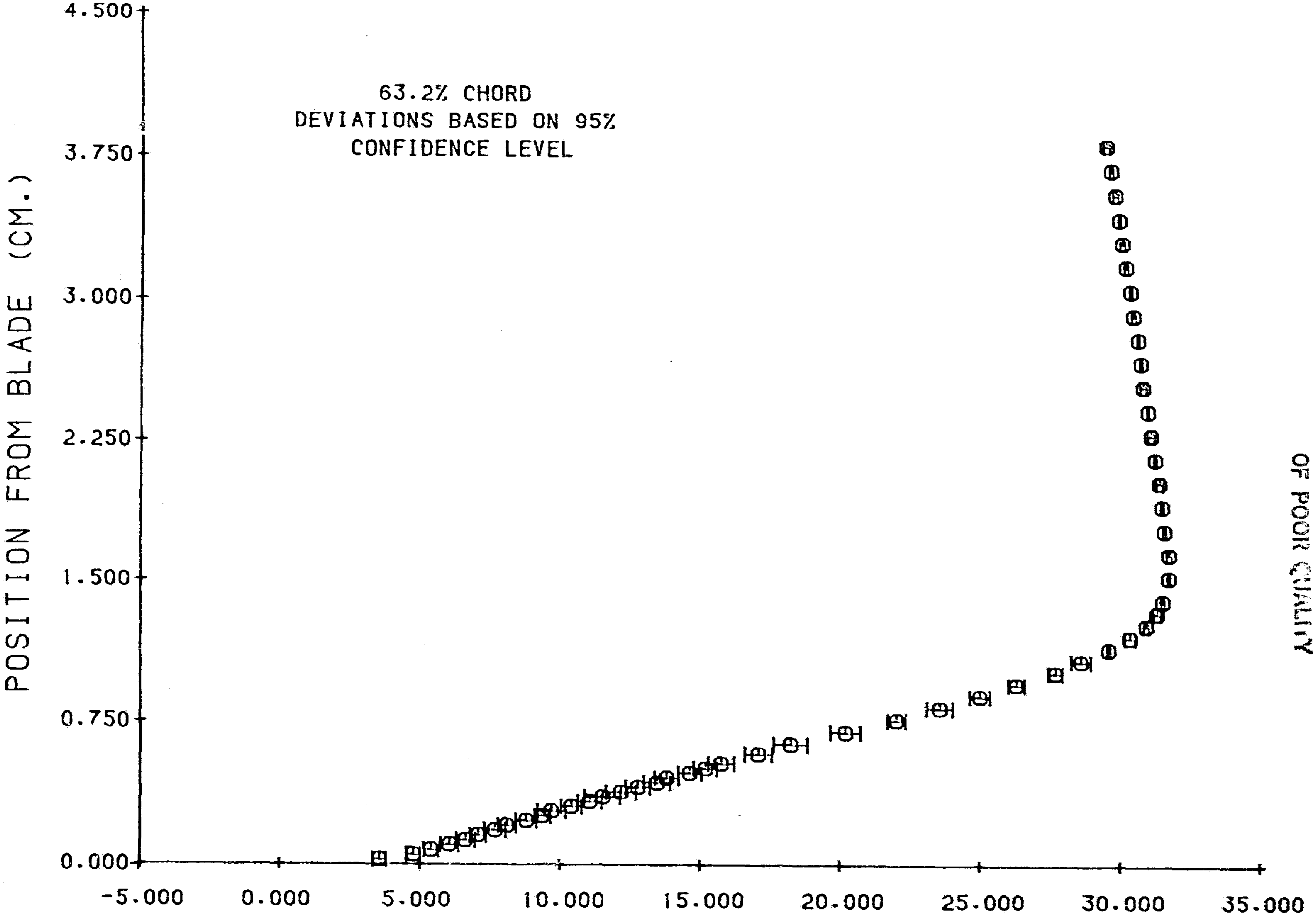
63.2% CHORD
DEVIATIONS BASED ON 95%
CONFIDENCE LEVEL
POSITION FROM BLADE (CM.)
4.500
3.750
3.000
2.250
1.500
0.750
0.000
-5.000
0.000
5.000
10.000
15.000
20.000
25.000
30.000
35.000
U (M/SEC)

Figure 50.

ORIGINAL PAGE IS
OF POOR QUALITY

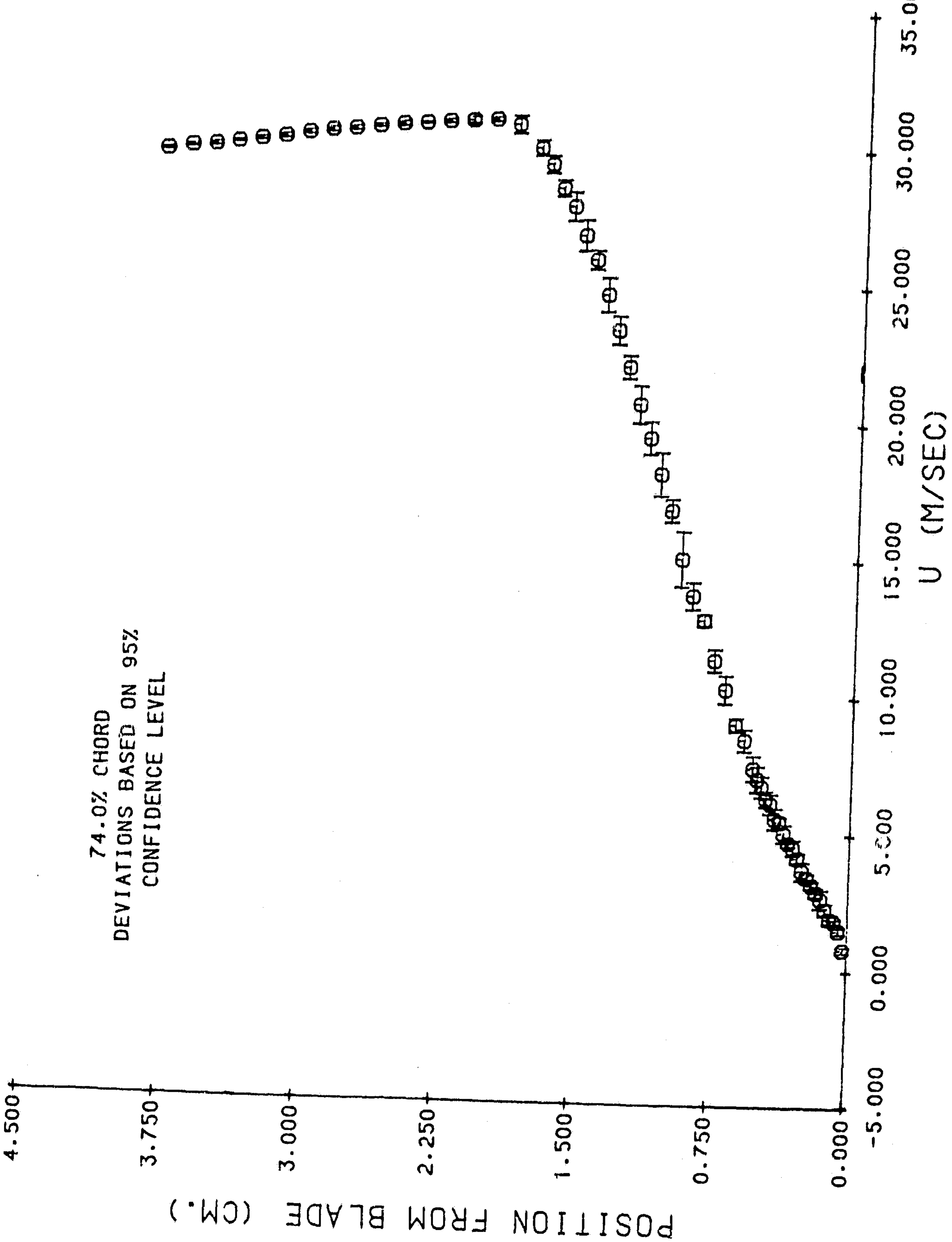

Figure 51.

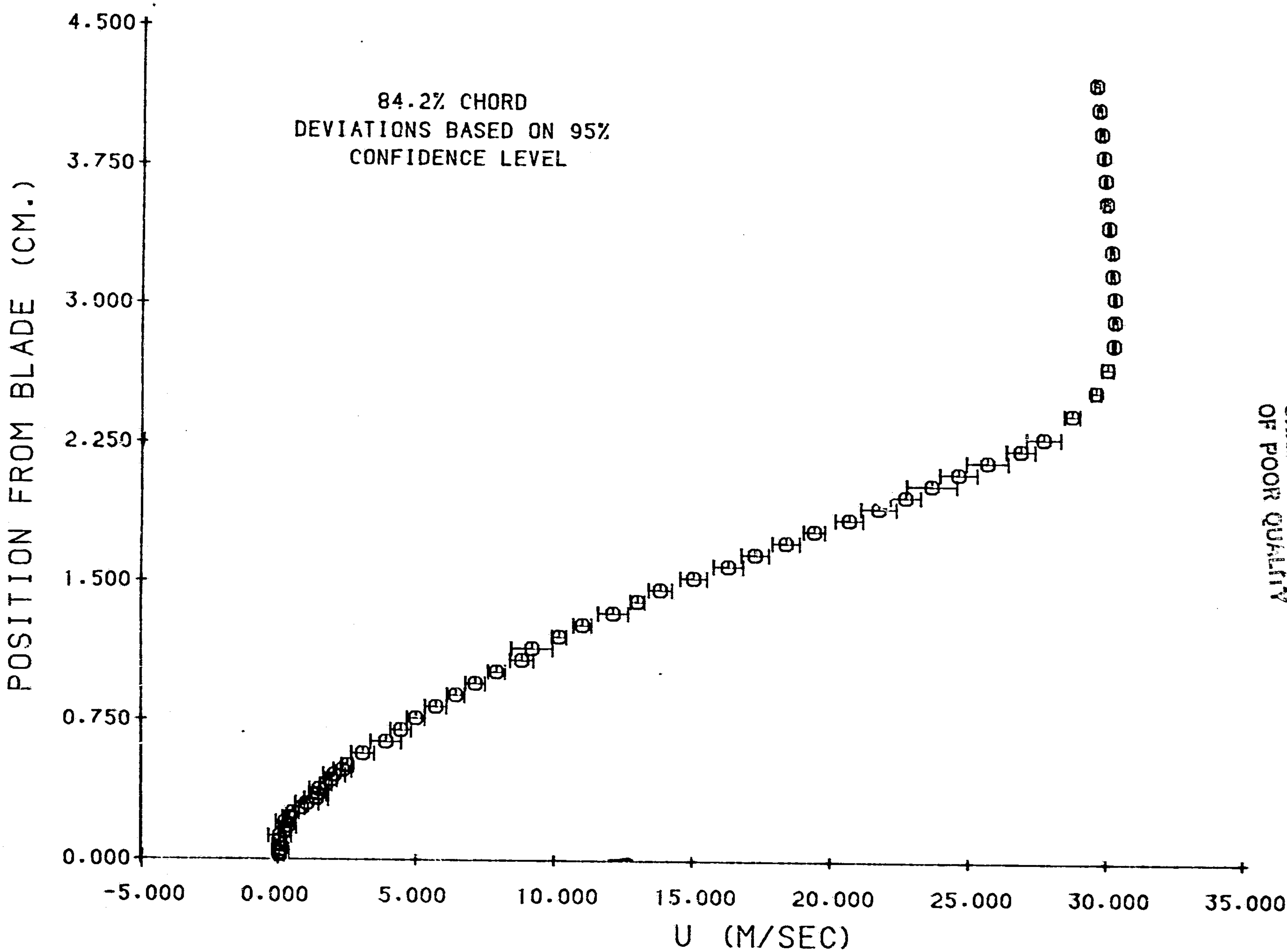
84.2% CHORD
DEVIATIONS BASED ON 95%
CONFIDENCE LEVEL
POSITION FROM BLADE (CM.)
4.500
3.750
3.000
2.250
1.500
0.750
0.000
-5.000
0.000
5.000
10.000
15.000
20.000
25.000
30.000
35.000
U (M/SEC)

Figure 52.

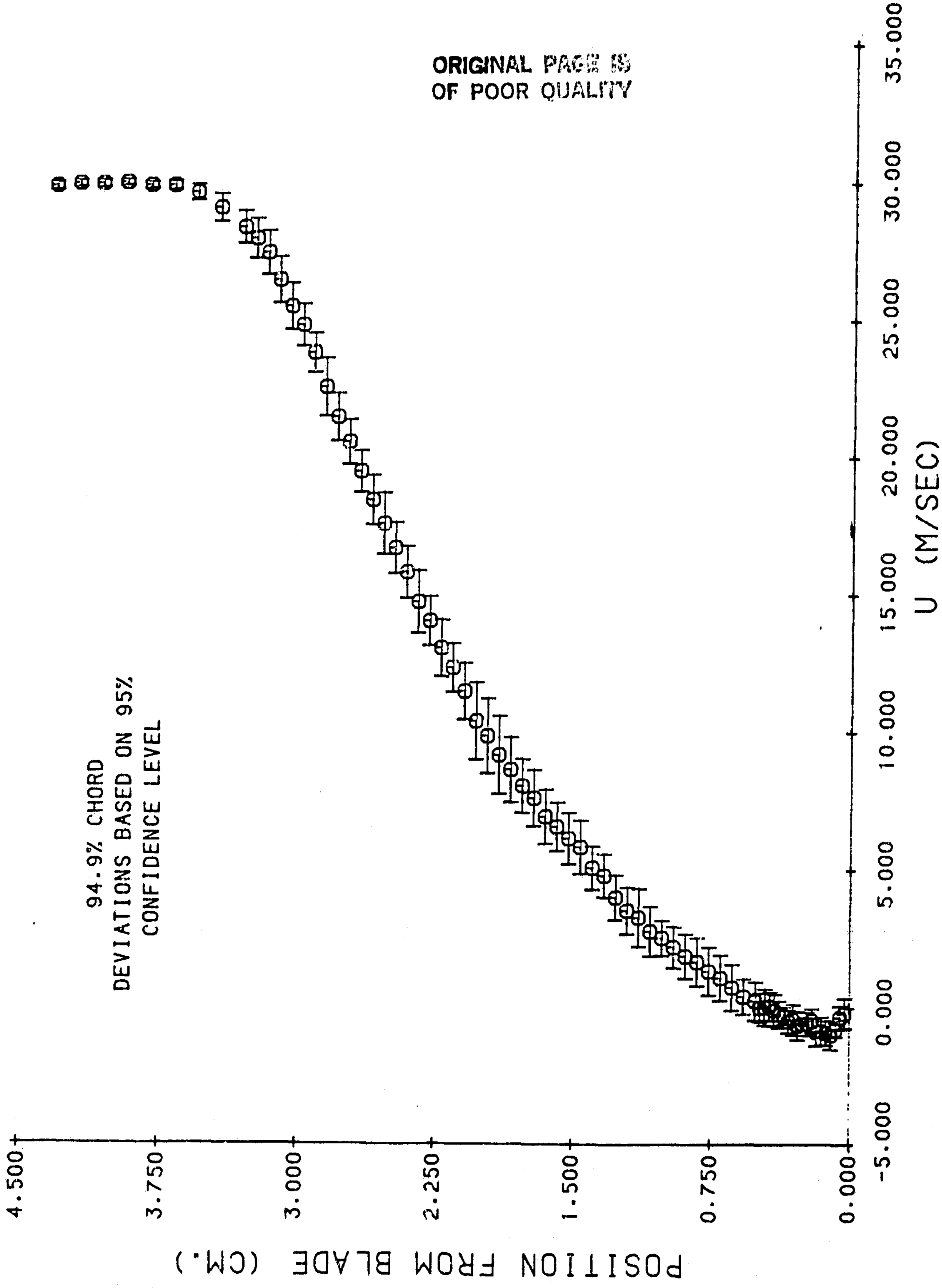
94.9% CHORD
DEVIATIONS BASED ON 95%
CONFIDENCE LEVEL
POSITION FROM BLADE (CM.)
4.500
3.750
3.000
2.250
1.500
0.750
0.000
U (M/SEC)
-5.000
0.000
5.000
10.000
15.000
20.000
25.000
30.000
35.000

Figure 53.

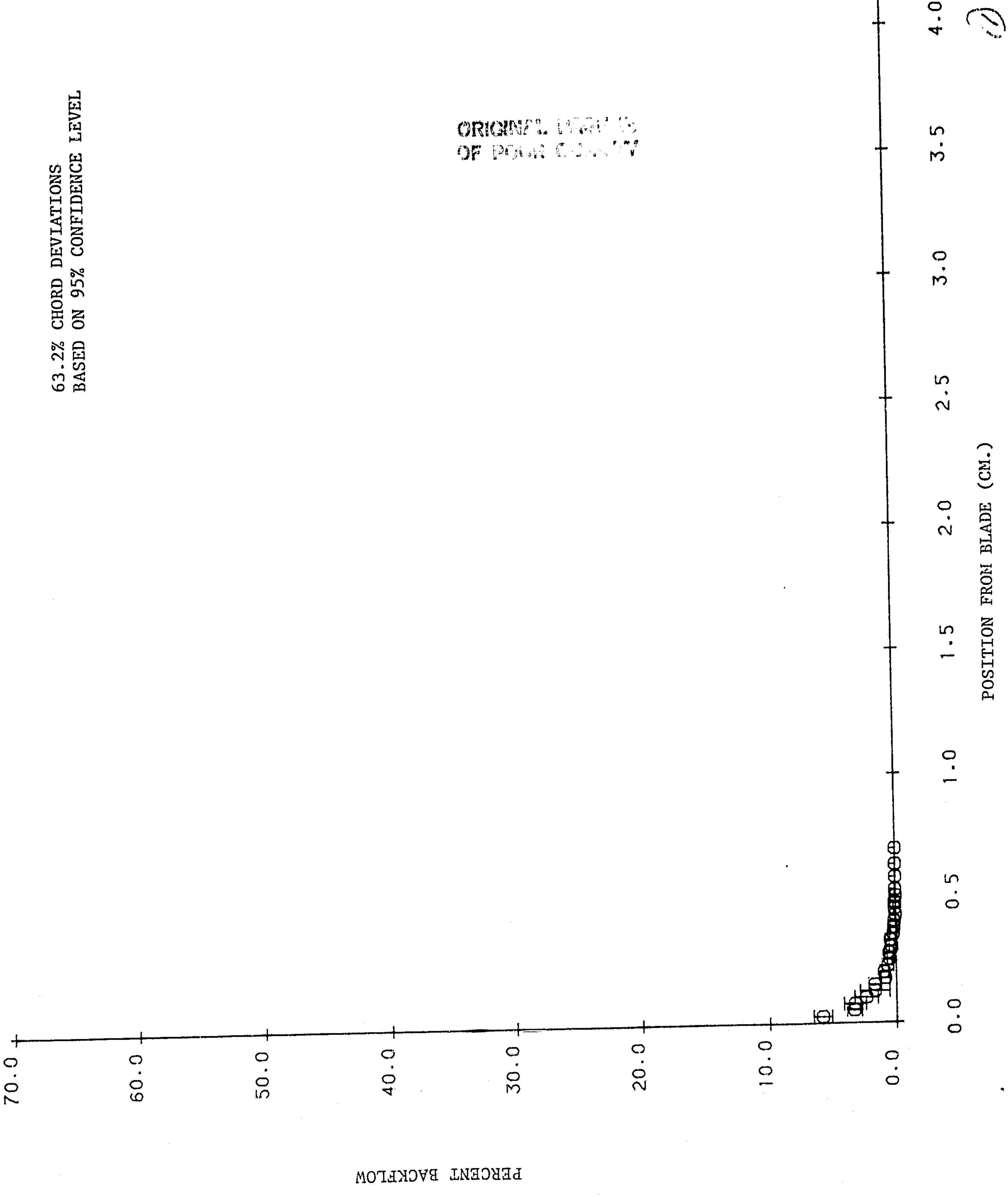
63.2% CHORD DEVIATIONS
BASED ON 95% CONFIDENCE LEVEL
PERCENT BACKFLOW
0.0
10.0
20.0
30.0
40.0
50.0
60.0
70.0
POSITION FROM BLADE (CM.)
0.0
0.5
1.0
1.5
2.0
2.5
3.0
3.5
4.0

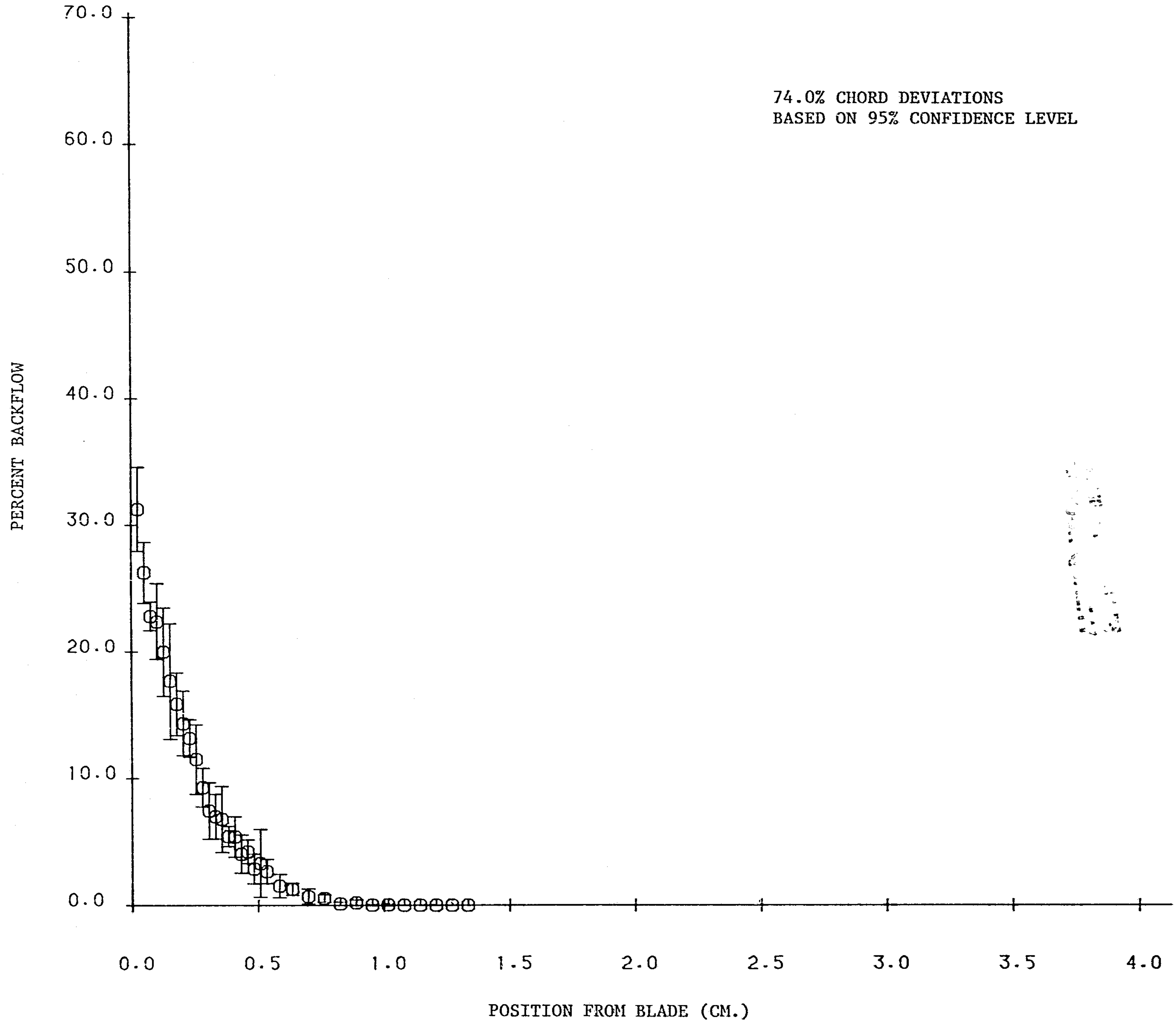
74.0% CHORD DEVIATIONS
BASED ON 95% CONFIDENCE LEVEL
PERCENT BACKFLOW
70.0
60.0
50.0
40.0
30.0
20.0
10.0
0.0
0.0
0.5
1.0
1.5
2.0
2.5
3.0
3.5
4.0
POSITION FROM BLADE (CM.)

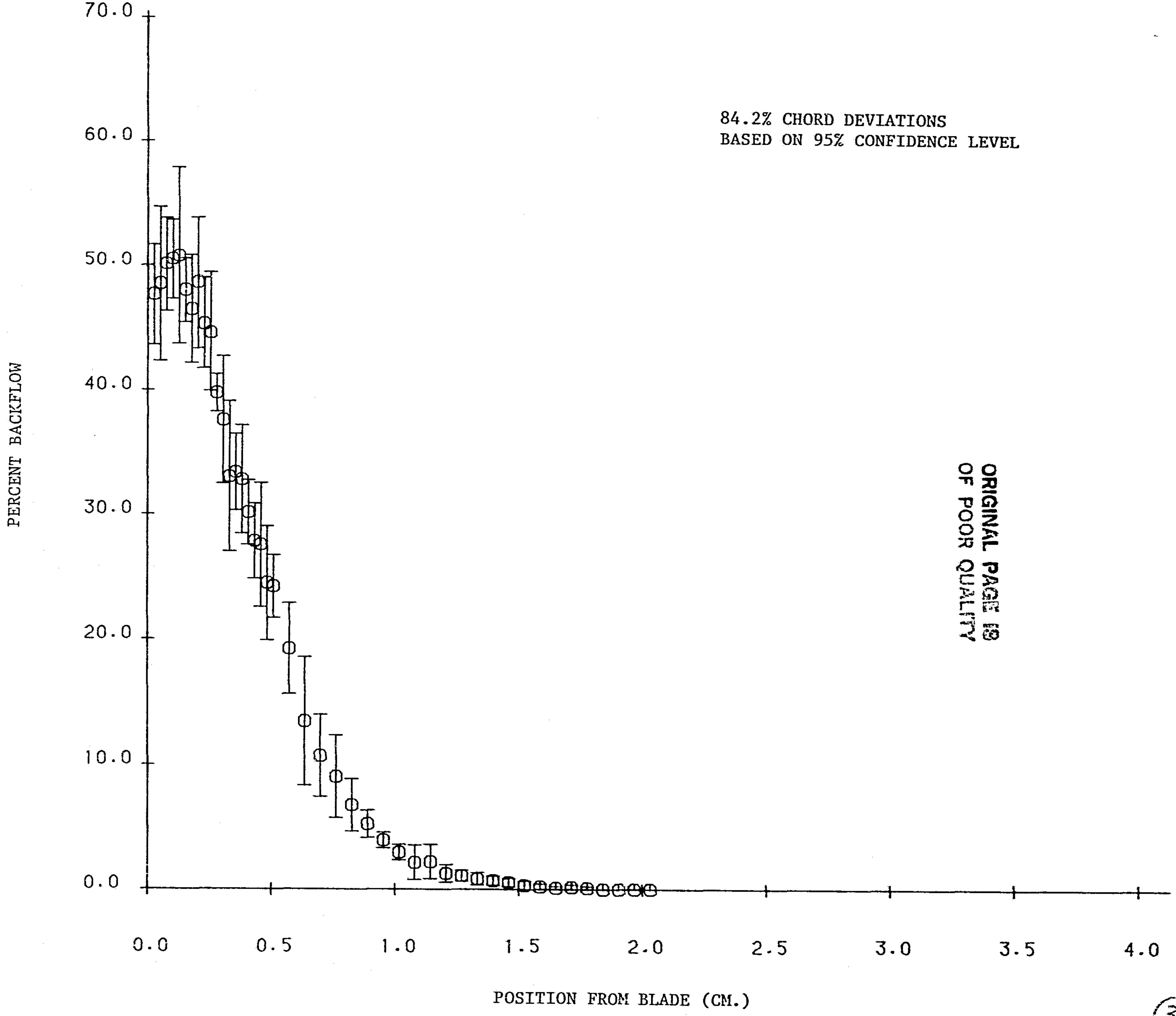
84.2% CHORD DEVIATIONS
BASED ON 95% CONFIDENCE LEVEL
PERCENT BACKFLOW
70.0
60.0
50.0
40.0
30.0
20.0
10.0
0.0
0.0
0.5
1.0
1.5
2.0
2.5
3.0
3.5
4.0
POSITION FROM BLADE (CM.)

3

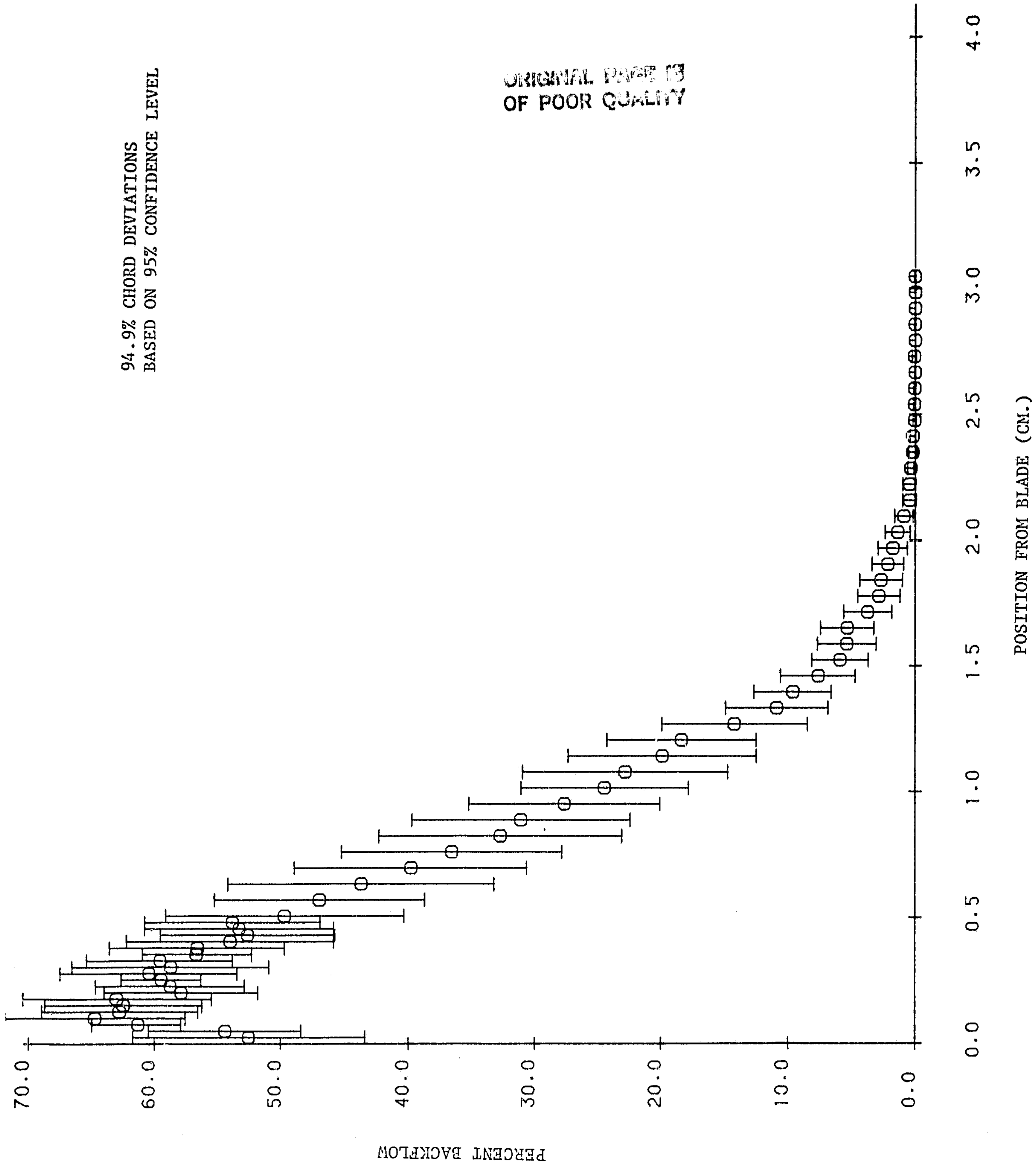
94.9% CHORD DEVIATIONS
BASED ON 95% CONFIDENCE LEVEL
PERCENT BACKFLOW
POSITION FROM BLADE (CM.)
0.0
10.0
20.0
30.0
40.0
50.0
60.0
70.0
0.0
0.5
1.0
1.5
2.0
2.5
3.0
3.5
4.0

Figure 57

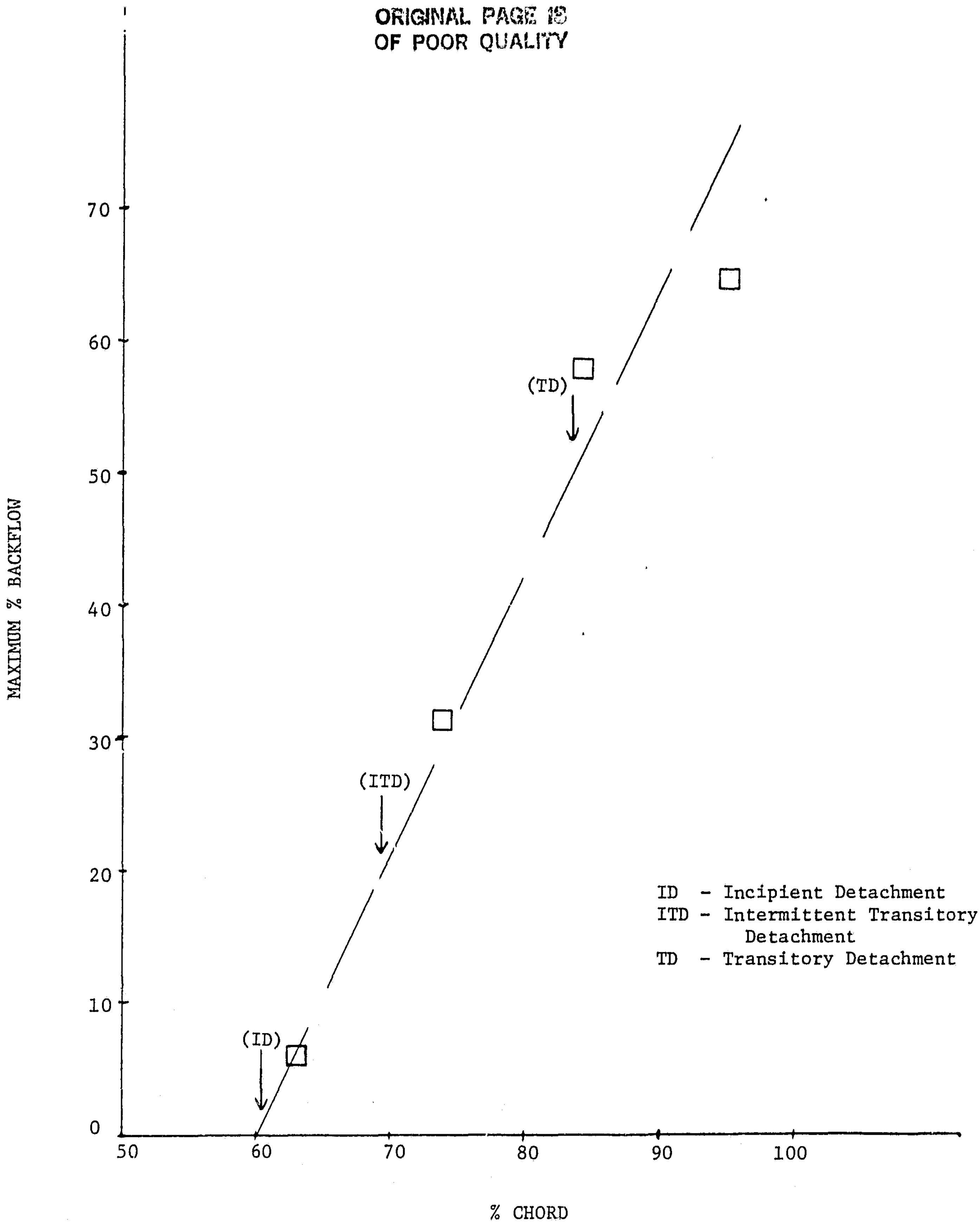
MAXIMUM % BACKFLOW
70
60
50
40
30
20
10
0
50
60
70
80
90
100
% CHORD
(TD)
(ITD)
(ID)
ID - Incipient Detachment
ITD - Intermittent Transitory Detachment
TD - Transitory Detachment

Figure 58.